(FOUO)

9 APRIL 1979 NO. 1, 1979 1 OF 2

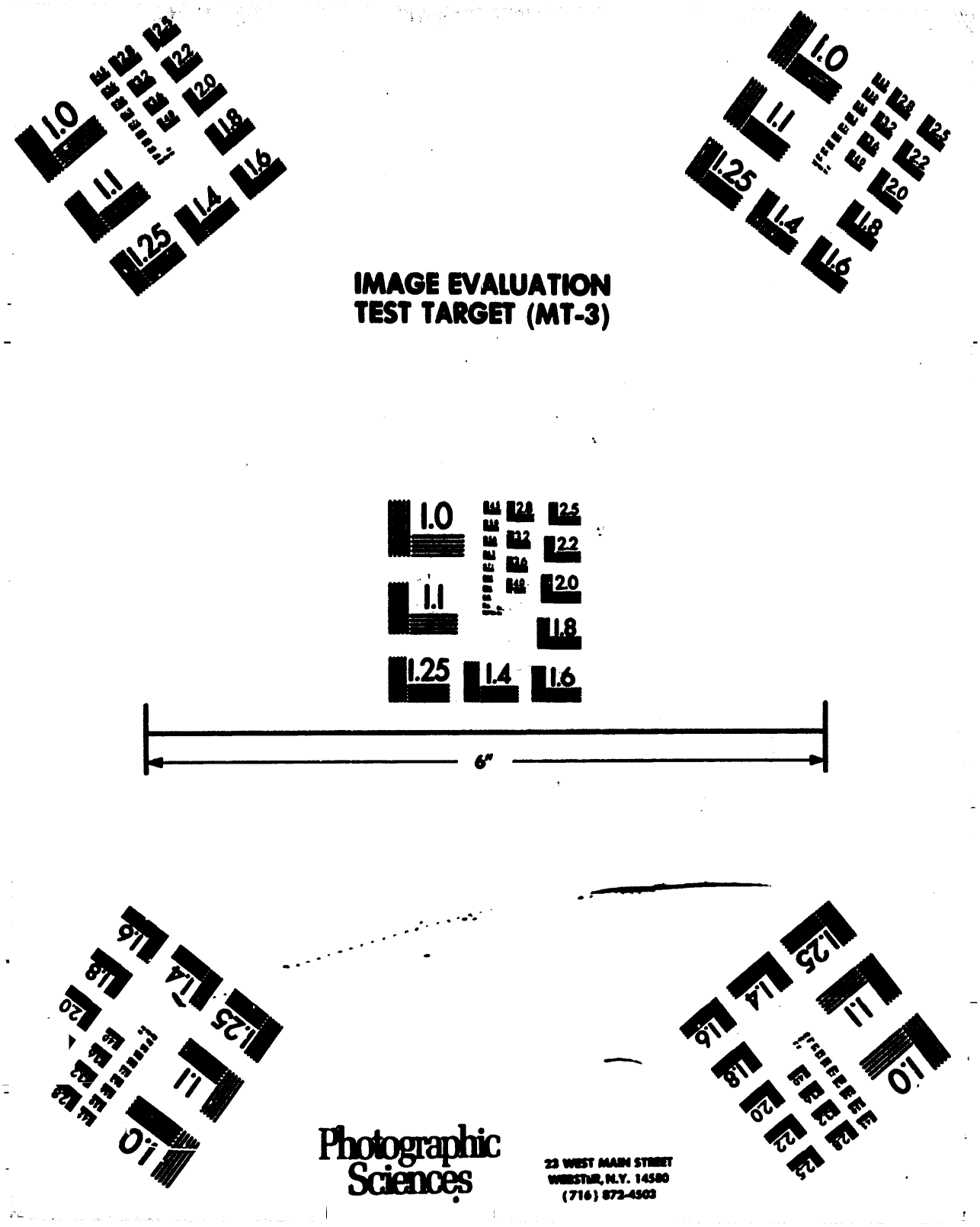

FOR OFFICIAL USE ONLY

JPRS L/8381

9 April 1979

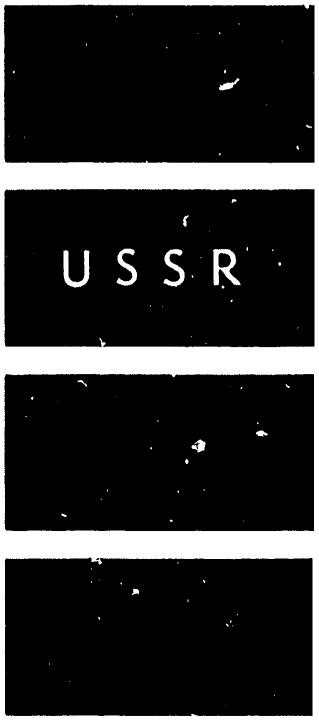

SELECTED ARTICLES FROM THE JOURNAL 'QUANTUM ELECTRONICS' No. 1, 1979

U. S. JOINT PUBLICATIONS RESEARCH SERVICE

FOR OFFICIAL USE ONLY

NOTE

JPRS publications contain information primarily from foreign newspapers, periodicals and books, but also from news agency transmissions and broadcasts. Materials from foreign-language sources are translated; those from English-language sources are transcribed or reprinted, with the original phrasing and other characteristics retained.

Headlines, editorial reports, and material enclosed in brackets [] are supplied by JPRS. Processing indicators such as [Text] or [Excerpt] in the first line of each item, or following the last line of a brief, indicate how the original information was processed. Where no processing indicator is given, the information was summarized or extracted.

Unfamiliar names rendered phonetically or transliterated are enclosed in parentheses. Words or names preceded by a question mark and enclosed in parentheses were not clear in the original but have been supplied as appropriate in context. Other unattributed parenthetical notes within the body of an item originate with the source. Times within items are as given by source.

The contents of this publication in no way represent the policies, views or attitudes of the U.S. Government.

APPROVED FOR RELEASE: 2007/02/08: CIA-RDP82-00850R000100040017-8

JPRS L/8381

9 April 1979

SELECTED ARTICLES
FROM THE JOURNAL 'QUANTUM ELECTRONICS'

No. 1, 1979

Moscow KVANTOVAYA ELEKTRONIKA in Russian Vol 6, No 1, Jan 79
pp 38-62, 78-85, 114-119, 127-133, 140-145, 177-188, 204-224, 231-248

CONTENTS PAGE

CONTENTS (Continued)

APPROVED FOR RELEASE: 2007/02/08: CIA-RDP82-00850R000100040017-8

PHYSICS

UDC 535.375

ON THE PROPERTIES OF CAVITIES WITH WAVEFRONT-REVERSING MIRRORS

Moscow KVANTOVAYA ELEKTRONIKA in Russian Vol 6, No 1, Jan 79 pp 38-44

[Article by I. M. Bel'dyugin, M. G. Galushkin and Ye. M. Zemskov]

[Text] An examination is made of the problem of the mode structure of a flat cavity with wavefront-reversing mirrors. An integral equation is derived for the modes of oscillations of such a cavity. It is shown that the modes of a cavity with wavefront-reversing mirrors coincide with the modes of a conformal cavity of the same length.

Methods of wavefront reversal based on various properties of nonlinear scattering of light in a medium have recently received intensive development [Ref. 1-4]. The use of such methods eliminates the distortions introduced by inhomogeneities of the index of refraction of optical media into the wave fronts of well collimated laser beams [Ref. 4]. It is also obvious that when the reflectivity is sufficiently high, a wavefront-reversing (WFR) medium can be used as one of the mirrors in the optical cavity of a laser. By analogy with Ref. 4 it can be expected that with use of such a cavity the optical inhomogeneities of the active medium will have little influence on the appearance of the laser field beyond its output mirror, the form of the field itself being determined by the properties of the cavity mirrors.

This paper deals with the investigation of the properties of flat cavities having a WFR mirror as one of the reflectors.

From the standpoint of optics, a WFR mirror is one that transforms the phase of the incident wave field. If the field at the input to this medium is denoted by U_i, and the field at the output from the medium is denoted by U_0, the action of the medium can be described by the equation

$$U_0(r)=cU_i^*(r)U_i(0)/U_i^*(0), \qquad (1)$$

where r is the distance to the optical axis, $|c|\leq 1$ is a complex constant that is independent of the form of field U_i and is determined by the reflecting properties of the medium. The factor $U_i(0)/U_i^*(0)$ in (1) is necessary

since without it the phase increment of the field with transition from a field $U_i(r)$ to the field $U_0(r)$ according to (1) depends on the zero for reckoning time, and the selection of the coordinate origin on the optical axis. It should be noted that the considerations given here relative to the phase factor $U_i(0)/U_i^*(0)$ in (1) are important only for the case of media that reverse the wave fronts without altering their frequency. It is only for such media that the concept of modes of oscillations of the corresponding cavity makes sense, and it is only thanks to the factor $U_i(0)/U_i^*(0)$ that the modes of oscillations have a definite frequency, as will be shown below. On the other hand, if the medium reverses the wave fronts with a change in frequency, as in stimulated Mandelstam-Brillouin scattering, we are dealing not with modes of oscillations, but rather with modes of propagation of fields (see for instance Ref. 5) for which there is no definite steady-state frequency. In this case the phase factor $U_i(0)/U_i^*(0)$ is not important since it has no effect either on the form of the field of modes of propagation or on the magnitude of their losses.

Hereafter for the sake of definiteness we will assume that the WFR mirror of a flat resonator is rectangular in shape, and its transverse dimensions are much less than the corresponding transverse dimensions of the output mirror. As implied by the theory of open resonators [Ref. 6], it is sufficient to consider a cavity with mirrors in the form of infinite strips to determine the form of the field of modes of oscillations and the corresponding losses in cavities with mirrors of rectangular shape. With consideration of (1), where we set $c = 1$ for the sake of definiteness, the corresponding integral equation is written as

$$\gamma U(x) = \sqrt{j} \int_{-a}^{a} \exp\{-j\pi (x-y)^2\} U^*(y) \frac{U(0)}{U^*(0)} dy \qquad (2a)$$

or more briefly

$$\gamma U = \hat{K} U, \qquad (2b)$$

where $a = \tilde{a}/\sqrt{2L\lambda}$, $2\tilde{a}$ is the transverse dimension of the WFR mirror, L is the distance between the mirrors of the cavity. Integral equation (2a) relates the field on the WFR mirror to the field on a mirror that is the image of the WFR mirror in an output mirror that has an infinite transverse dimension.

Let us first find the solutions of equation (2) for the condition $a = \infty$. Assuming that there exists a Fourier transform

$$V(\xi) = \frac{1}{\sqrt{2\pi}} \int_{-\infty}^{\infty} U(t) \exp(-j\xi t)\, dt \qquad (3)$$

of the function U(x), and applying it to both sides of equation (2), we get the functional equation

$$\gamma V(\xi) = \exp[j\xi^2/(4\pi)]\, V^*(-\xi) U(0)/U^*(0). \qquad (4)$$

Introducing into consideration the function $\tilde{V}(\xi)$ according to the relation

$$V(\xi) = \tilde{V}(\xi) \exp[j\xi^2/(8\pi)], \qquad (5)$$

we transform (4) to

$$\gamma\tilde{V}(\xi)=\tilde{V}^*(-\xi)U(0)/U^*(0). \tag{6}$$

The general solution of equation (6) takes the form

$$\tilde{V}(\xi)=F(\xi), \quad |\gamma|=1, \tag{7}$$

where $F(\xi)$ is an arbitrary complex function subject to the conditions

$$|F(\xi)|=|F(-\xi)|, \arg F(\xi)+\arg F(-\xi)+\arg[\gamma U(0)/U^*(0)]=2k\pi, \; k=0,\pm1\ldots \tag{8}$$

Relations (7) and (8) together with (5) give solutions that are symmetric relative to the axis coincident with the optical axis of the cavity with finite mirrors (i. e. solutions that have a definite frequency), as well as solutions that are symmetric relative to other axes displaced parallel to the optical axis. We will concern ourselves only with solutions of equation (6) with a definite frequency. In this case, we write relations (7) and (8) in the form

$$\tilde{V}(\xi)=F(\xi), \; F(\xi)=\pm F(-\xi); \; \gamma U(0)/U^*(0)=\pm1. \tag{9}$$

Substituting (9) in (5) and using the inverse Fourier transform, we get

$$U(x)=\sqrt{2j}\int_{-\infty}^{\infty} f(y)\exp[-j2\pi(x-y)^2]\,dy. \tag{10}$$

Here $f(x)$ is the Fourier transform of the function $F(\xi)$. Since $F(\xi)$ is essentially an arbitrary real function that has a definite frequency, $f(x)$ is also an arbitrary function that satisfies relations $f(x)=f(-x)$ when $F(\xi)=F(-\xi)$, and $f(x)=jf_1(x)$, where $f_1(x)=-f_1(-x)$ is a real function when $F(\xi)=-F(-\xi)$. Equation (10) also implies that $f(x)$ is the distribution of the field on the output mirror. A general solution that corresponds to relations (5), (7), (8) is also given by expression (10), where $f(x)$ is a real function of arbitrary form now with accuracy to multiplication by a complex constant.

If we set

$$f(x)=j^nH_n(\sqrt{2}x/w_0)\exp(-x^2/w_0^2), \tag{11}$$

where w_0 is the half-width of the gaussian beam $\exp(-x^2/w_0^2)$, then

$$U(x)=j^n(w_0/w)^{1/2}H_n(\sqrt{2}x/w)\exp(-j2\pi x^2/q)\exp[j(n+1/2)\operatorname{arctg}(2\pi w_0^2)^{-1}], \tag{12}$$

where

$$w=w_0[1+(2\pi w_0^2)^{-2}]^{1/4}, \; q=1+j2\pi w_0^2. \tag{13}$$

Thus the modes of oscillations of a cavity with WFR mirrors may be Hermitian-Gaussian beams having a plane phase front and arbitrary half-width w_0 on the output mirror. For comparison let us recall that for cavities with symmetric concave mirrors the modes are also Hermitian-Gaussian beams, but with a fixed half-width w_0 that is determined by the radius of curvature of the mirrors and the distance between them.

If we set

$$\exp(-j2\pi x^2/q)=\exp[-(\alpha+j\beta)x^2], \tag{14}$$

we have the relation

$$\alpha^2+(\hat{\mu}+\pi)^2=\pi^2. \tag{15}$$

This implies that the minimum half-width of the Gaussian beam on the WFR mirror of the cavity takes the form

$$\tilde{w}=w(2L\lambda)^{1/4}=(2L\lambda/\alpha)^{1/4}=(2L\lambda/\pi)^{1/4}, \tag{16}$$

which corresponds to the half-width of a Gaussian beam on the mirror of a confocal cavity having length 2L.

Let us go on now to find the solutions of equation (2a) at finite values of α. It can be readily seen that equation (2a) differs from the corresponding integral equation for the case of ordinary flat mirrors only in the sign of complex conjugation over function U(x) in the integrand. Since the solutions of this equation for finite values of α are complex (see for instance Ref. 6), they cannot be solutions of equation (2a). However, it is known that the eigenfunctions corresponding to the modes of a symmetric confocal cavity (and only such a cavity) are real for any values of the transverse dimensions of the mirrors [Ref. 5]. If we introduce into consideration the function V(x) that is related to function U(x) by the expression

$$U(x)=V(x)\exp(-j\pi x^2), \tag{17}$$

then equation (2a) takes the form

$$\gamma V(x)=\sqrt{j}\int_{-a}^{a}\exp\{-j2\pi xy\}\,V^*(y)\,\frac{V(0)}{V^*(0)}\,dy. \tag{18}$$

With accuracy to the operation of complex conjugation under the integral, equation (18) has the form of the equation for a confocal cavity. Therefore since the solutions of the integral equation for a confocal cavity are real, they will be solutions of equation (18) as well. These solutions (see for instance Ref. 5) take the form

$$\begin{aligned} V_m(x)&=S_m(2\pi a^2, x/a);\\ \gamma_m&=2j^{m+1/2}R_m(2\pi a^2, 1), \end{aligned} \tag{19}$$

where the functions S_m, R_m are real, and are called spheroidal. Since spheroidal functions form a complete orthogonal system of functions and

$$|\gamma_m|>|\gamma_{m+N}|, \quad N=1, 2, \ldots, \tag{20}$$

then the functions $V_m(x)$ defined by (19) are not just some of the solutions of (18), but represent all its possible solutions.

When $\alpha^2\gg 1$ and $(x/a)^2\ll 1$ we have the relation

$$S_m\left(2\pi a^2, \frac{x}{a}\right)\approx\frac{\Gamma(m/2+1)}{\Gamma(m+1)}H_m(\sqrt{2\pi}x)\exp(-\pi x^2). \tag{21}$$

Thus the solutions $U_m(x)$ of equation (2a) defined by expressions (17), (19) are approximately Gaussian-Hermitian beams (12) with parameter $w=\pi^{-1/2}$ corresponding to the case of a confocal cavity. We also note that we have

found solutions of form (21) when m = 0.1 by using a computer iteration method to solve equation (18). There is an understandable reason why such a wide variety of solutions (10) of equation (2a) for $a = \infty$ are transformed to Hermitien-Gaussian beams with $w = \pi^{-\frac{1}{2}}$ in the case of finite mirrors. For instance let us assign the actual field on the output mirror of the cavity in the form of a Gaussian beam: $f(x) = \exp(-x^2/w_0^2)$. Then when $w_0 \gg 1$ such a beam will have greater losses on WFR mirrors because of its large transverse dimensions over the entire space between mirrors, and when $w_0 \ll 1$ the losses will be large due to strong diffraction broadening of the beam. Simple exact calculation shows that the minimum losses for all finite mirrors a will occur at $w_0 = (2\pi)^{-\frac{1}{2}}$, which corresponds precisely to the field distribution of the lowest mode of a confocal cavity.

The way that the described transformation takes place can be traced on the example of the integral equation

$$\gamma U(x) = \sqrt{j} \int_{-a}^{a} \exp\{-j\pi(x-y)^2\} \exp\left\{-\frac{y^2}{a^2}\right\} U^*(y) \frac{U(0)}{U^*(0)}\, dy, \qquad (22)$$

which is approximately equivalent in its properties to equation (2a). Substituting the function U(x) in the form

$$U(x) = \exp[-(\alpha + j\beta)x^2], \qquad (23)$$

in (22), we find that (23) is a solution of equation (22) with satisfaction of the conditions

$$\frac{\pi^2}{(\alpha + a^{-2}) - j(\beta + \pi)} + j\pi = -\alpha - j\beta \qquad (24a)$$

or

$$\begin{cases} \alpha^2 + (\beta + \pi)^2 + \alpha/a^2 = \pi^2; \\ (\beta + \pi)/a^2 = 0. \end{cases} \qquad (24b)$$

System of equations (24) uniquely defines the values of parameters α and β:

$$\beta = -\pi, \quad \alpha = -(2a)^{-1} + \sqrt{(2a)^{-2} + \pi}. \qquad (25)$$

At arbitrarily large but finite values of a

$$\alpha \approx \pi, \quad \beta = -\pi, \qquad (26)$$

and solution (23) corresponds to the mode of a confocal cavity, and at $a = \infty$ conditions (24b) are converted to (15) and the half-width of the Gaussian beam is not uniquely defined.

Our presentation has shown that cavities with WFR mirrors have certain disadvantages as compared with ordinary flat mirrors, specifically: in an ordinary flat resonator the characteristic transverse dimension of the field of the lowest mode on the mirror is of the order of the transverse dimension of the mirror itself, whereas in a cavity with WFR mirrors the size of the field on the output mirror

$$\tilde{w}_0 = (L\lambda/\pi)^{\frac{1}{2}} \qquad (27)$$

does not depend on the transverse dimensions of the mirrors, and for typical experimental situations is quite small. For instance when $L = 1$ m, $\lambda = 1$ μm the half-width $W_0 = 0.25$ cm. To some extent, this circumstance probably places under doubt the advisability of using such cavities in lasers with large transverse dimensions of the active medium. Nonetheless, in our view the use of cavities with WFR mirrors for pulse lasers may be considered sound.

In actuality, with large transverse dimensions of mirrors it can be expected that the solutions of (10) with functions f(x) that have characteristic dimensions less than the mirror size a and that vary fairly smoothly with respect to the transverse coordinate within the limits of this dimension will be approximate solutions of equation (2a), or in other words will be approximate modes of oscillations of the cavity. Here the term "approximate modes of oscillations of the cavity" is understood to mean that the form of the field described by such functions with satisfaction of stipulated conditions will be practically duplicated on the mirrors over the extent of a large number N of passes through the cavity. The number of passes N for pulse lasers may be greater than the number of passes of emission over the length of the cavity during a lasing pulse, and then such an approximate mode of oscillations will be practically realizable.

Thus for pulse lasers in addition to the problem of finding the exact solution of equation (2a) the question arises of studying the nature of the change in approximate solutions (10) of equation (2a) depending on the form of the function f(x), the transverse dimensions a of the mirror and the number N of passes, and as far as we know this problem has no analogs in the conventional theory of open resonators. Probably the consideration of such a problem will in future be the basis of research on the theory of cavities with WFR mirrors.

In conclusion, let us consider the problem of the influence that optical inhomogeneities have on the mode structure of fields in a cavity with WFR mirrors. In doing so, we limit ourselves to media for which the index of refraction n depends on the coordinate according to the law

$$n(r, z) = n_0(z) + n_1(z) r^2. \qquad (28)$$

It is known [Ref. 7, 8] that in this case the optical properties of the medium located between the mirrors can be described by a transfer matrix:

$$T = \begin{pmatrix} A & B \\ C & D \end{pmatrix}, \quad AD - CB = 1. \qquad (29)$$

The transfer matrix that relates the field on the WFR mirror to the field on its image in a flat output mirror takes the form

$$T_1 = \sigma T^{-1} \sigma T = \begin{pmatrix} AD + CB & 2BD \\ 2AC & AD + CB \end{pmatrix}, \quad \sigma = \begin{pmatrix} 1 & 0 \\ 0 & -1 \end{pmatrix}. \qquad (30)$$

Using the elements of matrix T_1, we get an integral equation for fields on the WFR mirror:

$$\gamma U(x) = \sqrt{i} \int_{-a}^{a} \exp\{\mp i\pi(gx^2 + gy^2 - 2xy)\} U^*(y) \frac{U(0)}{U^*(0)} dy, \quad (31)$$

where $a = \tilde{a}/\sqrt{2|BD|\lambda}$, $g = AD - CB$, the sign "-" in the exponential function corresponds to $BD>0$, and the sign "+" -- to $BD<0$. If we introduce into consideration the function $V(x)$ in accordance with the relation

$$U(x) = V(x)\exp(\mp i\pi g x^2), \quad (32)$$

then equation (31) is transformed to equation (18), which we considered in detail above.

Thus we find that when there is a medium between mirrors described by matrix T, the fields of the cavity on a WFR mirror are Hermitian-Gaussian beams with half-width

$$\tilde{w} = (2|BD|\lambda/\pi)^{1/2} \quad (33)$$

and radius of curvature

$$\tilde{R} = \mp 2|BD|/(AD+CB). \quad (34)$$

If now in agreement with Ref. 7 we introduce into consideration the parameter q such that

$$1/\tilde{q} = 1/\tilde{R} - i\lambda/(\pi\tilde{w}^2), \quad (35)$$

and take into consideration that the parameter $\tilde{q}_0$ on the output mirror is related to $\tilde{q}$ by the expression

$$\tilde{q}_0 = (A\tilde{q}+B)/(C\tilde{q}+D), \quad (36)$$

then for the parameters $\tilde{w}_0$, $\tilde{R}_0$ we get

$$\tilde{R}_0 = \infty, \quad \tilde{w}_0 = [(\lambda/\pi)|B/D|]^{1/2}. \quad (37)$$

For an ampty cavity $D = 1$, $B = L$ and (37) coincides with (27). In other cases the half-width of the beam (37) generally speaking is not equal to the half-width of the beam (27), and optical inhomogeneities have a definite effect on the form of the field on the output mirror of the cavity.

Let us illustrate what we have said on the basis of an example of a thin lens with focal length f, located a distance l from the output mirror of the cavity. In this case we have

$$T = \begin{pmatrix} 1-l/f & L-l(L-l)/f \\ -1/f & 1-(L-l)/f \end{pmatrix} \quad (38)$$

and

$$\tilde{w}_0 = \left(\frac{\lambda}{\pi}\left|\frac{fL-l(L-l)}{f-L+l}\right|\right)^{1/2}. \quad (39)$$

Thus when $l = L$, i. e. when the lens is up against the WFR mirror, it has no influence on the form of the output field, regardless of lens power. Contrariwise, when $l = 0$ the lens has the maximum effect on the form of the field, but this effect is insignificant when $|f| \gg L$, i. e. in the case of small optical inhomogeneities of the medium.

REFERENCES

1. B. Ya. Zel'dovich, V. I. Popovichev, V. V. Ragul'skiy, F. S. Fayzullov, PIS'MA V ZHURNAL EKSPERIMENTAL'NOY I TEORETICHESKOY FIZIKI, Vol 15, 1972, p 160.

2. V. V. Ragul'skiy, TRUDY FIZICHESKOGO INSTITUTA IMENI P. N. LEBEDEVA, Vol 86, 1976, p 3.

3. V. I. Bespalov, A. A. Betin, G. A. Pasmanik, "Tezisy dokladov Vos'moy Vsesoyuznoy konferentsii po kogerentnoy i nelineynoy optike" [Abstracts of Reports to the Eighth All-Union Conference on Coherent and Nonlinear Optics], Tbilisi, Metsniyereba, 1976.

4. O. Yu. Nosach, V. I. Popovichev, V. V. Ragul'skiy, F. S. Fayzullov, PIS'MA V ZHURNAL EKSPERIMENTAL'NOY I TEORETICHESKOY FIZIKI, Vol 16, 1972, p 617.

5. "Lazery" [Lasers, Collection of Papers], Moscow, Inostrannaya literatura, 1963.

6. L. A. Vaynshteyn, "Otkrytyye rezonatory i otkrytyye volnovody" [Open Resonators and Open Waveguides], Moscow, Sovetskoye radio, 1966.

7. H. Kogelnik, BELL SYST. TECHN. J., Vol 44, 1965, p 455.

8. D. Markuze, "Opticheskiye volnovody" [Optical Waveguides], Moscow, Mir, 1974.

6610
CSO: 1870

PHYSICS

UDC 539.2

INVESTIGATION OF LASER DAMAGE TO CRYSTALS UNDER THE ACTION OF A $CaF_2:Er^{3+}$ LASER ($\lambda = 2.76$ μm)

Moscow KVANTOVAYA ELEKTRONIKA in Russian Vol 6, No 1, Jan 79 pp 45-48

[Article by G. V. Gomelauri and A. A. Manankov, Physics Institute imeni P. N. Lebedev, Academy of Sciences USSR]

[Text] A study is done on laser destruction of a number of alkali halide and other crystals on $\lambda = 2.76$ μm using a laser on a crystal of $CaF_2:Er^{3+}$ (pulse duration 85 ns). Results obtained on the most optically stable specimens of NaCl at different temperatures (in the range of 300-1000 K) are compared with data of measurements on other wavelengths and discussed on the basis of the avalanche breakdown mechanism. It is found that the measured threshold on $\lambda = 2.76$ μm at $T = 300$ K together with data found previously on $\lambda = 10.6$, 1.06 and 0.69 μm are satisfactorily explained by the theory of avalanche ionization at a value of the parameter of effective rate of electron-phonon collisions $\nu_{ef} = 6 \cdot 10^{14}$ s^{-1}, although the theory does not explain the temperature dependence of the destruction threshold observed on $\lambda = 2.76$ μm.

1. Introduction

Until recently the study of laser destruction in the infrared range has been limited to only two wavelengths: 10.6 μm (CO_2 laser) and 1.06 μm (neodymium or garnet lasers). At the same time, the study of laser destruction on other wavelengths of the infrared range is of undoubted interest for explaining the mechanism of laser destruction since the frequency dependence of the threshold of destruction is one of the most characteristic criteria of the mechanism of destruction [Ref. 1, 2]. Studies done in Ref. 3 on laser destruction of a number of alkali halide crystals on $\lambda = 0.53$, 0.69, 1.06 and 10.6 μm showed that the mechanism of destruction for the most stable specimens may be avalanche ionization. However, an analysis of experimental data on the temperature dependence of the threshold of destruction at $\lambda = 10.6$ μm based on the theory of avalanche ionization showed

considerable discrepancies between theory and experiment for which the causes remain unexplained. In this connection, in our research we studied the same crystals as in Ref. 3, using a laser on a $CaF_2:Er^{3+}$ crystal [Ref. 4] ($\lambda = 2.76$ μm). An investigation was made of the temperature dependence of the threshold of destruction in NaCl crystals, and destruction thresholds were also measured for a number of alkali halide and other crystals (KCl, KBr, KI, CsI, CsBr, LiF, NaF, RbCl, BaF_2) at room temperature.

2. Description of the facility and experimental method

A diagram of the experimental setup is shown in Fig. 1. The laser operated in the mode of isolated pulses on the fundamental TEM_{00} mode, and pulse duration at half-height was 85 ns. A small part of the laser beam was coupled out by a CaF_2 plate to monitor pulse energy. Beam attenuation was handled by using calibrated BS glass filters. The emission was focused inside the study specimens by using a CaF_2 lens with focal length $f = 24$, 31, 40 mm; the lenses were placed in the far zone of the laser beam. A method of "photoemulsion burn" similar to that described in Ref. 3 was used to determine the distribution of intensity in the focus of the lenses. The distribution of intensity in the cross section of the caustic was near Gaussian. The beam diameter in the minimum cross section of the caustic for

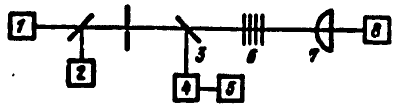

Fig. 1. Diagram of the experimental installation: 1--$CaF_2:Er^{3+}$ laser; 2--He-Ne laser; 3--CaF_2 plate; 4--calorimeter; 5--chart recorder; 6--BS glass attenuating filters; 7--CaF_2 lens for focusing emission inside the specimen; 8--specimen

the lens most frequently used with focal length of $f = 24$ mm on a level of 1/e of the maximum intensity was 20 μm, which is close to the diffraction limit (18.5 μm). The radiation was focused in the body of the specimens at a depth of a few millimetres. Destruction was determined visually by a spark and by scattering in the helium-neon laser beam. A new point of the specimen was tested each time, regardless of destruction.

Measurements of threshold intensities of destruction using lenses of different focal lengths gave close results, indicating the absence of influence of self-focusing of radiation. The accuracy of measurement of the threshold intensities of destruction was 10% for relative quantities, and 50% for the absolute values. The temperature dependence of the thresholds was studied in a range of 300-1000 K.

3. Experimental results and their discussion

In the investigation of laser destruction of different crystals, considerable variations in the threshold of destruction were observed from one specimen

to another. The results of distribution studies for a large number of NaCl crystals with respect to threshold of volumetric destruction at room temperature are shown in Fig. 2 in the form of a histogram. Given here for comparison are analogous results for the same NaCl crystals as found previously [Ref. 5] on $\lambda = 10.6$ and 1.06 μm. A comparison of the distributions shown in Fig. 2 shows that in the main, the same group of crystals has a maximum threshold both on $\lambda = 2.76$ μm and on $\lambda = 10.6$ μm, whereas on $\lambda = 1.06$ μm the thresholds of crystals of this group are not maximum. Besides, on $\lambda = 2.76$ μm the distribution has a single maximum, in contrast to the distributions for the two other wavelengths.

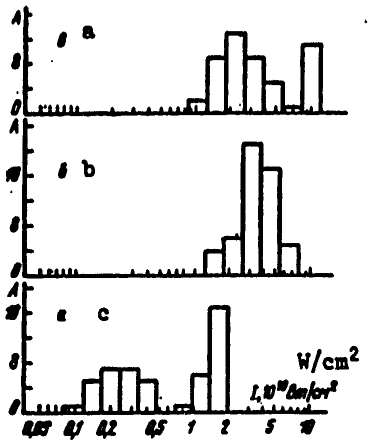

Fig. 2. Histograms of the distribution of thresholds of laser destruction of crystals of sodium chloride (A--number of specimens) at room temperature for $\lambda = 10.6$ (a, Ref. 5), 2.76 (b) and 1.06 μm (c, Ref. 5)

The observed variations of thresholds and the lack of correspondence of the histograms on different frequencies shows the considerable influence that impurities and defects have on the process of destruction, which differs on different frequencies. However, it can be expected that the natural mechanism of destruction, which does not necessarily occur in the same crystal on all frequencies, is realized only in crystals that have a maximum threshold of destruction on each of the frequencies. From this point of departure, in analyzing the frequency dependence we used the data found on crystals having maximum thresholds of destruction.

In addition to NaCl, other crystals were also studied in our research. The thresholds of volumetric destruction for the most stable of the specimens at our disposal are summarized in the Table. Since we did not have an adequate supply of such specimens, it remains unclear whether the measured thresholds are maximum on $\lambda = 2.76$ μm. A comparison of these thresholds with

Thresholds of laser destruction (in 10^{10} W/cm^2) of some crystals at room temperature

Кристалл Crystal	I, 10^{10} Вт/см^2 W/cm^2				
	λ=0.53 μm мкм, τ=8 нс ns	λ=0.69 μm мкм, τ=10 нс ns	λ=1.06 μm мкм, τ=10 нс ns	λ=2.76 μm мкм, τ=85 нс ns	λ=10.6 μm мкм, τ=60 нс ns
LiF	24	36	36	12	
NaF	9	14	14	5	
KCl	2.5	8	7	2	0.1
KBr	6	5.8	5	0.8	1.2
CsJ	0.9	1.3	1.5	0.4	0.05
KJ		1.0	2.2	0.2	
CsBr		0.4	2.7	0.6	
RbCl				0.3	
BaF_2				12	

Note: Destruction thresholds on λ = 0.53, 0.69, 1.06 and 10.6 μm are taken from Ref. 5.

the thresholds of destruction on λ = 1.06 μm indicates that they are apparently close to the limiting values, and therefore the given results, supplementing available experimental data on frequency dependence, may be of interest in elucidating the mechanism of destruction in the investigated crystals.

We did a detailed study of the temperature dependence of thresholds of laser destruction of NaCl crystals on λ = 2.76 μm. In this research, the values of the thresholds with rising and falling temperature were not reproduced on specimens with relatively low initial thresholds (at T = 300 K): the threshold of destruction increased with a change in temperature in the cycle 300 K → 1100 K → 300 K. An analogous hardening effect was observed previously for the same crystals on λ = 1.06 and 0.69 μm [Ref. 3], and was qualitatively attributed to the influence of impurities on the basis of a model of formation and degradation of impurity clusters during heat treatment. It was shown in Ref. 3 that the true temperature dependences of the thresholds of destruction typical of the natural mechanism of destruction can be obtained only on specimens that are not subject to the mentioned effect of hardening. Such a relation for one of the most stable NaCl specimens plotted on λ = 2.76 μm in a range of 300-900 K is shown in Fig. 3.

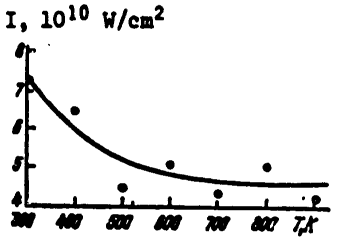

Fig. 3. Temperature dependence of the threshold of intensity of laser destruction of a sodium chloride crystal on a wavelength of 2.76 μm

Assuming that the observed dependence is inherent in a natural destruction mechanism such as impact ionization, let us compare this dependence and that predicted by electron avalanche theory [Ref. 1, 2]. According to the theory, a falling temperature dependence can be observed if the effective frequency of electron-photon collisions ν_{ef} is less than the frequency of laser emission [Ref. 1]. A quantitative comparison with the formula for the critical field in this case leads to $\nu_{ef} = 2 \cdot 10^{14}$ s^{-1}.

The frequency of electron-photon collisions can also be evaluated from the frequency dependence of the threshold of laser destruction. Using the data of Ref. 3 for measurements of the thresholds of destruction on $\lambda = 10.6$, 1.06 and 0.69 μm*, we find that the threshold measured by us on $\lambda = 2.76$ μm agrees well with electron avalanche theory if a value of $6 \cdot 10^{14}$ s^{-1} is taken for ν_{ef}. It is evident that this value differs appreciably (outside the range of experimental error) from that found from temperature dependence. This discrepancy is still unexplained. It can be assumed that the quantity $\nu_{ef} = 6 \cdot 10^{14}$ s^{-1} is apparently more preferable since it gives a good explanation of the frequency dependence of the threshold of destruction over a fairly wide range of emission wavelengths λ (from 10.6 to 0.69 μm).

Let us note that an analogous discrepancy in data for ν_{ef} obtained from the temperature and frequency dependences of the thresholds of destruction was observed previously in studies of laser destruction in alkali halide crystals on $\lambda = 10.6$, 1.06 and 0.69 μm in Ref. 3, where it was shown that the developed theory of avalanche ionization gives a good explanation of the temperature dependence for high-frequency radiation ($\lambda = 0.69$ and 1.06 μm), but does not explain the lack of dependence of the destruction threshold on temperature for low-frequency radiation ($\lambda = 10.6$ μm). Our results also indicate such a discrepancy. All this leads to the thought that in the low-frequency region the process of avalanche ionization differs from that in the high-frequency region. A final explanation of this problem requires further theoretical and experimental research.

REFERENCES

1. A. S. Yepifanov, A. A. Manenkov, A. M. Prokhorov, PIS'MA V ZHURNAL EKSPERIMENTAL'NOY I TEORETICHESKOY FIZIKI, Vol 21, 1975, p 483.

2. A. S. Yepifanov, A. A. Manenkov, A. M. Prokhorov, ZHURNAL EKSPERIMENTAL'NOY I TEORETICHESKOY FIZIKI, Vol 70, 1976, p 728.

*Although our measurements on $\lambda = 2.76$ μm were done at a pulse length of $\tau = 85$ ns, and in Ref. 3 on wavelengths of 0.53, 0.69 and 1.06 μm at a pulse length of about 10 ns, in comparing the results we assumed weak dependence of the thresholds of destruction on pulse length, which is typical of the avalanche breakdown mechanism [Ref. 1]. Actually, the experiments of Ref. 5 on a wavelength of $\lambda = 1.06$ μm in the range of pulse durations τ from 1.5 to 15 ns showed practical independence of the threshold of laser destruction on the durztion of the damaging pulse.

3. B. G. Gorshkov, Yu. K. Dalineyko, A. S. Yepifanov, V. A. Lobachev, A. A. Manenkov, A. V. Sidorin, ZHURNAL EKSPERIMENTAL'NOY I TEORETICHESKOY FIZIKI, Vol 72, 1977, p 1171.

4. G. V. Gomelauri, L. A. Kulevskiy, V. V. Osiko, A. D. Savel'yev, V. V. Smirnov, KVANTOVAYA ELEKTRONIKA, Vol 3, 1976, p 628.

5. B. G. Gorshkov, Candidate's Dissertation, Lebedev Physics Institute, Moscow, 1977.

6610
CSO: 1870

PHYSICS

UDC 621.373.826.038.823

CHARACTERISTICS OF RADIATION EMITTED BY A PERIODICALLY PULSED CO_2 LASER USING AN AIR-CO_2 MIXTURE

Moscow KVANTOVAYA ELEKTRONIKA in Russian Vol 6, No 1, Jan 79 pp 49-56

[Article by S. V. Drobyazko and L. G. Zhuravskiy]

[Text] It is experimentally demonstrated that laser pulse duration can be regulated over a wide range (0.1-80 μs) by changing the composition of the mixture and the Q of the cavity of a periodically pulsed CO_2 laser on an air-CO_2 mixture with average power of 500 W. A semi-empirical model is proposed for calculating the parameters of the lasing pulse that enables optimization of the cavity and analysis of energy losses for different mixture compositions based on measuring the output characteristics of emission for a known cavity and known dimensions of the active medium. The theoretical results agree well with the experiment.

Periodically pulsed CO_2 lasers (PPL's) with average power of the order of 1 MW are needed for solving a number of scientific and technical problems. For some applications (location, isotope separation, initiation of chemical reactions) short (0.01-1 μs) powerful laser pulses are required, while in other applications (cutting, welding, drilling, tempering) the pulse duration must lie in a range of 0.01-1 ms to prevent optical breakdown of the medium in front of the target.

The emission pulse of a high-pressure CO_2 laser with transverse excitation consists of a short powerful spike and a long low-power component [Ref. 1] that as a rule contains an appreciable part of the total pulse energy. The energy in the spike is determined chiefly by the degree of excitation of the ν_3 mode of CO_2 by the instant of onset of lasing, while the energy in the long component is determined by the degree of excitation of vibrational levels of nitrogen. In the very earliest research on pulsed CO_2 lasers with transverse excitation [Ref. 2-4] it was noticed that the emission pulse shape is influenced by the composition of the mixture, but not until Ref. 5, and later on in Ref. 6 and 7 was a systematic study done on the

influence that the composition of the mixture and the Q of the cavity have on the characteristics of laser emission. The research was done on mixtures containing from 60 to 90% He.

In connection with the feasibility of developing open-cycle and closed-cycle PPL's on helium-free mixtures, and in particular using an air-CO_2 mixture, an urgent problem is the study of the characteristics of laser radiation for these mixtures. Ref. 8 describes a PPL on an air-CO_2 mixture with open gas cycle and average power of 500 W. Here we give the emission characteristics of this laser for different compositions of the working mixture and Q's of the cavity. A semi-empirical model is proposed for calculating the parameters of the emission pulse; this model can be used to optimize the cavity and to analyze energy losses for different compositions of the working mixture.

The experiments were done on the facility described in Ref. 8. The circuit diagram and cathode design are shown in Fig. 1. In all experiments

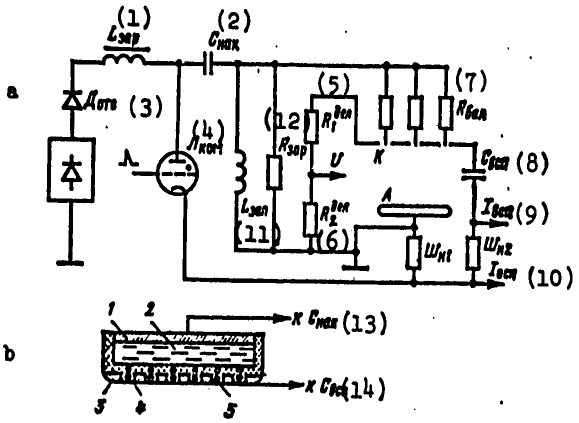

Fig. 1. Electric circuit of the setup of Ref. 8 (a), and cathode design (b): 1--common contact of ballast resistance; 2--ballast resistance (electrolyte); 3--copper plate (base electrode; 4--insulator; 5--cathode pins; $Ш_{1,2}$--shunts

KEY:
1--L_{ch}
2--C_{res}
3--D_{ref}
4--V_{com}
5--R_1^{div}
6--R_2^{div}
7--R_{bal}
8--C_{aux}
9--I_{aux}
10--I_{base}
11--L_{bl}
12--R_{ch}
13--to C_{res}
14--to C_{aux}

C_{res} = 0.1 μF, C_{aux} = 0.05 μF, R_{bal} = 500 Ω, and the voltage across the reservoir capacitor was varied from 22 to 36 kV. The cathode device (Fig. 1b) consisted

of a base electrode -- a copper plate 5 mm thick with apertures 3 mm in diameter (spaced 5 mm apart) -- cooled by water around the perimeter, and auxiliary electrodes made in the form of pins 1 mm in diameter coaxial with the apertures in the plate and insulated from the plate, so that at one end the pins are flush with the plate and face the anode, while the other ends of the pins are connected through ballast resistances to a common bus. This electrode system produced a stable glow discharge for any ratios of the components of the air-CO_2 mixture at pressures of up to 150 mm Hg and energy inputs up to 300 J/(l·atm).

The technique for measuring electrical, gasdynamic and optical parameters is described in Ref. 8. The pressure of water vapor and ionizable additives was determined from the dew point by a vacuum hygrometer. Typical oscillograms of current I, discharge voltage U and emission power W are shown in Fig. 2. The characteristic E/p for the given mixture was determined at the point dI/dt = 0. The total energy Q introduced into the plasma was determined by graphic calculation of the integral $Q = \int IUdt$, where U is the voltage drop across the plasma, I is the current through the discharge gap and t is time. The delay of the laser pulse $\tau_з$ was determined with respect to the start of the current pulse (Fig. 2b), whose duration in our experiments did not vary with a change in the composition of the working mixture. The total duration of the laser pulse τ was determined from its base, while the duration of the spike τ_n was determined at half-height. In all experiments the laser radiation receiver operated in the linear region, making it possible to determine the energy and power in the spike and long component of the laser pulse if the total energy and shape of the emission pulse are known.

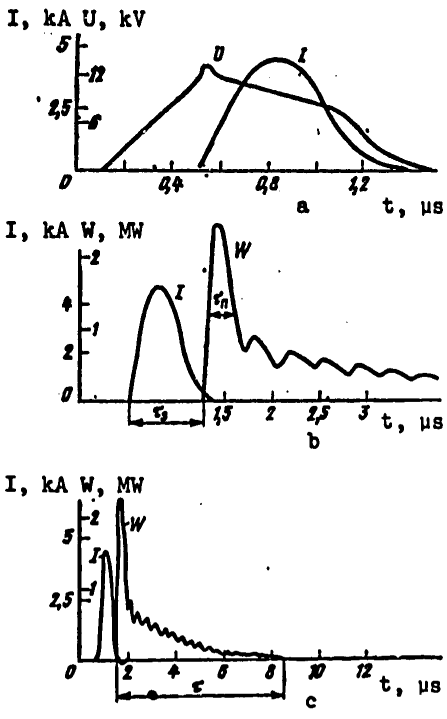

Fig. 2. Typical oscillograms of current I, voltage U and power W of laser emission: U_{res} = 30 kV, p = 114 mm Hg, mixture CO_2:air=1:2.

Shown in Fig. 3 are cruves for E/p, Q and electro-optical efficiency $\eta = \mathcal{E}/Q$ ($\mathcal{E}$ is the energy of the laser pulse for reflectivity R = 85% on the output mirror) as functions of the

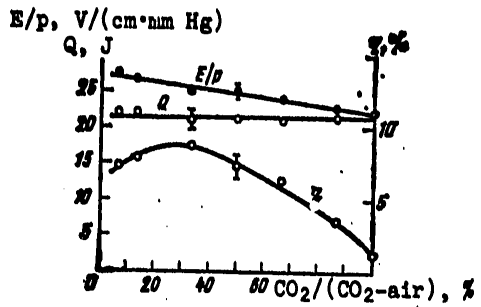

Fig. 3. Curves for E/p, energy input Q and electro-optic efficiency η as functions of the percentage of CO_2 in the mixture

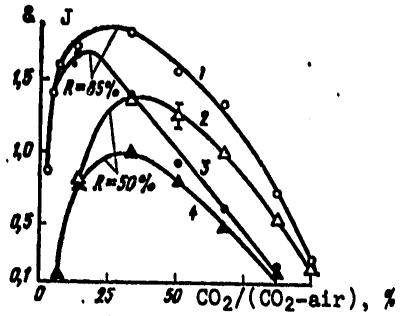

Fig. 4. Curves for the total energy of the radiation pulse (1, 2) and the energy in its long component (3, 4) as functions of the percentage of CO_2 in the mixture for output mirrors with R = 50% (2, 4) and R = 85% (1, 3)

composition of the mixture. It can be seen that with a change in the percentage of CO_2 in the mixture from 2.7 to 100% the E/p decreased from 27 to 22 V/(cm·mm Hg), while Q remained practically constant, since there is an increase in the current amplitude with a reduction in E/p. At the same time, η changes by nearly an order of magnitude, and has a flat maximum in the region of 20-40%. Fig. 4 shows the curves for the total energy of a radiation pulse and the energy contained in the long component for output mirrors with R = 50 and 85% as functions of the composition of the mixture. The total energy of the laser radiation and its distribution in the pulse, as we can see, depend considerably on the composition of the mixture and the Q of the cavity.

For analysis of energy losses in a PPL on a CO_2-air mixture, and also for optimizing the cavity and the dimensions of the optical active medium, the computational model of Ref. 9 was used to describe stimulated emission. It was assumed that vibrational intramode exchange is rapid enough that for each vibrational mode of CO_2 and N_2 we can introduce a specific temperature. Taken as the reference origin was the instant when the gain was equal to zero, i. e. it was assumed that discharge does not lead to population inversion of laser levels, which arises as a result of emptying of the lower laser level, so that there is an instant when the gain is equal to zero. Such an assumption is valid since the experimentally measured times of delay between the start of the current pulse and the emission pulse (see below) are greater than the total duration of the current pulse and the lasing "rise time," which for our conditions was about 0.1 μs. In this connection, we can examine the evolution of the populations of vibrational levels in time under certain initial conditions rather than describing the process of their excitation.

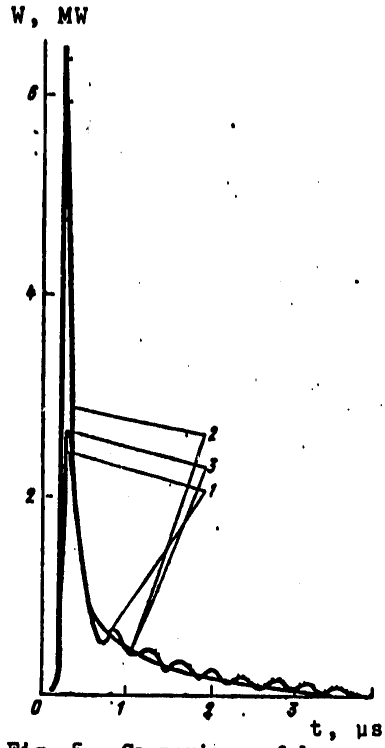

Fig. 5. Comparison of laser pulses found experimentally (1) and in calculation with an infinite (2) and a finite (3) rate of rotational exchange

At time zero it was assumed that the temperatures of symmetric and deformation modes of CO_2 were equal; however, in the lasing process consideration was taken of the difference in these temperatures caused by the heavy flux of quanta to level 100 of the symmetric mode of CO_2. Zero gain implies equality of the populations of the upper and lower laser levels. The initial gas temperature was taken as equal to the wall temperature, and the initial intensity was taken as equal to that of spontaneous emission. To solve the system of equations it is necessary to determine the initial populations of the vibrational levels of nitrogen and the antisymmetric mode of CO_2. Lack of information on the electron distribution function for the air-CO_2 mixture precludes determination of the initial populations of vibrational levels from the current-voltage curve of the discharge. Therefore the initial populations of nitrogen levels and the antisymmetric mode of CO_2 were determined by comparing a reference emission pulse with the experimentally measured pulse for given values of the dimensions of the active zone, the Q and the degree of filling of the cavity. An important point in this connection is coincidence not only of the total energy, but also the fraction of energy in the spike and the long component of the pulse, since the former is determined chiefly by the vibrational temperature of the antisymmetric mode of CO_2, while the latter is determined by the vibrational temperature of nitrogen. It was found that the equilibrium distribution by rotational levels during lasing does not settle down instantaneously, and accounting for the rate of rotational exchange is essential for proper calculation of pulse shape.

Fig. 5 shows an experimentally measured emission pulse, and pulses calculated with and without consideration of the finite rate of rotational exchange [Ref. 10]. It can be seen that accounting for the finite rate of rotational exchange leads to broadening of the spike and eliminates the disagreement between the calculated and experimentally measured emission pulse shapes that was noted in Ref. 9, 11.

In accordance with what we have said, the vibrational temperatures of nitrogen and the antisymmetric mode of CO_2 were chosen from conditions of coincidence of the calculated and experimentally measured total energy of the pulse and

the energy of the spike for a cavity with output mirror having R = 50%, length of the active medium 64 cm and distance between mirrors 120 cm. To check the correctness of the method of calculation and the selected initial conditions, the parameters of the lasing pulse were calculated for an output mirror with R = 85% under the same conditions of excitation of the active medium.

The results of the comparison of experiment with theory for p = 114 mm Hg and U_{res} = 30 kV are summarized in Table 1.

TABLE 1

$\{CO_2\}$, %	$\mathcal{E}_\Sigma$, J[1] R=50% эксп. [3]	$\mathcal{E}_\Sigma$, J[1] R=50% расч. [4]	$\mathcal{E}_\Sigma$, J[1] R=85% эксп. [3]	$\mathcal{E}_\Sigma$, J[1] R=85% расч. [4]	$\mathcal{E}_\pi$, J[1] R=50% эксп. [3]	$\mathcal{E}_\pi$, J[1] R=50% расч. [4]	$\mathcal{E}_\pi$, J[1] R=85% эксп. [3]	$\mathcal{E}_\pi$, J[1] R=85% расч. [4]	τ, μs[2] R=50% эксп. [3]	τ, μs[2] R=50% расч. [4]	τ, μs[2] R=85% эксп. [3]	τ, μs[2] R=85% расч. [4]	τ_π, μs[2] R=50% эксп. [3]	τ_π, μs[2] R=50% расч. [4]	τ_π, μs[2] R=85% эксп. [3]	τ_π, μs[2] R=85% расч. [4]	Z_{30}	Z_{40}
6.7	0.16	0.16	1.0	1.5	0.013	0.02	0.08	0.1	15	12.5	30	40	0.5	0.5	0.2	0.25	0.04	0.09
13.3	0.8	0.69	1.73	1.64	0.2	0.2	0.156	0.17	15	19	20	27.3	0.2	0.2	0.3	0.33	0.04	0.09
33.4	1.37	1.26	1.83	1.89	0.36	0.28	0.44	0.39	5.25	10	7.25	10	0.1	0.12	0.28	0.20	0.03	0.12
50	1.27	1.18	1.56	1.86	0.48	0.38	0.64	0.66	3.5	7	5	8	0.1	0.16	0.3	0.29	0.1	0.18
66.7	1	0.93	1.33	1.45	0.52	0.39	0.71	0.7	2.5	3	3.5	3	0.08	0.14	0.3	0.28	0.09	0.2
83.7	0.53	0.49	0.75	0.82	0.37	0.32	0.52	0.533	0.75	1	3	3	0.125	0.14	0.22	0.22	0.07	0.23
100	0.2	0.19	0.27	0.28	0.16	0.15	0.28	0.22	0.3	0.4	0.75	0.8	0.14	0.14	0.28	0.28	0.06	—

Note: $\{CO_2\} = CO_2/(CO_2 + air)$, $\mathcal{E}_\Sigma$ is the total energy of the laser pulse, $\mathcal{E}_\pi$ is the energy in the spike, τ is the total duration of the lasing pulse, τ_π is the duration of the spike at half-height, $Z_{30} = \exp(-\theta_3/T_3)$, where θ_3 is the characteristic energy of vibrational mode ν_3 of CO_2, equal to 3880 K, T_3 is the vibrational temperature of mode ν_3 of CO_2, Z_{40} is the analogous quantity for the vibrational mode of nitrogen.

KEY: 1--joules 3--experimental
2--μs 4--calculated

The selected values of initial populations Z_{30} and Z_{40} ensure that the theoretical and experimental values of $\mathcal{E}_\Sigma$ and $\mathcal{E}_\pi$ coincide within 15% for output mirrors with R = 50 and 85% for all mixtures when the experimental error of determination of $\mathcal{E}_\Sigma$ is of the order of 10%.

Using the values of Z_{30} and Z_{40} from Table 1, and setting $Z_{10} = Z_{30}$, $Z_{10} = Z_{20}^2$ at time zero, we can determine the energies contained in each vibrational mode and analyze the losses of energy invested in the discharge. The results of such an analysis are summarized in Table 2. The quantity Q_{CO_2} in Table 2 was determined from the reduction in the concentration of CO_2 after discharge in additional experiments on a hermetically sealed chamber while preserving the conditions of the foregoing experiment. It was assumed that dissociation of CO_2 takes place as a result of collisions with an electron, and an energy of 7 eV must be expended on each act of dissociation. The rate constant of dissociation of O_2 for our values of E/p according to Ref. 12 is 3-5 times as high as for CO_2. Utilizing this fact, as well as

TABLE 2

$[CO_2]$, %	χ_{z_0}	z_0	(1) Q_1, Дж	(1) Q_2, Дж	(1) Q_3, Дж	(1) Q_4, Дж	(2) $Q_{вых}$, Дж	(1) Q_{O_2}, Дж	(1) Q_{CO_2}, Дж	(1) Q_X, Дж	(3) $(Q_{вых}+Q_X)$, Дж	(4) $Q_{эксп}$, Дж	(1) (Q_3+Q_4), Дж	(5) $\eta_{раз}$, %	(6) $\eta_{раз}$, % $R=50\%$	(6) $\eta_{раз}$, % $R=85\%$	τ_3, мкс (7) $R=50\%$	τ_3, мкс (7) $R=85\%$
6.7	0.04	0.09	0.14	0.51	0.25	10.5	11.4	7.7	0.5	8.2	19.6	22	10.75	54.8	3.63	36.3	4.4	1.5
13.3	0.02	0.09	0.28	1.02	0.5	9.73	11.53	5.74	0.6	6.54	18.07	22	10.23	56.6	19.1	41.2	1.4	1.05
25.4	0.08	0.12	0.61	2.6	1.48	10.4	15.52	2.82	1.44	3.98	19.5	21.1	11.87	60.9	28.2	37.3	0.9	0.73
50	0.1	0.18	1.96	5.35	3.44	12.42	23.18	1.4	1.8	3.2	26.37	21.2	15.86	60.1	19.5	24	0.7	0.7
85.7	0.09	0.2	2.44	6.88	4.29	9.57	23.18	0.66	2	2.66	25.81	21	13.86	53.6	17.6	23.4	0.65	0.58
93.7	0.07	0.23	2.7	8.22	4.76	4.52	20.2	0.23	2.3	2.53	22.73	21.5	9.28	40.8	13.9	19.7	0.8	0.6
100	0.06	—	3.06	9.7	5.27	—	18.23	—	2.75	2.75	20.78	22	8.27	25.4	9.25	12.4	1.1	0.8
100	—	—	—	—	5.8	—	16.6	—	4.4	4.4	20.9	—	—	—	—	—	—	—

Note: Q_1-Q_4 are the energies expended respectively in modes ν_1-ν_3 of CO_2 and vibrations of nitrogen, $Q_{vib} = \sum_{i=1}^{4} Q_i$, Q_{O_2} and Q_{CO_2} are the energies expended on dissociation of O_2 and CO_2, $Q_X = Q_{CO_2} + Q_{O_2}$, $\eta_{dis} \equiv (Q_3 + Q_4)/(Q_{vib} + Q_X)$, $\eta_{cav} = \mathcal{E}_{\Sigma exp}/[^{0,41}(Q_3 + Q_4)]$ is the fraction of the emitted energy out of the maximum possible; the values in the last row are taken from Ref. 13.

KEY: 1--joules
2--Q_{vib}, J
3--$(Q_{vib} + Q_X)$, J
4--Q_{exp}, J
5--η_{dis}, %
6--η_{cav}, %
7--τ_3, μs

the rate constant for dissociation of CO_2 as determined for our discharge for different mixtures, we calculated the quantity Q_{CO_2}.

It can be seen that the energy going to chemical reactions fluctuates from 11 to 42% depending on the composition of the mixture, and depends strongly on the oxygen concentration in the mixture. Therefore the presence of oxygen in the working mixture is undesirable.

The experimentally measured energy input to the discharge and the calculated value of $Q_{vib} + Q_X$ coincide with an accuracy of up to 25%, which is quite satisfactory when one considers that the experimental error in measurement of Q is about 10%, and the choice of initial conditions ensured agreement with experimental results with accuracy of the order of 15%.

Let us note that for a low CO_2 content in the mixture (6.7 and 13.3%) there is time for an appreciable part of the energy stored in the deformation mode of CO_2 to be converted to heat before lasing starts (for these mixtures $\tau_3 = 4.4$ and 1.4 μs respectively). The initial gas temperature for these mixtures was taken as 380 and 360 K respectively.

For pure CO_2 the energy balance was compared with the results of calculation in Ref. 13. As can be seen from Table 2, the discrepancy does not exceed 10%. When the percentage of CO_2 in the mixture is less than 70%, discharge efficiency varies little with the composition of the mixture, and reaches 60%, which is only 20% lower than for mixtures with a high He content [Ref. 14].

The fraction of the emitted energy out of the maximum possible (η_{cav}) was less than 42% in all experiments. An appreciable part of the energy at the instant of cessation of lasing, as implied by the calculations, remains stored in vibrations of nitrogen and the antisymmetric mode of CO_2, which can be attributed to a growth in population of the lower laser level as a result of gas heating. As shown by the results of calculations presented in Table 3, reducing the initial gas temperature enables us to raise η_{cav} by a factor of 1.5 (the calculation was done for a mixture of CO_2:air = 2:13,

TABLE 3

T, K	$\mathcal{E}_\Sigma$, Дж (1)	τ, мкс (2)	$\eta_{рез}$, % (3)
380	1,64	27,3	39
295	2,11	30,4	50,3
200	2,40	29,6	57,2

KEY: 1--joules
2--μs
3--η_{cav}, %

pressure p = 114 mm Hg and values of U_{res} = 30 kV, R = 85%, Z_{30} = 0.04, Z_{40} = 0.09). A maximum pulse duration of 80 μs is realized experimentally with 2.7% CO_2 in the mixture. In this case $\mathcal{E}_\Sigma$ = 0.83 J. To increase the pulse duration further it is necessary to reduce the percentage of CO_2 in the mixture. As implied by calculations, at a CO_2 fraction in the mixture of 1.7%, τ = 150 μs, and when the fraction is 1%, τ = 250 μs. In doing this, to maintain the laser efficiency on a constant level it is necessary to increase the length of the active medium and to raise the Q of the cavity.

The dependence of pulse parameters on the Q of the resonator for a mixture with pressure of 114 mm Hg and $\{CO_2\}$ = 13.3% is shown in Table 4 (U_{res} = 30 kV). The absence of a drop in $\mathcal{E}_\Sigma$ at R ≥ 0.9 that was observed in Ref. 6 can be attributed to the fact that the coefficient of reflection of the opaque mirror in our experiments was taken as 100%.

Thus we have experimentally demonstrated the feasibility of regulating the duration of a pulse emitted by a CO_2 laser on air-CO_2 mixtures over a wide range (from 0.1 to 80 μs) by using the composition of the mixture and the Q of the cavity.

TABLE 4

R, %	γ_g, дБ/м (1)	$\gamma_в$, дБ/м (1)	$\tau_в$, мкс (2)	$\tau_г$, мкс (2)	$\tau_в$, мкс (2)
40	0,36	0,06	0,2	15,6	2
50	0,69	0,09	0,2	19	1,4
60	0,92	0,11	0,2	22	1
70	1,17	0,13	0,25	24,2	0,7
80	1,49	0,17	0,3	26,3	0,6
85	1,64	0,17	0,35	27,3	0,5
90	1,76	0,24	0,35	28,2	0,5
95	1,87	0,28	0,8	29,2	0,4

KEY: 1--joules
2--μs

The dependence of laser emission energy on the voltage across the reservoir capacitor for different compositions of the working mixture is shown in Table 5. An identical content of CO_2 and N_2 was maintained in all mixtures,

TABLE 5

$U_{рез}$, кВ (1)	(2) Энергия излучения в импульсе, Дж		
	$CO_2:N_2:O_2:H_2O$ = 38:60:16:0,8, мм рт. ст. (3)	$CO_2:N_2:H_2$ = 38:60:4, мм рт. ст. (3)	$CO_2:N_2:He$ = 38:60:102, мм рт. ст. (3)
20	—	0,5	0,6
23	1	1,7	1,3
25	1,4	2,1	1,8
28	2	2,8	2,8
30	2,4	3,3	3,6
32	2,8	3,8	4,2

KEY: 1--U_{res}, kV
2--Emission energy in pulse, J
3--mm Hg

and the amount of H_2O, H_2 and He ensured an identical rate of emptying of the lower laser level. The difference in energy inputs for different mixtures did not exceed 10%.

The proposed computational model with semi-empirical determination of initial conditions enables calculation of the initial populations of levels and emission pulse shape for any mixture compositions, cavity Q and dimensions of the active medium. Accounting for the finite rate of rotational exchange brought the calculated length of the spike into agreement with that measured experimentally. Analysis of the energy balance showed that with a working mixture of air-CO_2 an appreciable fraction of energy is expended on dissociation of O_2, and therefore there is a better outlook for helium-free

mixtures such as CO_2-N_2-H_2 and CO_2-N_2-H_2O. The efficiency of discharge utilization in a CO_2-air laser is fairly high (up to 60%). To achieve a further improvement of laser efficiency it is necessary to increase the η_{cav}, optimizing the Q of the cavity for each size of the active medium, a . increasing the rate of emptying of the lower laser level through a reduction in the initial gas temperature.

In conclusion the authors consider it their pleasant duty to thank Professor A. A. Vedenov for formulating the problem and interest in the work, and V. M. Knizhnikov for constructive criticism and assistance with the calculations.

REFERENCES

1. J. Gilbert, J. L. Lachambre, F. Rheault, R. Fortin, CANAD. J. PHYS., Vol 50, 1972, p 2523.

2. J. A. Beaulieu, PROC. IEEE, Vol 59, 1971, p 667.

3. P. R. Pearson, H. M. Lamberton, IEEE J., QE-8, 1972, p 145.

4. Y. L. Pan, A. F. Bernardt, J. R. Simpson, REV. SCI. INSTR., Vol 43, 1972, p 662.

5. A. Girard, A. J. Beaulieu, IEEE J., QE-10, 1974, p 521.

6. K. J. Andrews, P. E. Dyer, D. J. James, J. PHYS. E., Vol 8, 1975, p 493.

7. D. C. Hamilton, D. J. James, S. A. Ramsden, J. PHYS. E., Vol 8, 1975, p 849.

8. A. A. Vedenov, S. V. Drobyazko, A. A. Yegorov, L. G. Zhuravskiy, V. B. Turundayevskiy, KVANTOVAYA ELEKTRONIKA, Vol 3, 1976, p 2480.

9. V. Yu. Baranov, V. M. Borisov, A. P. Napartovich, Ye. Sh. Napartovich, Yu. A. Satov, Preprint, Institute of Atomic Energy, Moscow, 1974, No 2398.

10. V. K. Garside, J. Raid, Ye. A. Ballik, IEEE J., QE-11, 1975, p 583.

11. K. R. Manes, H. J. Sequin, J. APPL. PHYS., Vol 43, 1972, p 5073.

12. D. I. Slovetskiy, Doctoral dissertation, Institute of Petrochemical Synthesis imeni A. V. Topchiyev, Academy of Sciences USSR, Moscow.

13. L. Nighan, PHYS. REV. A., Vol 2, 1970, p 1989.

14. J. J. Lowke, A. V. Phelps, B. W. Irwin, J. APPL. PHYS., Vol 44, 1973, p 4664.

PHYSICS

UDC 681.787

LIMITING RESOLUTION OF A POLARIZATION INTERFEROMETER AND MEASUREMENT OF THE RADIUS OF CURVATURE OF THE PHASE FRONT OF LASER BEAMS

Moscow KVANTOVAYA ELEKTRONIKA in Russian Vol 6, No 1, Jan 79 pp 57-62

[Article by V. B. Pakhalov, A. S. Chirkin and F. M. Yusubov, Moscow State University imeni M. V. Lomonosov]

[Text] A theoretical and experimental study is done on the problem of the limiting resolution of a polarization interferometer in measurement of the correlation radius. It is shown that the limiting resolution of the polarization interferometer is determined by the effect of diffraction and in the realized experiment is of the order of 10 μm. In addition, it is demonstrated that a polarization interferometer can be used to measure the radius of curvature of the phase front of light beams.

Introduction

Recently a polarization interferometer proposed by Arutyunyan, Tunkin and one of the authors [Ref. 1] has been used to do a number of experiments in studying the spatial coherence of laser emission and scattered light radiation. In particular, measurements have been made of the space correlation function (SCF) of the field and the intensity of multimode laser emission [Ref. 2] and its second harmonic [Ref. 3]. A study has been done on the formation of spatially coherent light beams in a laser [Ref. 4, 5] and the limiting spatial coherence of laser emission has been measured [Ref. 6, 7]. The enumerated range of possibilities of the PI in combination with the photocount method of registering optical radiation is due to its capacity for measuring small radii of correlation and SCF with high accuracy. Errors of measurement of the degree of coherence with the PI are considered in Ref. 6.

This research is devoted primarily to elucidation of the problem of the limiting resolution of the PI in measurement of the correlation radius. Theoretical and experimental studies have shown that the phenomenon of

diffraction plays a major role in limiting the measurable correlation radius. In addition, a study is done on a new possibility for using the PI -- for measuring the radius of curvature of the phase front of light beams. The measurements of the latter reduce to measurement of the phase difference of two photons, and can be done electronically [Ref. 8] or by an interference method [Ref. 9, 10], including with a Young interferometer [Ref. 10].

1. Working principle of the polarized interferometer

The main element of the PI (Fig. 1) is a plane-parallel plate cut from a birefringent crystal parallel to the optical axis. This plate is placed in an immersion liquid with index of refraction n_i, equal for instance to the index of refraction n_e for the extraordinary wave in the plate. The plate can be rotated about the optical axis oriented perpendicular to the incident beam and making an angle of 45° with its polarization. Thus the initial beam in the plate is divided into two beams with ordinary ("o") and extraordinary ("e") polarizations.

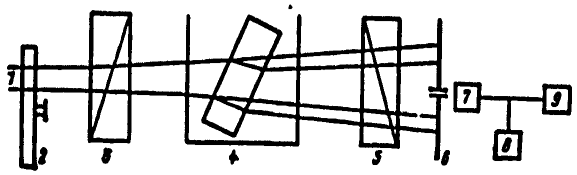

Fig. 1. Diagram of the experimental setup: 1--laser beam; 2--rotatable matte disk; 3--polarizer; 4--cell with rotatable plane-parallel plate; 5--analyzer; 6--diagram; 7--photon counting device; 8--chart recorder; 9--digital printer

At the output of the PI the analytical signal of field strength is

$$V(r, t)=V_o(r, t)+V_e(r-s, t-\tau_3). \quad (1)$$

Here s is transverse displacement of the beams relative to one another; τ_3 is the delay time between beams. In this connection

$$s=d\frac{\Delta n}{n_o}\varphi; \quad \tau_3 c=d\Delta n+\frac{d}{2}\frac{n_e}{n_o}\Delta n\varphi^2, \quad (2)$$

where $\Delta n=n_o-n_e$; d is the thickness of the plate; ϕ is the angle of incidence of the beam on the plate; c is the speed of light.

In the region of overlap of the beams, depending on the path difference there is a transition from linear to elliptical polarization. When beams pass through the analyzer in the XY plane perpendicular to the direction of propagation Z, the distribution of average intensity $I=\langle VV^*\rangle$ is given by the expression

$$I=I_o(x, y)+I_e(x, y)+2\mathrm{Re}\langle V_o^* V_e\rangle. \quad (3)$$

where the angle brackets denote statistical averaging; $V_{o,e} = |V|_{o,e} \cos \psi_{o,e}$; $\psi_{o,e}$ is the angle between the direction of polarization of the analyzer and the corresponding beam.

Let the analytical signal of the initial beam, and hence the interfering beams be representable as

$$V_{вх}(\rho, t, z=0) = A(\rho)e^{i\omega t} = A_{рег}(\rho)A_{сл}(\rho)e^{i\omega t}, \qquad (4)$$

where the functions $A_{рег}(\rho)$ and $A_{сл}(\rho)$ describe the regular and random modulation of the beam in plane XY, where

$$A_{рег}(\rho) = A(0)\exp[-\rho^2(1/2a^2 + ik/2R)] \qquad (5)$$

and the SCF of the random field is

$$\langle A_{сл}(\rho_2)A^*_{сл}(\rho_1)\rangle = \gamma(\rho_1 - \rho_2 = s) = \exp[-(\rho_2 - \rho_1)^2/r_0^2 - i\beta(\rho_2^2 - \rho_1^2)],$$

where a, R and r_0 are the beam radius, the radius of curvature of the phase front and the correlation radius respectively, the parameter $\beta > 0$ accounts for the phase of the SCF. With consideration of (4), (5), the term $\mathrm{Re}\langle V_o^* V_e\rangle$ that appears in (3) takes the form

$$\mathrm{Re}\langle V_o^*(\rho, z, t)V_e(\rho+s, z, t-\tau)\rangle = A_o A_e |\gamma(s)| \exp[-[\rho^2 + (\rho+s)^2]/2a^2]\cos\Phi.$$

Disregarding the slight difference in the radii of curvature of beams with ordinary and extraordinary polarization as compared with R ($\Delta R/R \ll 1$) we have for phase Φ

$$\Phi = (\beta + k/2R)(s^2 - 2\rho s) + \Delta z,$$

where $\Delta z = \tau_{зс}$ is the difference in the lengths of the optical paths.

As usual, knowledge of the extremum values of intensity I (3) that correspond to $\cos\Phi = \pm 1$ enables us to determine the degree of coherence from the visibility v of the interference pattern

$$v = \frac{I_{max} - I_{min}}{I_{max} + I_{min}} = \frac{2\sqrt{I_o I_e}}{I_o + I_e}|\gamma(s)|, \qquad (6)$$

where $I_{o,e} = |V_{o,e}|^2$.

Let us determine the distance between the interference extrema with change in ρ and s. These coordinates can be conventionally assigned to the planes of measurement of the radius of curvature and the correlation radius respectively.

Limiting ourselves for the sake of simplicity to consideration of displacement along the X axis, we have the following equation for the positions of the maxima I_{max} in the case of beams with phase $\beta = 0$:

$$-\frac{\rho s}{R} + \frac{s^2}{2R} + \frac{n_o n_e}{2d\Delta n}s^2 = \lambda m,$$

where (2) is taken into consideration, m = 0, 1, 2... is interference order.

If displacement s is fixed, the distance between interference maxima in the plane of measurement of the radius of curvature is

$$\Delta\rho = \lambda R/s \qquad (7)$$

and does not depend on the order of interference. Let us estimate the order of magnitude of $\Delta\rho$. Assuming λ 0.5 μm, s≈100 μm, R≈1-10 m, we get $\Delta\rho$≈5-50 mm. Since the typical value of Laser beam diameter is about 1 cm, only a single interference maximum or minimum alternating with a change in s (rotation of the plane-parallel plate) will be observed in the region of beam overlap in the given example.

In the plane of measurement of the correlation radius (i. e. when $\rho = 0$, which corresponds to the conditions of experiments [Ref. 1-7]) the difference between interference maxima when $\Delta z \neq 0$ is

$$\Delta s_m = s_{m+1} - s_m = \sqrt{\lambda \frac{2d\Delta n}{n_e n_o}} \left(\sqrt{m+1} - \sqrt{m}\right). \qquad (8)$$

If the time delay is totally compensated ($\Delta z = 0$) by synchronous rotation of a special second plate [Ref. 1], then

$$\Delta s_m = \left(\sqrt{m+1} - \sqrt{m}\right)\left(\frac{2R\lambda}{1+2\beta R/k}\right)^{1/2}. \qquad (9)$$

In the experiments the plate of the PI was cut from a uniaxial calcite crystal ($n_o = 1.66$, $n_e = 1.49$, $\Delta n = 0.17$) and placed in castor oil with index of refraction coinciding with that for the extraordinary wave.

For our PI (see below) in case (8), $\Delta s_o = 41.6$ μm, which agrees with the experiment; in case (9) with a compensating plate $\Delta s_o = 1.6$ mm, and the alternation of maxima and minima will be very sharp. Therefore in measurements without total compensation, time shift acts as a phasing element and enables measurement of small correlation radii down to 15-20 μm.

2. Theory of resolving capacity of the PI

In the preceding discussion we examined the principle of using the PI to measure the SCF. In doing this, we disregarded diffraction effects on the path of light beam propagation from the source of emission to the recording device. Let us show that diffraction limits the minimum measurable correlation radius.

In the quasi-optical approximation, diffraction effects are described by the parabolic equation

$$\left(\frac{\partial}{\partial z} + \frac{i}{2k(z)}\Delta_\perp(x,y)\right) A(x,y) = 0. \qquad (10)$$

The relation $k(z) = (2\pi/\lambda)n(z)$ accounts for optical inhomogeneity of the path of propagation ($\Delta_\perp$ is the transverse Laplacian). Equation (10) with the appropriate substitution of wave number k is applicable to PI waves with ordinary and extraordinary polarizations.

The solution of equation (10) takes the form

$$A_{o,e}(\rho, z) = \iint_{-\infty}^{\infty} A_{o,e}(\xi, \eta, z=0)\, G_{o,e}(\rho, \xi, \eta, z)\, d\xi d\eta, \qquad (11)$$

where $G_{o,e}$ is the Green's function ($k = 2\pi/\lambda$)

$$G_{o,e}(\rho, \xi, \eta, z) = \frac{ik}{2\pi L_{o,e}} \exp\left\{-\frac{ik}{2L_{o,e}}(x - s_{o,e} - \xi)^2 - \frac{ik}{2L_{o,e}}(y-\eta)^2\right\}.$$

For the extraordinary wave $s_e = 0$, and

$$L = L_e = L_1 + (n_e - 1)d + (n_i - 1)(l - d),$$

where L_1 is the distance from the source to the photomultiplier, l is the size of the cell with immersion liquid.

For the ordinary wave $s_o = s$ (displacement of the beam takes place only along the X axis). Under the conditions of the experiment, disregarding the difference in optical paths we can assume $L_o = L$. The measurable degree of spatial coherence in accordance with (11) is

$$|\gamma^{\text{изм}}(s)| = \frac{|\Gamma^{\text{изм}}(s)|}{(I(0, s)\, I(s, s))^{1/2}} =$$

$$= \exp\left\{-\frac{(s/r_0)^2}{L^2\left[(2l_{\text{д}})^{-2} + (l_{\text{д}} l_{\text{н}})^{-1}\right] + \left[1 + \alpha\left(2L/k\right)\right]^2}\right\}. \qquad (12)$$

Here we have introduced the characteristic lengths -- diffraction $l_{\text{д}}$ and longitudinal correlation $l_{\text{н}}$

$$l_{\text{д}} = ka^2/2; \quad l_{\text{н}} = kr_0^2/2; \quad \alpha = \beta + k/2R. \qquad (13)$$

According to (12), the correlation radius is equal to [cf. Ref. 3]

$$r_{\text{н}} = r_0\left[L^2\left[(2l_{\text{д}})^{-2} + (l_{\text{д}} l_{\text{н}})^{-1}\right] + (1 + 2\alpha L/k)^2\right]. \qquad (14)$$

The minimum value of $r_{\text{н}}$ for $L \neq 0$ occurs at ($ar_0\alpha \gg 1$)

$$1 + 2\alpha L/k = 1 + L/R + 2\beta L/k = 0.$$

For $\beta = 0$, this is satisfied when $R = L$, i. e. in the focal plane of the lens in the case of beams that pass through a collecting lens ($R < 0$). However, since the parameter $\beta > 0$ for partly coherent beams, in reality the correlation radius reaches a minimum at a distance $L = (1/|R| - 2\beta/k)^{-1}$, which exceeds the focal length of the lens. According to Ref. 3, the beam diameter assumes the minimum value at this same distance.

The value of the measurable correlation radius when $a \gg r_0$ and $\alpha = 0$ is

$$r_{\text{н}}^{\text{изм}} = r_0\left[1 + L^2/(l_{\text{д}} l_{\text{н}})\right]^{1/4} = \left[r_0^2 + \lambda/(\delta\pi)\right]^{1/4}, \qquad (15)$$

where $2\delta = 2a/L$ is the angular size of the source. Thus $r_{\text{н}}^{\text{изм}} > r_0$ because of the diffraction effect.

Let us introduce the apparatus parameter f and require that the relative broadening of the correlation radius be less than this quantity: $(r_{\text{н}} - r_0)r_0^{-1} \leq f$. This condition is met at distances $L \leq \sqrt{f/2k}ar_0$ from which we

get the value of the limiting measurable correlation radius (Ref. 2 gives an inexact formula without derivation for limiting resolution of a PI)

$$r_{\text{н}}^{\text{пред}} = \frac{\sqrt{2\eta}L}{ka} = (\delta k\sqrt{\eta/2})^{-1}. \qquad (16)$$

With increasing angular size δ of the source of emission the influence of diffraction decreases, and consequently the smaller will be the radius of correlation that can be measured. However, as L decreases there comes a time when the maximum value of δ is limited by the aperture of the optical elements. For our PI, $a/L = 0.04$; taking $f = 0.1$ we get $r_{\text{н}}^{\text{пред}} = 10$ μm for $k = 10^5$ cm^{-1}.

3. Experiment. Discussion

Limiting resolution of the PI. To study the limiting resolution of the PI a quasi-coherent light source was used [Ref. 11], which was a rotating matte disk illuminated by the beam of a helium-neon laser ($\lambda = 0.63$ μm) through a collimating system. The correlation radius in the measurement plane was varied by changing the following parameters: diameter of the illuminated section of the matte disk, distance to the measurement plane L, dimensions of inhomogeneities on the disk (correlation radius r_0).

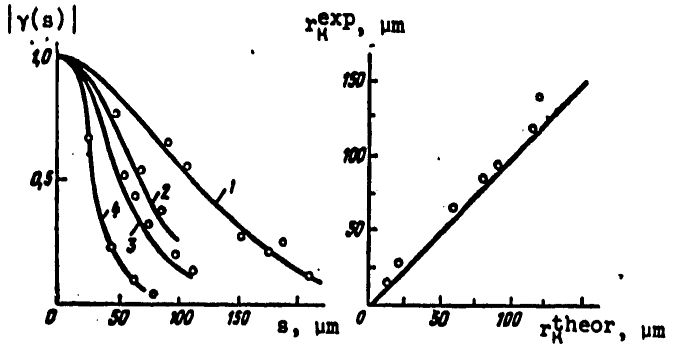

Fig. 2. Experimental curves for the normed correlation function of a quasi-optical source with correlation radius $r_0 = 12$ μm for different angles δ. The value of δ increases with the number of the curve

Fig. 3. Theoretical and corresponding experimental values of correlation radii

When the birefringent plate of the PI was continuously rotated an interference pattern was recorded on the chart recorder, and at the same time the result of frequency meter readings for the averaging time T = 1 s was printed out on a digital printer and chart-recorded (see Fig. 1). To determine the antiphase values of interference, the results of measurements were repeated,

but this time with the output analyzer turned through 90° as compared with the former case (See also Ref. 5).

The values of $|\gamma^{изм}(s)|$ were determined from the measurement results, using formula (6). One series of measurements of $|\gamma^{изм}(s)|$ for a matte disk with size of inhomogeneities $2r_0 \approx 25$ μm is shown in Fig. 2. As can be seen from Fig. 2, the measurable correlation radius decreases with an increase in the angular size of the source of emission.

The correlation radii theoretically calculated by formula (15) and experimentally measured values are shown in Fig. 3 for convenicence of comparison. The bisector of the angle of the $r_н^{теор}$-$r_н^{эксп}$ coordinate system corresponds to exact coincidence of the given results. It can be seen that although somewhat greater $r_н^{эксп}$ corresponds to the values of $r_н^{теор}$, the agreement of the results is rather good. The mentioned slight systematic deviation is caused according to (14) by the value of the phase of the SCF ($\beta > 0$, $R \to \infty$).

Experimental and theoretical values of the radius of curvature R of the phase front of focused laser beams for different displacements s_n

s_n	R, cm	
	exp.	theor.
s_1	66	84
s_2	49	49
s_3	56	57
s_4	88	92
s_5	49	49
s_6	50	49

Note. $s_1 = s_2 = s_3 = s_4 > s_5 > s_6$

Thus the results of measurement of the correlation radius are described well by formula (15), and consequently the limiting resolution of the PI realized by us is ~10 μm.

Measurement of the radius of curvature of the phase front. These measurements are based on formula (7). In our experiments with the He-Ne laser the radius of curvature of the phase front of focused laser beams was measured at different distances from the center of constriction. Lenses were used with different focal lengths, and the displacement s was varied.

The results of measurement of R are summarized in the table. Measurement accuracy was 2%. The given data show that the PI can be used to determine the curvature of the phase front of light beams with good precision. The upper limit for possible measurements of R is determined by the transverse dimensions of the studied beam; according to (7), $R < a^2/\lambda \approx L_д$.

REFERENCES

1. A. G. Arutyunyan, V. G. Tunkin, A. S. Chirkin, "Kvantovaya elektronika" [Quantum Electronics], edited by N. G. Basov, No 1, 1973, p 111; Soviet Patent No 421880, OFITSIAL'NYY BYULLETEN', No 12, 1974, p 115.

2. A. G. Arutyunyan, S. A. Akhmanov, Yu. D. Golyayev, V. G. Tunkin, A. S. Chirkin, ZHURNAL EKSPERIMENTAL'NOY I TEORETICHESKOY FIZIKI, Vol 64, 1973, p 1511.

3. S. A. Akhmanov et al., KVANTOVAYA ELEKTRONIKA, Vol 2, 1975, p 1171.

4. S. A. Akhmanov, V. B. Pakhalov, A. S. Chirkin, PIS'MA V ZHURNAL EKSPERIMENTAL"NOY I TEORETICHESKOY FIZIKI, Vol 23, 1976, p 391.

5. V. B. Pakhalov, A. S. Chirkin, KVANTOVAYA ELEKTRONIKA, Vol 4, 1977, p 1268.

6. S. M. Arakelyan, A. G. Arutyunyan, S. A. Akhmanov, V. G. Tunkin, A. S. Chirkin, KVANTOVAYA ELEKTRONIKA, Vol 1, 1974, p 215.

7. S. M. Arakelyan, S. A. Akhmanov, V. G. Tunkin, A. S. Chirkin, PIS'MA V ZHURNAL EKSPERIMENTAL'NOY I TEORETICHESKOY FIZIKI, Vol 19, 1974, p 571.

8. J. T. Ruscio, BELL SYST. TECHN. J., Vol 45, 1966, p 1583.

9. Svêtlik, APPL. OPTICS, Vol 13, 1974, p 1276.

10. N. K. Berger, V. V. Dembovetskiy, A. V. Mikheyenko, "Tezisy dokladov na Tret'yem Vsesoyuznom simpoziume po rasprostraneniyu lazernogo izlucheniya v atmosfere" [Abstracts of Reports to the Third All-Union Symposium on Propagation of Laser Radiation in the Atmosphere], Tomsk, 1975, p 222.

11. W. Martienssen, E. Spiller, AMER. J. PHYS., Vol 32, 1964, p 919.

6610
CSO: 1870

PHYSICS

UDC 535.21+621.378.33

HEATING OF METALS BY PULSED CO_2 LASER EMISSION

Moscow KVANTOVAYA ELEKTRONIKA in Russian Vol 6, No 1, Jan 79 pp 78-85

[Article by V. P. Ageyev, A. I. Barchukov, F. V. Bunkin, V. I. Konov, S. B. Puzhayev, A. S. Silenok and N. I. Chapliyev, Physics Institute imeni P. N. Lebedev, Academy of Sciences USSR, Moscow]

[Text] An experimental study is done on processes of heating of metal targets by a pulsed CO_2 laser for different ambient air pressures (10^{-5}-1 atm) and emission intensity of 1-100 MW/cm^2. It is established that there is a considerable increase in the laser energy input to the target in the case of initiation of breakdown of the vapor of the target material or low-threshold breakdown of the air. Under such conditions one observes a size effect -- an increase in the effective absorbing capacity of metal targets with an increase in the ratio of their radius to the radius of the emission spot. The results are attributed to contact of the breakdown plasma with the target surface as the plasma disperses into the ambient medium.

Introduction

A number of recently published papers [Ref. 1-4] deal with investigation of the principles governing heating of metal targets by pulsed emission of CO_2 lasers in the case where optical breakdown of air takes place close to the surface of the metal.

It has been established that in the case of emission intensity $I > I_{thr}$ ($I_{thr} \approx 10^6$-10^7 W/cm^2 is the threshold of breakdown of air close to the target) up to 50% of all the laser energy may be converted to thermal energy of the specimen, which is an order of magnitude greater than the natural "cold" absorptivity of the metal A_0. In this case the characteristic of energy input of laser emission to the metal is no longer A_0, but rather the so-called effective absorptivity of the target $A = E_1/E$, where E_1 is the percentage of laser energy E expended in heating the target. When a plasma

arises on the surface of the target, heating of the target by laser emission may take place through several channels. In the first place there is the absorption proper in the target of the radiation that has passed through the plasma. In the second place the target is heated through direct thermal contact with the plasma heated by the radiation; in this case the heating of the target is determined to a great extent by the geometry of the problem. For instance if the plasma of air breakdown is created on large exposure spots, heating of the metal target takes place chiefly across the area of the spot [Ref. 1]. In the third place, dispersal of the plasma with formation of a shock wave in the ambient gas may lead to considerable additional heating of the target across sections of its surface that are fairly distant from the exposure spot [Ref. 2, 3].

This paper, which is a continuation and development of Ref. 2, is devoted to the study of the basic principles that govern heating of metal targets in air by pulsed CO_2 laser emission under conditions of appreciable influence of plasma dispersal on the mechanism of heat transfer. Also investigated are cases of reduced air pressure and air-vacuum transition where there are changes in the properties of the plasma initiated close to the target: the plasma of air breakdown is transformed to a vapor jet of target materials.

In both cases a "size" effect is observed -- the dependence of the value of A for the metals on the ratio of the areas of the exposure spot and the target for a given emission intensity.

In the experiments a CO_2 laser was used with half-height pulse duration $\tau \approx 2.5$ μs and energy E up to 10 J. The radiation was focused in the center of steel or copper disks in spots with radius $R_s \approx 0.45$ and 1 mm. The targets were placed inside a vacuum chamber that was filled with air at a pressure of $p_0 = 10^{-5}$-1 atm. Cemented to the back of the specimens was a chromel-copel thermocouple used to determine the temperature increment ΔT of the specimen as a result of laser action. Heating of specimens was slight, and the temperature was quickly leveled out. Disregarding heat losses from the specimen, and using the relation $cm\Delta T = E_1$ (c, m are the specific heat and mass of the specimen), the effective absorptivity A was determined from ΔT.

1. Pulse heating of metals in a rarefied atmosphere

First consider heating of specimens at reduced air pressures, where emission intensity I is insufficient for initiating breakdown of air close to their surface, but sufficient for well-developed vaporization. Shown in Fig. 1 is the function A(I) for steel specimens of different radii (R of the order of $R_s = 1$ mm or greater) at air pressure of $p_0 \approx 2 \cdot 10^{-2}$ mm Hg. It can be seen that there are two parts to the function A(I). In the first region, when the value of I is less than some threshold intensity $I^* \approx (2\text{-}3) \cdot 10^7$ W/cm^2 the value of A does not depend on target size and increases with increasing I from $A_0 \approx 5\text{-}6\%$ (which corresponds to the "cold" absorptivity of steel) to $A \approx 10\%$. A further increase of intensity in the region $I > I^*$ leads to a

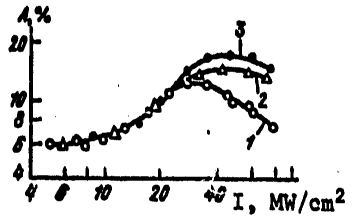

Fig. 1. Function A(I) for steel targets ($p_0 \sim 2 \cdot 10^{-2}$ mm Hg), $R/R_s = 1$ (1), 3 (2) and 4 (3).

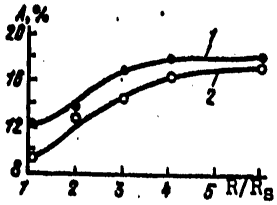

Fig. 2. Curves for A_{max} (1) and A at $I = 60$ MW/cm^2 (2) as a function of R/R_s

situation where laser energy is more effectively transmitted to specimens with a larger ratio of R/R_s. Let us note that the function A(I) in this region is nonmonotonic: for each specimen there is a maximum value of A at the value $I_{opt}(R/R_s)$. For targets with $R/R_s \approx 1$ the optimum energy input is reached close to I*, while for specimens with $R/R_s > 1$ the value of I_{opt} shifts toward larger values of I.

Shown in Fig. 2 are the maximum (for each specimen) effective absorptivity A_{max} as a function of target radius, and the function A(R) for a fixed emission intensity. It can be seen that the increase in A practically stops at $R/R_s \approx 4$, and the saturation value of A is approximately 1.5-2 times the effective absorptivity due to heat transfer across the exposure spot alone, where $R = R_s$.

The results shown in Fig. 1 and 2 can be interpreted as follows. In the region $I < I^*$ no appreciable vaporization of the targets takes place. Under laser exposure the surface temperature in the exposure zone increases with increasing I. According to Ref. 5 this should lead to an increase in the natural absorptivity of the metal. At $I \gtrsim I^*$ a luminescent jet of vapor of the exposed material appears at the surface of the target, i. e. I* can be identified as the threshold of well-developed vaporization of the target I_{vap}. Within the framework of well-developed vaporization of metal (see for instance Ref. 5) heat transfer into the specimen through the exposure spot takes place only during settling of the process

$$\tau_{set} \approx (\rho q/A)^2(\chi/I^2) \qquad (1)$$

(ρ, q and χ are the density, specific heat of vaporization and thermal diffusivity of the metal). Beyond this point, practically all the energy of the plaser pulse is expended on vaporizing the metal and heating its vapor. Taking the absorbed energy as $E_1 \approx A\pi R_s^2 \tau_{set} I$ and $A \approx A(I_{vap})$, we readily find from (1) that in the mode of well-developed vaporization the absorptivity in the exposure spot is

$$A(I) \approx A(I_{vap})(I_{vap}/I)^2 \qquad (2)$$

(here we use the definition of the threshold of well-developed vaporization from the condition $\tau_{set}(I_{vap}) = \tau_{rad}$, i. e. when $I > I_{vap}$ the quantity A should drop as I^{-2}. According to the data presented in Fig. 1 the experimental function A(I) differs from that predicted by formula (2) and takes the form $A \propto I^{-2/5}$. This difference is apparently the result of two causes. In the first place, in experiments with microsecond CO_2 laser pulses the vaporization of metals as a rule is accompanied by vapor breakdown, which should lead to additional heating of the metal due to thermal contact with the vapor plasma. In the second place, the laser pulse is close to triangular in shape, and therefore the energy in the "tail" of the pulse where emission intensity is no longer adequate for target vaporization should be absorbed in the plasma once more with efficiency $\sim A(I_{vap})$.

The "size" effect -- dependence of A on R_1 -- is due to spatial dispersal of the plasma and additional heating of the target across peripheral sections of the surface outside of the exposure spot. To make certain that it is the dispersal of the vapor cloud into vacuum that is responsible for this effect, we measured the thermal response of an additional copper plate located to the side of the axis of the laser beam at a distance $R_1 > R_s$ with its surface (area about 14 sq. mm) facing the plasma. Fig. 3 shows thermal response A

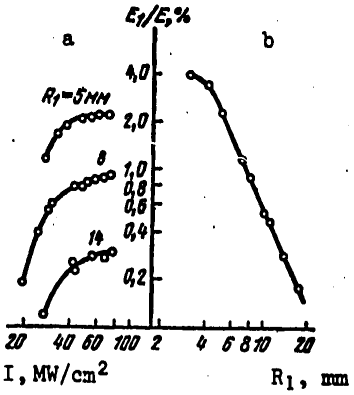

Fig. 3. Thermal response E/E_1 of auxiliary target with vaporization of a steel target ($p_0 = 2 \cdot 10^{-2}$ mm Hg) at different distances R_1 of the target from the axis of the beam (a) and at a fixed intensity $I = 60$ MW/cm^2 (b)

of this target as a function of I and R_1. It can be seen that for all values of R_1 (Fig. 3a) noticeable thermal action on the additional target starts at $I > I_{vap}$ when a luminescent vapor jet arises on the steel target. Fig. 3b gives an idea of the change in A with distance R_1. At a fixed emission intensity $I \approx 6 \cdot 10^7$ W/cm^2, $A(R_1) \propto R_1^{-2}$ with fair accuracy. Such behavior of $A(R_1)$ shows that the energy input to the auxiliary target is proportional to the time-integrated flux density of energy in the case of unbounded spherically symmetric vapor dispersal.

Control experiments with a plate of NaCl located in front of the auxiliary target to eliminate direct contact of the target with the dispersing vapor have shown that natural radiation of the vapor plasma makes no appreciable

contribution to heating of specimens in the investigated range of intensities at reduced air pressures.

2. Thermal effect on a metal target due to the plasma of low-threshold breakdown of air close to its surface

Let us go on now to examination of results that demonstrate the change in effective absorptivity A of targets with an increase in ambient air pressure p_0. Supersonic dispersal of the plasma of optical breakdown of vapor produces a shock wave in the ambient gas. Under certain conditions the absorption of laser emission behind the front of a shock wave propagating opposite to a laser beam gives rise to a light-detonation wave in the ambient gas (air). The breakdown plasma on the front of this wave shields the target from incident radiation and prevents further vaporization. Propagation of the light-detonation wave redistributes the energy release of laser emission in space, which should have an influence on the mechanism of heating of targets. The threshold of light-detonation with respect to intensity I depends strongly on the pressure and the kind of gas, and decreases with increasing p_0. Therefore in the problem of the laser energy input to the target it is important to know the pressures below which the rarefied gas medium is equivalent to a vacuum, i. e. the values of p_0 where the medium has no significant effect on heating of targets.

Fig. 4. Dependence $A(p_0)$ for a steel target

Shown in Fig. 4 are curves for $A(p_0)$ for steel targets with $R/R_s \geq 4$ (curve 1) and $R/R_s \approx 1$ (curve 2). The emission intensity I was held constant and equal to $\sim 6 \cdot 10^7$ W/cm^2 in an exposure spot with $R_s \approx 1$ mm. Let us note that in the pressure range of $p_0 < p_{cr} \approx 5$ mm Hg, $A(p_c) \approx$ const. This means that when $I \approx 6 \cdot 10^7$ W/cm^2 the pressure p_{cr} is critical, and at lower pressures the residual air is equivalent to a vacuum from the viewpoint of energy release of laser emission to the target. With increasing I there is a reduction in p_{cr}. An increase in pressure above the critical point (see Fig. 4) leads to a sharp reduction in the quantity A. Visual observations and high-speed photography show that when $p_0 > p_{cr}$ a light-detonation wave propagates through the air in opposition to the laser beam.

It is interesting to trace the heat response of an auxiliary target located to the side of the beam axis under the same experimental conditions. The results of measurements shown in Fig. 5 were found in the same arrangement of the experiment as in the study of vapor dispersal in vacuum (see Fig. 3). Curve 1 corresponds to a value of $R_1 = 10$ mm, and curve 2 was found at $R_1 = 17$ mm. An examination of these curves shows that the efficiency A of energy release over the auxiliary target at $p_0 \leq 0.1$ mm Hg does not depend on the residual air pressure. At high pressures the value of A increases, reaches a maximum at $p = p_{cr}$ and then decreases.

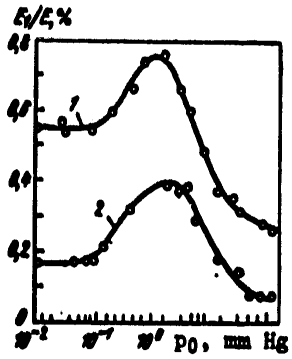

Fig. 5. Heat response E_1/E of an auxiliary target as a function of ambient air pressure p_0

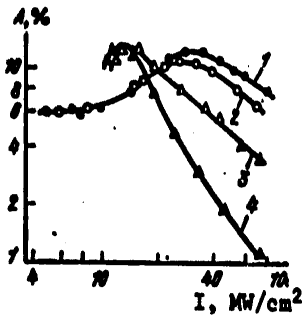

Fig. 6. General evolution of the dependence A(I) of a steel target ($R/R_s = 1$) when $p_0 \approx 5$ (1), 20 (2) and 60 mm Hg (3), and 1 atm (4)

In the preceding we have examined the behavior of A at different air pressures, but at constant emission intensity $I \approx 6 \cdot 10^7$ W/cm^2. Fig. 6 gives an idea of the functions A(I) at different pressures p_0 based on the example of a steel target with $R = R_s = 1$ mm. We note here first of all one very important experimental result. At each pressure p_0 there is an optimum emission intensity I_{opt} at which A(I) has a maximum, the value of I_{opt} always being close to the threshold value for formation of a plasma close to the target. In the case of exposure of a steel target "in vacuum" (curve 1, common to all $p_0 < p_{cr}$) this occurs at $I \approx I^* \approx 3 \cdot 10^7$ W/cm^2, i. e. close to the threshold of target vaporization and development of optical breakdown in the vapor. For pressures approximating atmospheric pressure (curves 3, 4) the value of I_{opt} decreases to 10^7 W/cm^2 -- typical threshold intensities for breakdown of air close to a target [Ref. 6]. In this case the breakdown of air is initiated by breakdown of microimpurities on the target surface, and no longer by breakdown of the vapors of target material itself (steel).

In general terms the function A(I) at different pressures p_0 behaves like the curves of Fig. 6 in the case of targets that have a larger diameter of the exposure spot as well.

Let us now take up some of the differences in the thermal action of pulsed radiation of CO_2 lasers on metals in atmospheric and rarefied air. In the first case, the "size" effect shows up more clearly in atmospheric air. Fig. 7 shows the dependence of A at $p_0 = 1$ atm for copper and steel specimens as a function of the ratio R/R_s (points corresponding to A for copper targets were found at $R_s \approx 0.45$ mm, and for steel -- at $R_s \approx 1$ mm; in both cases $I \approx 1.4 \cdot 10^7$ W/cm^2, exceeding the breakdown threshold of air). It can be seen that regardless of target material A is determined by the ratio R/R_s and

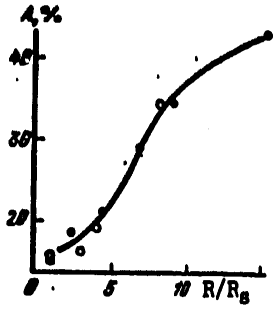

Fig. 7. Size effect in air on copper (black circles) and steel (light circles) targets at I=1$\frac{1}{4}$ MW/cm^2

reaches about 40% for targets with R/R_g=12, which is approximately triple the efficiency of energy input when R/R_g=1.

The results of the corresponding measurements are given in Fig. 2 for low pressures.

Another distinguishing feature of the behavior of effective absorptivity of metals in air is the sharper drop of A in air than in vacuum with increasing intensity when the threshold intensity is exceeded for plasma formation close to the target.

The experimental results, and particularly the "size" effect can be interpreted in terms of model representations of an air breakdown plasma as a source of explosion. Such an approach is fairly fruitful, and for instance has enabled a satisfactory description of the mechanical pressure pulse that is experienced by a target when a low-threshold breakdown of air produces a plasma that is ignited on the target surface [Ref. 6]. In this case, as well as in the discussion of Ref. 2 concerning experiments in which a dependence A(R) was observed in air, a model of a point explosion was used. In a more detailed approach to the problem of plasma heating of targets, one cannot fail to consider that the energy release in the course of a laser pulse occurs in some finite volume of air V_b, i. e. the breakdown plasma generally speaking is not the source of a point explosion. Let us illustrate this by a simple estimate that agrees well with experimental data.

Let all the energy E of a laser pulse be released in an initial volume V_b within which the pressure p_b is approximately constant and considerably greater than atmospheric pressure. Then we can set $E = p_b V_b/(\gamma - 1)$ (γ is the Poisoon adiabatic constant for air). The plasma focus expands rapidly with volume V_b to some volume V_0, wherein the pressure p_0 approaches atmospheric pressure. This expanded plasma space contains an appreciable fraction of laser energy $E_1 = p_0 V_0/(\gamma - 1)$ that is not converted to shock wave energy, but rather dissipates due to thermal radiation and heat conduction into the ambient air and target. We can readily see that the energy stored in volume V_0 is transferred chiefly to the metal target. The contact areas of the plasma with target and with air are close to each other. The heat flux Q from volume V_0 at each instant of time t is proportional to $\kappa|\nabla T|$, where T is the temperature in the plasma volume, $|\nabla T| \sim T/\sqrt{\chi t}$, κ and χ are the coefficients of heat conduction and thermal diffusivity of the ambient medium. The values of χ for air and metals are of the same order of magnitude, while the values of κ in metal are three or four orders of magnitude greater than in air.

We did the following experiments to determine the relative contribution of natural emission of plasma to the process of heating of a metal target.

An air breakdown plasma was created on one surface of a thin salt plate, and a steel target with thermocouple was pressed against the other surface. With such an arrangement of the experiment, the fraction of laser energy absorbed by the target fell by more than an order of magnitude as compared with the case where the breakdown plasma was initiated directly on the surface of the target. In both cases the emission intensity and breakdown plasma dimensions were about the same. Experiments were also done to study thermal radiation of a plasma by using an auxiliary copper target with area of about 0.1 cm^2 that was separated by a plate of NaCl from direct contact with the dispersing plasma. It was established that the angular distribution of heat radiation at intensities close to the threshold values is isotropic. Besides, at distances of 1.5-6 cm from the center of the plasma region the thermal response of a target with NaCl plate and without it is the same, i. e. the heat radiation of the plasma falls in the region of transmission of the plate of 0.2-15 μm. Let us note that plasma radiation in the UV region is strongly absorbed by air, and it was not recorded in the given arrangement of the experiment. Two versions of the auxiliary target were used: with a clean and with a blackened surface. The thermal response of the target with blackened surface was four times as high as for the clean surface. Such a difference can be readily explained if consideration is taken of the frequency dependence of target reflectivity. Blackened targets absorb practically all radiant energy that passes through the salt plate, while the thermal response of clean targets is determined chiefly by plasma radiation in the visible and ultraviolet regions of the spectrum. These experiments showed that when $I \approx I_{thr}$ the radiation losses from the plasma are rather small (about 10% of the laser energy). In the light-detonation mode these losses increase and may reach about 50%.

Assuming that the dimensions of the target are greater than the dimensions of the plasma volume, and taking the expansion process as adiabatic, we can estimate the effective absorptivity of the target in the region adjacent to the plasma:

$$A = E_1/E = (p_0/p_b)^{(\gamma-1)/\gamma}. \qquad (3)$$

Such an approach is valid for threshold conditions of air breakdown plasma formation when about 70% of the laser energy is absorbed in the plasma, the initial volume has dimensions of the order of the exposure spot and dispersal into the ambient air is spherically symmetric [Ref. 6]. In this case the radius of the expanded hemisphere $R = R_s/(p_b/p_0)^{1/3\gamma}$. For the conditions of our experiments ($I \approx 1.4 \cdot 10^7$ W/cm^2, $R_s \approx 1$ and 0.45 mm, $\gamma \approx 1.2$-1.25) the value of $R_0/R_s \approx 6$-8 and the quantity A≈20-30%, which is in satisfactory agreement with the data shown in Fig. 7. When $R/R_s > R_0/R_s$ The energy transfer to the target is determined by the shock wave as well, and gas heating takes place behind the wavefront. If the exposure spots on the target are sufficiently large, lateral expansion of the plasma volume is insignficant, and practically all the energy remaining in this volume after detachment of the shock wave is transferred to the exposure spot, which is confirmed by the results of experiments [Ref. 1].

In considering heating of metals under conditions where an air breakdown plasma is formed on their surface, we did not consider convective transfer of hot air along the target. Such an assumption is apparently valid since control experiments in which emission was focused on the target from the top downward and horizontally gave the same values of A within the limits of error of the measurements. These experiments show that the characteristic time during which the main portion of the energy stored in the plasma is transmitted to the target is less than the time of convective motion of hot air along the target.

On the other hand if the target is not in direct contact with the air plasma and is situated above it, then the contribution of convection to the thermal response of the target may be considerable. We measured the quantity E_1/E for two identical copper disks located one above the other at a distance of $2R_1$, and the air breakdown plasma was localized in the middle of the straight line joining their centers. The measurement results are shown in Fig. 8, where curves for laser energy input $A = E_1/E$ as a function of distance R_1 are given for two targets (reduced to the solid angle Ω at which the targets are visible from the center of the plasma region). The experiments were done at a laser pulse energy E=8-8.5 J. It can be seen that the energy input to the upper target throughout the entire investigated range of variations in R_1. This can be attributed to the fact that the lower target was heated only by the hot air behind the shock wave front, after it had reached the target surface, while the upper target was heated by ascending airflows as well.

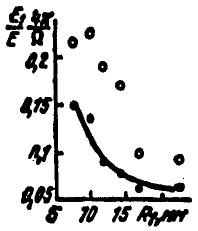

Fig. 8. Influence of convection on heating of a copper target in air: Lower target -- black circles, upper target -- white circles

REFERENCES

1. S. Marcus, J. E. Lowder, D. L. Monney, J. APPL. PHYS., Vol 47, 1976 p 2966.

2. V. P. Ageyev, V. I. Konov, A. S. Silenok, N. I. Chapliyev, PIS'MA V ZHURNAL TEKHNICHESKOY FIZIKI, Vol 3, 1977 p 677.

3. S. Marcus, J. E. Lowder, S. Manlief, D. L. Mooney, IEEE J., QE-11, 49D, 1975.

4. J. E. Robin, APPL. PHYS. LETTS., Vol 30, 1977, p 401.

5. S. I. Anisimov, Ya. A. Imas, G. S. Romanov, Yu. V. Khodyko, "Deystviye izlucheniya bol'shoy moshchnosti na metally" [Effect of High-Intensity Radiation on Metals], Moscow, Nauka, 1970.

6. V. P. Ageyev, A. I. Barchukov, F. V. Bunkin, V. I. Konov, S. M. Metev, A. S. Silenok, N. I. Chapliyev, IZVESTIYA VUZOV: SERIYA FIZIKA, No 11, 1977, p 34.

6610
CSO: 1870

PHYSICS

UDC 621.373.826.038.825

MEASURING THE POPULATION OF THE UPPER LASER LEVEL OF THE CO_2 MOLECULE AND THE GAIN OF THE ACTIVE MEDIUM IN A WAVEGUIDE DISCHARGE CHANNEL

Moscow KVANTOVAYA ELEKTRONIKA in Russian Vol 6, No 1, Jan 79 pp 114-119

[Article by B. A. Kuzyakov, Institute of Radio Electronics, Academy of Sciences USSR, Moscow]

[Text] A method involving registration of the intensity of gas discharge luminescence on a wavelength of 4.3 μm is used to investigate the way that the population of the upper laser level of the CO_2 molecule depends on the pressure of a working mixture of $CO_2 + N_2 + He$. It is shown that the population of the upper laser level is proportional to the discharge current at low pumping intensities and is weakly dependent on the pressure p of the active medium in the range of 70-120 mm Hg. The paper gives the results of experimental measurement of the gain of a weak signal with wavelength of 10.5 μm as dependent on the discharge parameters. The resultant experimental data are compared with analytical calculation.

The investigation of waveguide gas lasers that operate on gas mixtures that contain CO_2 [Ref. 1-6] is prompted by the outlook for developing miniature lasers with high gains, emission densities [Ref. 2] and frequency tuning range of the order of several gigahertz. Higher values of these parameters than those of the conventional CO_2 laser are realized by producing a uniform glow discharge at a higher pressure of the working mixture in a discharge tube of small diameter. Since there is a considerable difference between gas discharge parameters at high and low pressures, it is of interest to consider the fundamental characteristics of the active medium of a CO_2 waveguide laser (CO_2-WL).

1. One of the main characteristics of the active medium is the population of the upper laser level. The luminescence intensity J of a steady-state gas discharge is directly proportional to the population N of the upper laser level. Therefore in this paper the population of the upper laser level 00^01

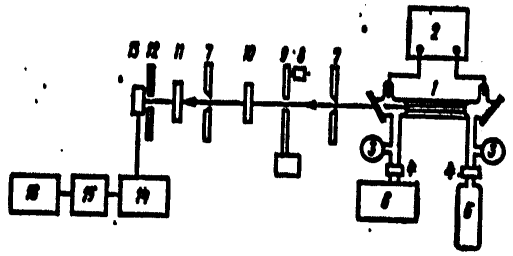

Fig. 1. Diagram of the experimental setup: 1--discharge tube; 2--source of supply; 3--vacuum meter; 4--vacuum valve; 5--gas tank with working mixture; 6--vacuum pump; 7--diaphragm; 8--reference signal source; 9--interrupter; 10--long-wave germanium filter; 11--short-wave sapphire filter; 12--screen; 13--photoreceiver; 14--narrow-band amplifier; 15--synchronous detector; 16--chart-recording potentiometer

of the CO_2 molecule was measured in relative units by the method of recording the number of photons with wavelength $\lambda = 4.3$ μm emitted per unit of time from the active volume with spontaneous transitions from the upper laser level to the ground state for the CO_2 molecule (00^00).

The experimental setup diagrammed in Fig. 1 enabled verification of the intensity of luminescence at different pressures of the working mixture and gas discharge current. Three-component gas mixtures of $CO_2 + N_2 + He$ were used as the working mixtures of the CO_2-WL. The discharge tube was a molybdenum glass tube 12.5 cm long with inside diameter of 1 mm and wall thickness of 1.5 mm. The discharge tube was placed in an envelope of the same material through which water was passed at a temperature of 17-19°C. Installed in the ends of the tube were mica windows 0.5 mm thick. The gas discharge was ignited between molybdenum electrodes soldered into side branches of the envelope of the discharge tube. A stabilized power supply with limiting voltage of 20 kV gave a stable discharge in the chosen range of electric field strength E and pressure p of the working mixture. The necessary value of the discharge current I was provided by selection of the appropriate ballast resistor of 2-3 MΩ. Depending on the mode of operation the maximum power dissipation of the ballast resistor was chosen at 30-50 W.

The systems for pumping and inlet of the gas mixture made it possible to vary the composition of the working mixture and the rate of circulation through the discharge tube. At a low pumping rate the pressure was determined as the arithmetical mean of the readings of manometers located at both ends of the discharge tube. Emission with a wavelength of $\lambda = 4.3$ μm was recorded by a standard Ge:Au resistor cooled to the temperature of liquid nitrogen. The signal from the photoresistor was sent to a synchronous detection system. To reduce the level of background radiation incident on the IR detector, directly behind the output window of the discharge tube and in front of the

window of the IR detector were diaphragms and special heat shields. The useful signal was isolated in the wavelength band of $\lambda = 4.3$ μm by a long-wave germanium filter 2 mm thick and a short-wave sapphire filter 4 mm thick [Ref. 7].

The results of relative measurements of luminescence intensity as a function of the pressure of the working mixture are shown in Fig. 2 (solid lines).

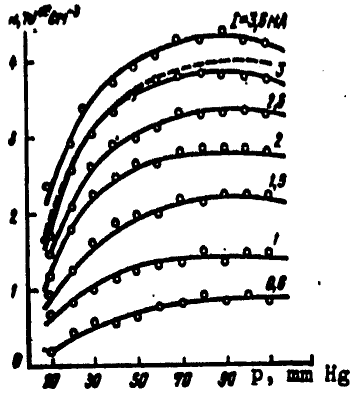

Fig. 2. Curves for the population of the upper level of the CO_2 molecule as a function of the pressure of the gas mixture $CO_2:N_2:He = 1:1:8$ for different values of pumping current; the experimental values are shown by solid lines, and the theoretical curve is shown by the broken line

Measurement errors without consideration of inhomogeneity of the distribution of luminescence flux through the volume of the discharge tube and effects of self-absorption were 7-10%. It is clear from the given figure that the pressure dependence of the population of the upper laser level of the CO_2 molecule is nonlinear; population increases with pumping current, and when the pressure ranges from 70 to 120 mm Hg the population is weakly dependent on the pressure of the working mixture. The scale of population in absolute units shown in Fig. 2 was obtained on the basis of a comparison of experimental data with the results of analytical calculation [Ref. 8]. The resultant values of laser level population play a major role in determination of the gain of the active medium.

2. To measure the gain of the active medium of the CO_2-WL, an experimental facility designed for measurements on a wavelength of 10.6 μm was used. The main units of this facility are shown in Fig. 1. The probing signal source was a series-produced LG-23 laser with stabilized power supply. An attenuator-polarizer was used to cut the intensity of the probing signal down to a level considerably below the intensity of saturation of the active medium of the discharge tube, so that signal level was 5 mW. The gain was

determined as the ratio of the values of the reference signal with and without the glow discharge plasma in the tube. The system used for measuring gain gave an accuracy of 10-12% in the chosen range of variation of parameters. The resultant relations for gain as a function of the parameters of the active medium are shown in Fig. 3.

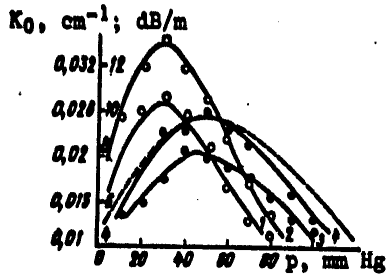

Fig. 3. Curves for gain of the active medium of a CO_2-WL as a function of pressure for mixtures of CO_2:N_2:He = 1:1:4 (1, 2) and 1:1:8 (3, 4); discharge currents 2 (1, 3) and 3 mA (2, 4); the experimental values are shown by the solid lines, and the calculated values are shown by the broken curve.

In addition to the experimental investigation of CO_2-WL laser operation, a theoretical study is also of interest to explain factors that would optimize the parameters. In this paper we compare the experimental results with the analytical description of weak-signal gain. In the investigated range of variation of working parameters of the discharge tube, the emission line shape is Lorentzian, and signal gain in the center of the line takes the form [Ref. 9]

$$K_1 = \exp(K_0 l), \qquad (1)$$

where l is the length of the active part of the discharge tube, K_0 is a function of emission wavelength, amplification linewidth, the difference between populations of laser levels of the CO_2 molecule (00^01) and (10^00) and so on. In Ref. 8 an expression was found for the K_0 of the active medium with different CO_2 and N_2 percentages without consideration of the population of laser level (10^00). In this paper, an expression is found for K_0 based on solution of kinetic equations for a three-level molecule, and enabling consideration of the population of the lower laser level and analysis of active mixtures of different compoeitions. In this case K_0 is described by the following expression:

$$K_0 = \frac{A_{1,2}\lambda^2 hcB_1(2J+1)\,3{,}55\cdot 10^{19}\delta_c n_c}{4\pi^2 kT\cdot 7{,}036\,(p/T)^{1/2}\sum_n \delta_n \alpha_{cb}} \frac{\alpha\langle\sigma_c v\rangle\delta_c + \langle\sigma_N v\rangle\delta_N + \langle\sigma_e v\rangle + \varkappa_N}{\alpha(\varkappa_N\delta_N + \varkappa_c\delta_c) + \varkappa_c\varkappa_N} \times$$

$$\times \exp\left[-\frac{hcB_1}{kT}J(J+1)\right]\left\{1-\alpha_3\frac{B_3}{B_1}\exp\left[-\frac{hc}{kT}B_1J(J+1)-B_3J(J-1)\right]\right\}, \qquad (2)$$

where $A_{1,2}$ is the probability of spontaneous emission, λ is emission wavelength, $B_{1,2}$ are the rotational constants of the upper and lower laser level respectively, n_e is the electron density in the gas discharge plasma, $\delta_{c,N}$ are the volumetric contents of components CO_2 and N_2 in the active gas medium respectively, k is Boltzmann's constant, T is gas temperature, $\sigma_{c,N}$ are the respective cross sections of excitation of CO_2 and N_2 molecules by electron impact:

$$\alpha_{ab}=(D_a+D_b)^{1/2}(1/M_a+1/M_b)^{1/2} \quad \text{[Ref. 10]},$$

where D_{ab} are the optical parameters of collisions of type "a" and "b" molecules, M_{ab} is the molecular weight of the colliding molecules,

$$\varkappa_c=n_e\langle\sigma_c v\rangle_{01}+\beta_1\delta_c+\gamma_1\delta_N+\varepsilon_1\delta_a+\varkappa_1;$$
$$\varkappa_N=n_e\langle\sigma_N v\rangle_{12}+\beta_2\delta_c+\gamma_2\delta_N+\varepsilon_2\delta_a+\varkappa_2;$$

is the probability of excitation (de-excitation) of molecules of CO_2 (N_2) by electron impact, $\alpha_{1,2}$ are the rate constants of processes of transfer of excitation from N_2^* to CO_2 and back, $\beta_{1,2}$ are the rate constants of relaxation of vibrational levels $(00^01)CO_2$ and $(v=1)N_2$ in collision with molecules of CO_2, α_3 is the ratio of populations of laser levels (10^00) and (00^01) of the CO_2 molecule, $\gamma_{1,2}$ are the rate constants of relaxation of the level $(00^01)CO_2$ and $N_2(v=1)$ in collision with N_2 molecules, $\varepsilon_{1,2}$ are the rate constants of relaxation of CO_2 (level 00^01) and N_2 $(v=1)$ in collision with molecules of He, $\varkappa_{1,2}$ are the rates of de-activation of excited molecules of CO_2 and N_2 on the wall of the discharge tube.

The values of these quantities are given mainly in Ref. 8. In defining them it was assumed that the temperature of the inner wall of the discharge tube is the same as that of the cooling water. Such an assumption is completely valid for discharge tubes made of materials with a high coefficient of heat transfer such as BeO ceramic. However, when a gas discharge is burning in a tube made of glass a temperature gradient arises between the inner and outer surfaces of the tube, which leads to the necessity of more exact determination of gas temperature.

3. The gas temperature in the discharge tube can be determined from the following formula [Ref. 11]:

$$T_g=Wr^2[0.178/K_r+1/4K_M\ln(r_1/r)]+T_0, \qquad (3)$$

where W is pumping power, r and r_1 are the inner and outer radii of the discharge tube, $K_{r,M}$ are the respective heat conductivities of the gas mixture and the tube material, T_0 is the temperature of the outer surface of the tube.

The coefficient of thermal conductivity K_r of the gas mixture can be calculated by one of the methods of the theory of thermal conductivity, for instance by Brokau's method [Ref. 12]. In this case, K_r is determined as the superposition of the coefficients of thermal conductivity of the components of the gas mixture. At a gas temperature of 273-473 K the

coefficient of thermal conductivity of He (λ_{He} = 0.1346 kcal/(m·hr·deg)) is 7-10 times as high, and the coefficient of thermal conductivity of N_2 (λ_{N_2} = 0.0237 kcal/(m·hr·deg)) is 1.3-1.7 times as high as the coefficient of thermal conductivity of CO_2 (λ_{CO_2} = 0.0154 kcal/(m·hr·deg)) [Ref. 13] (the numerical values of the coefficients of thermal conductivity of the components of the gas mixture are given for T_r = 323 K). Therefore expression (3) at high percentage contents of He may be used to analyze both a two-component mixture of CO_2 + He and three-component mixtures of CO_2 + N_2 + He. The dependence of gas temperature on discharge current calculated by formula (3) for a gas mixture of CO_2:N_2:He = 1:1:8 is shown by the broken line in Fig. 4.

In addition to calculation of the gas temperature, an experimental study was made of the gas temperature as a function of the pumping parameters of the active medium. Gas temperature measurements were made with a graduated copper-constan thermocouple connected to a precision millivoltmeter. To eliminate the influence that electron and ion components of the glow discharge plasma have on the readings of the recording device, the thermocouple was

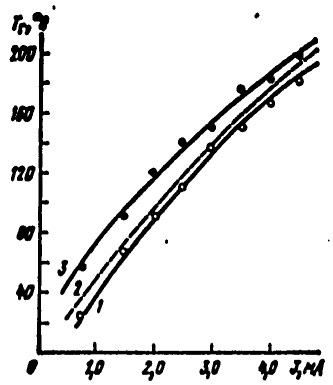

Fig. 4. Experimental (1, 3) and calculated (2) curves for gas mixture temperature as a function of discharge current in the weak circulation mode for mixtures of CO_2:N_2:He = 1:1:8 (1, 2) and 1:2:7 (3)

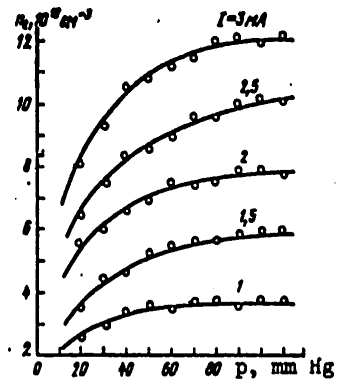

Fig. 5. Electron density in glow discharge as a function of the pressure of the active medium CO_2:N_2:He = 1:1:8 for different pumping currents

placed in a sealed thin-walled quartz tube with spherical cavity 0.4 mm in diameter on the end. This temperature sensor was installed inside the discharge channel close to its end face. The gas temperature measurements (solid lines on Fig. 4) were made under conditions with weak circulation of the gas mixture. The measurement error was 8-15%. The given data show that wich a change in pumping intensity from 100 to 400 mA/cm^2 the temperature of

gas mixture changes by nearly an order of magnitude. Therefore in calculating the gain of the active medium it is necessary to account for the resultant temperature dependences.

Consideration should also be taken of the circumstance that the gas temperature appears in the analytical expression for gain (2) not only as a parameter, but the coefficients of this expression also depend on gas temperature. The latter coefficients are determined on the basis of their temperature dependences [Ref. 14-17] with consideration of specific discharge conditions.

The electron density n_e in the gas discharge plasma, which appears in expression (2) for gain, is determined on the basis of measurement of the external discharge parameters with consideration of the drift velocity of electrons in the gas mixture, and is shown in Fig. 5. The parameter κ_c depends on the pressure and composition of the gas mixture [Ref. 8]. By using the resultant characteristics we can plot the calculated curves for the population of the upper laser level of the CO_2 molecule and the gain of the active medium as dependent on gas pressure (see Fig. 2, 3, broken curves). As can be seen from the resultant graphs, correction of the parameters appearing in the expressions for gain and population of the upper laser level with consideration of temperature dependences enabled us to reduce the discrepancy between experimental data and the theoretical results of Ref. 8.

Our analysis shows that the investigated characteristics of the CO_2-WL are complicated functions of many parameters with values determined by the specific conditions of creation of the population inversion. The complexity of the analytical description of the investigated characteristics is also due to the fact that many quantities appearing in the analytical formulas are determined on the basis of a large number of varied experiments and are semi-empirical in nature. However, under certain assumptions it is possible to estimate the relative error of the given expressions. As an example let us consider the analytical expression for gain K_0. Since the values of the function K_0 are positive, we have the following expression for the relative error δ_k under condition of small absolute errors of its argument Δx_i that are constant in the selected range of definition of K_0 [Ref. 18]:

$$\delta_k = \sum_{i=1}^{n} \frac{1}{K_0} \left| \frac{\partial K_0}{\partial x_i} \right| \Delta x_i. \qquad (4)$$

In doing calculations by formula (4) we get a relative error $\delta_k = 8\text{-}12\%$. The given errors of the analytical calculation are of the same order as the errors of the experimental results, which is an indication of the validity of the method chosen for calculation.

In conclusion the author thanks M. Ye. Zhabotinskiy and V. V. Grigor'yants for assistance and constructive criticism, and also T. V. Babkina for help with the measurements.

REFERENCES

1. R. E. Jensen, M. S. Tobin, APPL. PHYS. LETTS, Vol 20, 1972, p 508.

2. T. J. Bridges, E. G. Burkhardt, P. W. Smith, APPL. PHYS. LETTS, Vol 20, 1972, p 403.

3. P. W. Smith, T. J. Bridges, E. G. Burkhardt, O. P. Wood, APPL. PHYS. LETTS, Vol 21, 1972, p 420.

4. E. G. Burkhardt, T. J. Bridges, P. W. Smith, OPTICS COMMS, Vol 6, 1972, p 193.

5. A. S. Provorov, V. P. Chebotayev, KVANTOVAYA ELEKTRONIKA, Vol 2, 1975, p 748.

6. Ye. N. Bazarov, G. A. Gerasimov, Yu. N. Posidin, KVANTOVAYA ELEKTRONIKA, Vol 2, 1975, p 1160.

7. V. V. Kozelkin, I. F. Usol'tsev, "Osnovy infrakrasnoy tekhniki" [Principles of Infrared Technology], Moscow, Mashinostroyeniye, 1974.

8. V. V. Grigor'yants, B. A. Kuzyakov, A. M. Sinitsyn, KVANTOVAYA ELEKTRONIKA Vol 4, 1977, p 1482.

9. V. P. Tychinskiy, USPEKHI FIZICHESKIKH NAUK, Vol 91, 1967, p 407.

10. Ye. T. Gerry, D. A. Leonard, APPL. PHYS. LETTS, Vol 8, 1966, p 227.

11. H. Shirahata, T. Fujioka, J. APPL. PHYS., Vol 47, 1976, p 2453.

12. R. Rid, T. Shervud, "Svoystva gazov i zhidkostey" [Properties of Gases and Liquids], Moscow, Khimiya, 1971.

13. A. Misnar, "Teploprovodnost' tverdykh tel, zhidkostey, gazov i ikh kompozitsiy" [Thermal Conductivity of Solids, Liquids, Gases and Their Composites], Moscow, Mir, 1968.

14. R. I. Taylor, S. Bitteman, REV. MOD. PHYS., Vol 41, 1968, p 26.

15. J. E. Morgan, H. J. Shiff, CANAD. J. CHEM., Vol 41, 1963, p 903.

16. A. V. Yeletskiy, ZHURNAL PRIKLADNOY SPEKTROSKOPII, Vol 8, 1968, p 425.

17. W. L. Nighan, W. R. Bennet, APPL. PHYS. LETTS, Vol 14, 1969, p 240.

18. N. V. Kpochenova, I. A. Marov, "Vychislitel'naya matematika v primerakh i zadachakh" [Computational Mathematics in Examples and Problems], Moscow, Nauka, 1972.

6610
CSO: 1870

PHYSICS

UDC 621.378.325

DESIGN AND METHOD OF CALCULATING AN INDUCTIVE ACCUMULATOR FOR LASER PUMPING

Moscow KVANTOVAYA ELEKTRONIKA in Russian Vol 6, No 1, Jan 79 pp 127-133

[Article by I. I. Artamonov, V. A. Barikhin, V. V. Borovkov and V. I. Kashintsov]

[Text] Analytical expressions are obtained that describe the operation of an inductive accumulator into a load that contains inductance and resistance. It is shown that a reduction in the inductance and resistance of the load increases the energy dissipated in the load and the time of energy release, while an increase in inductance and resistance reduces the energy and time of its release. An experimental check is done on theoretical calculations based on the example of a laser using a solution of Rhodamine 6G in ethanol with flash-tube pumping. In this check, the use of an inductive accumulator as the pumping source increased the output energy of the laser by a factor of 1.5 while shortening the pulse front of the stimulated emission by a factor of 2.5 as compared with the parameters of a laser with capacitive accumulator under the same conditions.

At the present time nearly all the records being set for laser emission parameters are achieved on solid-state lasers. To a great extent, this is the result of development of powerful electric discharge light sources with capacitive accumulator supply. At the same time, light source requirements in the final analysis are determined by the specifics of the working laser transitions, and therefore the use of a given source of supply in each specific case must be based on the characteristics of the active medium rather than on the traditions that have evolved up to the given point in time.

It has been mentioned in the literature [Ref. 1-4] that inductive accumulators (IA) have advantages when rapid input of stored energy to a load is needed. Data of theoretical calculations [Ref. 5, 6] show that it is advantageous to use the IA for instance in dye lasers where the influence of the rate of increase in excitation is quite appreciable.

1. Operation of the IA into a mixed load

Usually the IA consists of a storage circuit and a load circuit [Ref. 1] connected in parallel. First the energy of the external source is stored in the inductance of the storage circuit, the switch of the load circuit being open. After the stored energy has reached a predetermined value, the switch of the storage circuit is opened simultaneously with closing of switch of the load circuit, and as a result the energy stored in the accumulator inductance is partly or completely released in the load, which may be either an inductance or a resistance, or both together. Usually electrically exploding wires (EEW) [Ref. 2] are used as the switches in the storage circuit, and dischargers are used in the load circuit.

Up until now the process of energy transfer to the load has been calculated in only two cases: for inductance without resistance, and for pure resistance without inductance [Ref. 1, 3]. Either numerical methods or qualitative representations have been used to describe the process of energy transfer to a mixed load. Nevertheless, even in this case analytical expressions can be found that describe the principles governing transfer.

If the instant of operation of the switches is taken as the time $t = 0$ of beginning of readout, the process of energy transfer to the load by analogy with Ref. 1 is described by the following system of differential equations

$$L_1\dot{I}_1+RI_3=0,\quad L_2\dot{I}_2+rI_2-RI_3=0,\quad I_1=I_2+I_3 \qquad (1)$$

with initial conditions $I_1(0) = I_0$, $I_2(0) = 0$, where L is inductance, I is current, $R = \text{const}$ is the pure resistance of the switch in the storage circuit when $t = 0$, $r = \text{const}$ is the pure resistance of the load, the subscripts 1-3 refer to the parameters of the storage circuit, the load circuit and the switch of the storage circuit respectively. It should be emphasized that system (1) describes transfer only for the case $R = \text{const}$ throughout the process. The validity of this assumption in the range of 10 ns-10 μs is shown by the experimental data given in Ref. 1-4.

It is convenient to use direct Laplace transformation to convert system (1) to a system of algebraic equations in image space:

$$L_1[si_1-I_1(0)]+Ri_3=0,\quad L_2[si_2-I_2(0)]+ri_2-Ri_3=0,\quad i_1=i_2+i_3, \qquad (2)$$

and then to find the originals of the solution of this system from a table of correspondences [Ref. 7]:

$$J_1(z)=\frac{2(1+x)-(A-\sqrt{A^2-4xy})}{2\sqrt{A^2-4xy}}\exp\left\{-\frac{A-\sqrt{A^2-4xy}}{2}z\right\}-$$

$$-\frac{2(1+x)-(A+\sqrt{A^2-4xy})}{2\sqrt{A^2-4xy}}\exp\left\{-\frac{A+\sqrt{A^2-4xy}}{2}z\right\}; \qquad (3)$$

$$J_2(z)=\frac{2\exp\{-Az/2\}}{\sqrt{A^2-4xy}}\operatorname{sh}\left\{\frac{\sqrt{A^2-4xy}}{2}z\right\}; \qquad (4)$$

$$J_3(z)=\frac{2x-(A-\sqrt{A^2-4xy})}{2\sqrt{A^2-4xy}}\exp\left\{-\frac{A-\sqrt{A^2-4xy}}{2}z\right\}-$$
$$-\frac{2x-(A+\sqrt{A^2-4xy})}{2\sqrt{A^2-4xy}}\exp\left\{-\frac{A+\sqrt{A^2-4xy}}{2}z\right\}. \qquad (5)$$

Here we have introduced the dimensionless functions $J_i = I_i/I_0$ ($i = 1, 2, 3$), the dimensionless variable $z = t/RL_2$ and the dimensionless quantities $x = r/R$, $y = L_2/L_1$ and $A = 1 + x + y$. A characteristic feature of the transfer process is that the quantities x and y enter symmetrically into expressions (3)-(5). In the limit as $r, L_2 \to 0$, we can get the conventional expressions [Ref. 1, 3] for a purely inductive and purely resistive load from (3)-(5).

It can be readily shown that at time

$$z_m = (A^2-4xy)^{-1/2}\ln\frac{A+\sqrt{A^2-4xy}}{A-\sqrt{A^2-4xy}}, \qquad (6)$$

when the current in the load circuit reaches the maximum value

$$J_3(z_m)=(xy)^{-1/2}\exp(-Az_m/2), \qquad (7)$$

the energy released in the load ($r \neq 0$) is

$$E_3(z_m)=\frac{L_3}{R}\int_0^{z_m} rJ_3^2(z)\,dz=\frac{E}{A}\left(1-\frac{A^2+xy}{xy}e^{-Az_m}\right), \qquad (8)$$

where $E = L_1 I_0^2/2$ is the energy stored in the inductance of the storage circuit, and the voltage across the load reaches the value

$$u_3 \approx rI_3(t_m)+L_3 I_3(t_m)/t_m = RI_0 J_3(z_m)(x+1/z_m). \qquad (9)$$

Expression (4) implies that the characteristic time of energy release in the load is

$$z_e \approx (A-\sqrt{A^2-4xy})^{-1}, \qquad (10)$$

and the total energy dissipated in the mixed load ($r \neq 0$) is

$$E_3=\frac{L_3}{R}\int_0^{\infty} rJ_3^2(z)\,dz=\frac{E}{A}. \qquad (11)$$

In some cases expressions (6)-(11) can be simplified. For instance for $x,\ y \gg 10$ $z_m \approx 2/A$; $J_3(z_m) \approx 0{,}38/\sqrt{xy}$; $E_3(z_m) \approx E/2A$; $u_3 \approx 0{,}19RI_0(3x+y)/\sqrt{xy}$; $z_e \approx 6/A$. In this case the pulse duration in the load circuit can be appreciably shortened, but the energy released in the load decreases by the same factor. Nonetheless, it is this case that is of the greatest interest in practice since the transfer process can be calculated by formulas (1)-(11) even if R and r vary slightly in time $\sim z_e$. Thus for instance one can realize nanosecond pulses with fairly high energy in electric-discharge sources for laser pumping with high impedance when breakdown occurs. Obviously the possibilities for shortening pulses in this case are limited in practice primarily by the electric strength of the switch in the load circuit [Ref. 8].

In the opposite case ($x, y \leq 0.1$) we can get: $z_m \approx -\ln xy$; $J_2(z_m) \approx I_0$; $E_2(z_m) \approx xyE$; $u_2 \approx RI_0(x - 1/\ln xy)$; $z_e \approx (2xy)^{-1}$; $E_1 \approx E$. In this case nearly all the energy stored in the storage circuit is released in the load; however, there is a considerable increase in the duration of the pulse in the load circuit. Here the current pulse in the load has a typical trapezoidal shape: in the interval $z_m \leq z \leq z_e$ there is almost no change in current: $J_2(z) \approx J_2(z_m)$. The operation of the IA into a mixed load in this state can be described by expressions (1)-(11) only when R = const and r = const at least up to values of $z \sim z_e$.

The transfer requires first of all that the energy stored in the inductance of the storage circuit be maximum, and secondly that vaporization of the EEW in the electric explosion be complete. These requirements are met if we can satisfy the condition that the integral of current be equal to the change of internal energy of the EEW during heating and vaporization [Ref. 2]:

$$\int_0^{\tau} j^2 dt = \int_{Q_1}^{Q_2} \sigma dQ, \qquad (12)$$

where j is the current density in the EEW before the explosion, σ is the conductivity of the EEW, Q is the density of internal energy of the EEW (initial Q_1, during explosion Q_2), τ is the instant when the current in the storage circuit reaches the maximum. We assume that all processes take place before operation of the switches of the IA, i. e. before the start of energy transfer to the load. From (12) we can find the cross section of the EEW

$$S = \sqrt{\left(\int_0^{\tau} j^2 dt\right) \Big/ k_1} \qquad (13)$$

if j(t) and the quantity $k_1 = \int_{Q_1}^{Q_2} \sigma dQ$, that is determined by the material and geometry of the EEW [Ref. 2] have been experimentally measured.

If we know the quantities E' (energy stored in the storage loop from the external source up until time τ) and E" (energy released up to this time in the EEW, where

$$E'' = \beta E', \qquad (14)$$

and $\beta < 1$), and also the energy E"' required for complete vaporization of the EEW,

$$E''' = \rho V q \qquad (15)$$

(ρ is density, V is volume, q is the specific energy of sublimation of the material of the EEW), then setting (14) equal to (15) we can readily find the length of the EEW:

$$l = \beta E'/S\rho q. \qquad (16)$$

Our analysis shows that when the IA works into a mixed load it is a fairly universal energy source, and in particular may be a source for pumping lasers.

2. Experimental facility

The experimental setup consisted of a capacitor bank and a coaxial flash tube (CFT) in which a circular vacuum discharger with forced ignition was the commutating element of the discharge loop. The capacitor bank with capacity $C = 57$ μF was charged to a voltage of $u_0 = 15$ kV in operation with the IA, and to $u_0 = 11$ kV in operation with a capacitive accumulator. The current and its derivative in the discharge circuit were recorded by Rogowski loops, and the output signals were sent to S1-26 and S1-37 oscilloscopes. The duration and shape of the pulses of laser radiation and pumping radiation were recorded by FEK-14 photocells through the S1-37 oscilloscope, and the rise time of the stimulated emission was recorded by a similar photocell on the S-1-26 oscilloscope. The active medium was a solution of Rhodamine-6G in ethanol. The concentration of dye molecules in all experiments was $5 \cdot 10^{-5}$ mole/cm^3. The design of the CFT is described in Ref. 9. Dimensions of the discharge cavity: length ~135 mm, inside diameter 27 mm, outside diameter 60 mm, working volume of the cell ~45 cm^3.

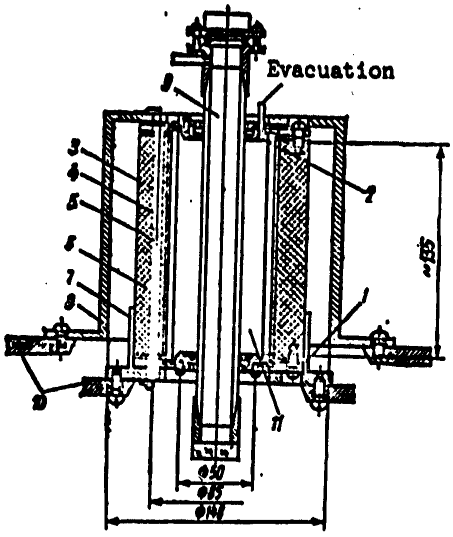

Fig. 1. Inductive accumulator

The main structural elements of the laser and the IA are shown in Fig. 1 (dimensions are given in mm). The flat mirrors of the cavity ($r' = 0.99$ and $r'' = 0.6$) were the ends of cell 9 with the dye solution, the output mirror being bellows-mounted for adjustment. The discharge cavity 11 of the CFT was formed by the cell and a quartz tube, and was filled with xenon to 10 mm Hg. Discharge took place between two metal electrodes 1 and 2. Teflon tubes 4 were set in 12 openings drilled axially with the discharge cavity in jacket 3 and in the electrodes of the tube. This was done to prevent possible damage to the CFT with explosion of the EEW. The exploding wires 5 were soldered on one side to brass spokes 6 fastened to the inside cup 7 within which the tube was tightly set, while the other was soldered to the face of the return current lead 8. Cup 7 and current lead 8 were attached to electrode 10 of the vacuum discharger. Spokes 6 enabled selection of the optimum length of the EEW in adjusting the switch of the storage circuit in experiments with the IA, and acted as the return current conductor in operation with the capacitive accumulator, making the discharge circuits equivalent with respect to the energy released in the load.

The dimensions of the coaxials were selected in such a way that the inductance of the storage circuit formed by the return current lead and the EEW would

be equal to the inductance of the load circuit formed by the EEW and the electric discharge plasma in the tube ($L_1 = L_2 = 40$ nH). This method of connecting coaxials was used in Ref. 2; in the given case, the gap between electrode 2 and return current lead 8 acted as an uncontrolled air-discharge arrester.

It was found from experiments with the capacitive accumulator that the pure resistance of the CFT after breakdown was $r = 3.5$ mΩ. In the IA experiments the value of the integral of current was determined for $u_0 = 15$ kV and $k_1 = 2 \cdot 10^9$ $A^2 \cdot s/cm^2$ for copper, and on this basis formula (13) was used to find the matching cross section of the EEW. It was found that in the optimum variant the EEW is a strand of 15 copper wires with cross sectional area of $S = 0.9$ mm^2. A preliminary evaluation of the length of the EEW was made by formula (16), and the final value of l was experimentally chosen. As can be seen from Fig. 2, the time for reaching the maximum R_{max} is a minimum for $l \approx 4$ cm, R_{max} in this case being 0.2 Ω.

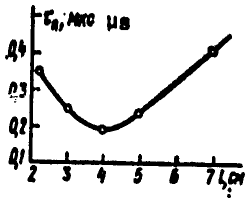

Fig. 2. Time for reaching R_{max} as a function of the length of the EEW

Thus in the given instance $x \approx 0.02$, $y = 1$, $A = 2.02$, and according to (11) $E_2 \approx 0.5E$, and consequently the choice of values of $u_0 = 15$ kV in operation with the IA and $u_0 = 11$ kV in operation with the capacitive accumulator makes the energy released in the load the same. It can be easily shown that for the given values of C, L_1, R, x and y in both cases $t_e \approx 10$ μs.

3. Discussion of the results

Measurement results are given in Fig. 3, 4. In operation of the CFT from a capacitive accumulator an oscillatory damped discharge was observed with maximum current being reached at $t_m \approx 2$ μs. In the case of excitation of the discharge in the CFT from an IA, energy transfer to the load started at the instant when the current (energy) in the oscillatory tank was maximum. In the load circuit the current reached the greatest value of ~300 kA within ~0.6 μs, the calculated values being 302 kA and 0.52 μs. Oscillations of the current in the

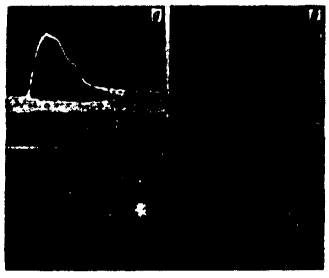

Fig. 3. Time behavior of pumping radiation (*а*, *б*) and stimulated emission (*в*, *г*) in operation with a capacitive accumulator (*а*, *в*) and with an IA (*б*, *г*); scale division 2.5 μs

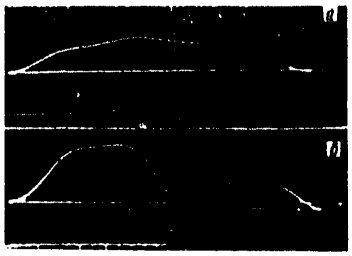

Fig. 4. Oscillograms of discharge current (top beams) and wavefront of stimulated emission (lower beams) for versions without transfer (*а*) and with transfer (*б*) of energy; time division 0.2 μs

discharge circuit after transfer were due only to the imperfection of the recording system, or possible "pinching" of the discharge in the tube.

In the version with capacitive accumulator the pumping pulse duration at half-height was 7.7 μs, the stimulated emission pulse 3 μs, and with the IA -- 2.2 and 3 μs respectively (see Fig. 3), a typical plateau being observed in this case in the vicinity of the maximum of the lasing pulse (see Fig. 3*а*), which is in total agreement with the conclusions of section 1 on the trapezoidal shape of the current pulse in the discharge circuit for small x, and experimental results (see Fig. 4). The absence of a plateau on the oscillogram of the pumping pulse (Fig. 3*б*) can be attributed to the specifics of the spectral characteristics of the FEK-14 photocell (light filters were not used in the experiments).

In operation with the capacitive accumulator stimulated emission arose practically at the maximum current, lasing intensity reached the greatest value within 8 μs, after which a rapid drop began, although the current up to this point did not have time to change much (Fig. 4). This shows the high thresholds of onset and interruption of lasing in the given instance. Use of the IA reduces the rise time of the lasing pulse to 0.7 μs, and lasing arises practically simultaneously with the current in the load, the energy in the pulse of stimulated emission increasing to 2.2 J as compared with 1.5 J in the first variant, primarily due to the reduction in rise time of the pumping pulse, leading to a reduction in the threshold of onset of stimulated emission [Ref. 6].

Thus the use of an IA as the pumping source for a laser on a Rhodamine 6G dye solution increases the output energy of the laser and shortens the duration of the lasing pulse front.

REFERENCES

1. G. Knopfel', "Sverkhsil'nyye impul'snyye magnitnyye polya" [Superstrong Pulsed Magnetic Fields], Moscow, Mir, 1972.

2. Ch. Maisonnier, J. G. Linhart, C. Gourlan, REV. SCI. INSTR., Vol 37, 1966, p 1380.

3. G. A. Mesyats, "Generirovaniye moshchnykh nanosekundnykh impul'sov" [Generation of Powerful Nanosecond Pulses], Moscow, Sovetskoye radio, 1974.

4. M. M. Bystrov, F. Z. Gal'chuk, B. A. Larionov, A. M. Stolbov, "Vsesoyuznoye soveshchaniye po inzhenernym problemam UTS" [All-Union Conference on the Engineering Problems of Controlled Nuclear Fusion], Abstracts of the Papers, 1974.

5. A. N. Rubinov, ZHURNAL PRIKLADNOY SPEKTROSKOPII, Vol 11, 1969, p 436.

6. B. A. Barikhin, B. S. Makayev, L. V. Sukhanov, A. I. Pavlovskiy, KVANTOVAYA ELEKTRONIKA, Vol 3, 1976 p 1211.

7. G. Dëch, "Rukovodstvo k prakticheskomu primeneniyu preobrazovaniya Laplasa" [Handbook on Practical Use of Laplace Transformation], Moscow, GIFML [State Physical-Mathematical Press], 1958.

8. A. I. Pavlovskiy, V. S. Bosamykin, ATOMNAYA ENERGIYA, Vol 37, 1974, p 228.

9. F. N. Baltakov, B. A. Barikhin, V. G. Kornilov, S. A. Mikhnov, A. N. Rubinov, L. V. Sukhanov, ZHURNAL TEKHNICHESKOY FIZIKI, Vol 42, 1972, p 1459.

6610
CSO: 1870

PHYSICS

UDC 621.375.9:535

HEAT LENSES IN THE ACTIVE ELEMENTS OF PULSE-PERIODIC GLASS LASERS

Moscow KVANTOVAYA ELEKTRONIKA in Russian Vol 6, Jan 79 pp 140-145

[Article by N. Ye. Alekseyev, A. K. Gromov, A. A. Izyneyev, Yu. L. Kopylov and V. B. Kravchenko, Institute of Radio Electronics, Academy of Sciences USSR, Moscow]

[Text] An analysis is made of the influence that the thermo-optical characteristics P, Q and $\theta = dP/dt$ of laser glasses have on the size of the heat lens induced in the active element of a pulse-periodic laser. The sizes of heat lenses and their temperature dependences are measured for a number of athermal phosphate glasses. A new method is proposed for determining P, Q and θ from the aberration parameters of the heat lens. The values of P, Q and θ determined by this method are compared with the known values of these parameters for the investigated glasses. The temperature dependences of lasing energy and divergence are measured. It is shown that glasses with the lowest value of θ have the minimum temperature dependence of these characteristics.

When a solid-state laser operates in the periodic-pulse mode with high average pumping power, considerable temperature differentials arise in the laser active element (AE) that lead to a change in the index of refraction and the development of a heat lens. This effect is especially considerable for glass because of its low thermal conductivity. Therefore the use of glass AE's in such devices requires consideration not only of thermo-optical characteristics of the glass used, but also of the way that these characteristics depend on temperature [Ref. 1-3].

Consider the case of a cylindrical AE with length much greater than its diameter. With volumetrically uniform heat release and uniform cooling of the lateral surface after the steady state is reached, a parabolic temperature distribution is set up in the AE

$$T(r)=T+\Delta T(1-\xi^2).$$

where T is the temperature of the lateral surface of the AE, ΔT is the temperature differential between the center and the surface of the AE, $\xi = r/R$, r is the running radius, R is the radius of the AE.

The following expression [Ref. 1] defines the optical difference of the path between the center and the point with running coordinate for radially (r) and tangentially (ϕ) polarized light for such a temperature distribution:

$$\Delta\mathfrak{L}_{r,\varphi} = l\Delta T\xi^2\left[P_0 \pm \frac{Q_0}{2} + \theta(T + 2\Delta T - \Delta T\xi^2)\right]. \qquad (1)$$

Here l is the length of the AE, P and Q are thermo-optical characteristics [Ref. 4] taken at the zero of temperature, $\theta = dP/dT$.

It should be pointed out that in Ref. 1 there was apparently a misprint in the given expression since the last term in parentheses is given as $\theta\Delta T^2\xi^2$. It is concluded in Ref. 1 that the minimum aberration in the AE is

$$\eta = (\Delta T)^2\theta\xi^2(2 - \xi^2) \qquad (2)$$

reached at a temperature of

$$T^0_{r,\varphi} = -(P_0 \pm {}^1/_2 Q_0)/\theta. \qquad (3)$$

For more detailed analysis of the behavior of the heat lens we introduce the quantity $P_T = P_0 + \theta T$ and determine the optical power of the lens from the formula

$$1/F = 2\Delta L/r^2. \qquad (4)$$

With consideration of formula (1), we find that the power of the heat lens is defined by the expression

$$1/F = 1/f_1 + 1/f_2, \qquad (5)$$

where

$$\frac{1}{f_1} = 2\Delta T\frac{l}{R^2}\left(P_T \pm \frac{Q_0}{2}\right); \qquad (6)$$

$$\frac{1}{f_2} = 2(\Delta T)^2\frac{l}{R^2}\theta(2 - \xi^2). \qquad (7)$$

The lens defined by expression (6) is spherical, and its power depends on the polarization of the light beam; lens (7) is aspherical, and its parameters are independent of polarization. Hints at such a nature of the heat lens without detailed analysis can be found in Ref. 3.

It is clear from expression (7) that the power of an aspherical lens is determined by the temperature differential between the center and edge of the AE and the quantity θ, depends on r and does not vanish anywhere, the change from center to edge being by a factor of two (the given property can be used to determine the quantity θ).

According to formulas (5) and (7), a heat lens for a given temperature differential ΔT can be compensated only for a certain value of r. Setting (5)

equal to zero, we can get the temperatures

$$T^{I}_{r,\varphi} = -\Delta T - (P_0 \pm {}^1/_2 Q_0)/\theta; \qquad (8)$$

$$T^{II}_{r,\varphi} = -2\Delta T - (P_0 \pm {}^1/_2 Q_0)/\theta, \qquad (9)$$

that correspond to compensation of the heat lens on the edge (r = R) and in the center (r = 0) of the AE and that differ from each other by the amount of the temperature differential ΔT.

Temperature $T^{II}_{r,\varphi}$ bounds the stability region of the laser cavity from below (below this temperature the heat lens becomes negative over the entire cross section of the AE). With increasing temperature the stability region expands, and at a temperature $T^{I}_{r,\varphi}$ the heat lens becomes positive over the whole cross section of the AE. It is significant that $T^{I}_{r,\varphi}$ and $T^{II}_{r,\varphi}$ depend not only on P, Q and θ, but on ΔT as well, i. e. on the pumping power. Thus the concept of the optimum temperature of the AE of the laser introduced in Ref. 3 becomes indeterminate.

Our mathematical analysis brings us to the question of accuracy of measurement of the thermo-optical constants P and Q by gradient methods (see for instance Ref. 4) that do not account for the temperature dependence of P. This should lead to an appreciable systematic error, which was indeed observed in Ref. 5.

Formulas (6), (7) or (8), (9) enable us to determine P_0 and Q_0 with consideration of the temperature dependence of P_0. To do this, we must know the optical power of the heat lens, and also θ and ΔT or $T^{I,II}_{r,\varphi}$. Measurements of this kind were done on cylindrical AE's 8 mm in diameter by 100 mm long made of GLS22, LGS-I and LGS-M phosphate glasses. Pumping was done by an ISP-600 tube placed together with the AE in a quartz monoblock with mirror reflecting surface. A liquid circulating at a rate of 5-15 l/min was used for cooling the AE and absorbing pumping emission shorter than 4500 nm. The recurrence rate of the pulses of stimulated emission varied over a range of 1-10 Hz, and the pumping energy in a pulse reached 100 J.

The focal length of the heat lens was determined by two methods: by the arrangement used in Ref. 6, and by using a three-slit Zernike interferometer (Fig. 1 [Ref. 8]), measuring the displacement of the focus Δc of an uaxiliary

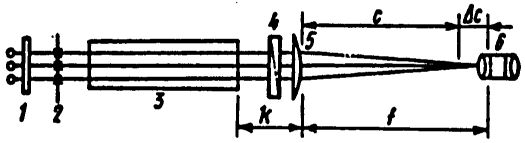

Fig. 1. Diagram of experimental setup: 1--quarter-wavelength plate; 2--diaphragm; 3--active element; 4--polarizer; 5--auxiliary lens; 6--ocular; f--focal length of auxiliary lens; Δc--displacement of the focus

lens. The principal measurements were done on a wavelength of 0.63 μm; an external diaphragm enabled measurement of focal length up to 50 m at any points of the cross section of the AE with accuracy no worse than ±10%.

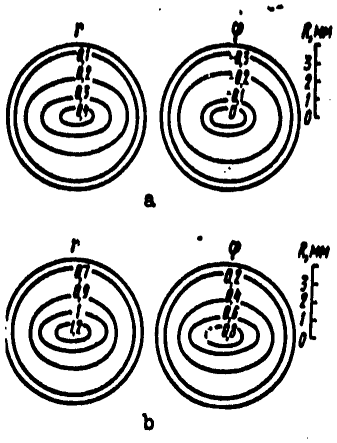

Fig. 2. Distribution of the heat lens power over the cross section of active elements made of LGS-M (a) and LGS-I (b) glass: r--for radial, ϕ—for tangential polarization; $\Delta T \approx 80°C$

The results of measurements for LGS-I and LGS-M glass are shown in Fig. 2. The lens had considerable spherical aberration and astigmatism. Lens power is close to a parabolic function of radius. Astigmatism is caused by imperfection of the cylindrical illuminating system and is expressed in the elliptical distribution of sections with the same focal length over the cross section of the AE. The axis ratio of the ellipse was close to 1:2.

The temperature differential was also determined by several methods: 1) from the temperature dependence of lens power (Fig. 3); 2) from the number of interference rings in the polarization pattern of birefringence; 3) by using a thermocouple inside an opening bored along the axis of the AE; 4) from the relative longitudinal extension of the AE due to heating. The lengthening with heating is proportional to the average temperature of the AE T_{av}; in the case of parabolic temperature distribution $\Delta T = 2T_{av}$.

All methods of measurement gave results that were close. The quantities P_0 and Q_0 were calculated by using the values of θ from Ref. 7; measurement results are given in Table 1. Also given there are the values of P_0 and Q_0 calculated from formulas (8) and (9) in terms of temperature T^I and T^{II}, from formulas (6) and (7) in terms of the heat lens power, and also the data of Ref. 3. The results agree well with the values of P and Q calculated by the analytical expressions of Ref. 4 (see Table 1). Comparison of the results for GLS22 with the results of Ref. 3 shows that the values of Q_0 coincide, while the value of P_0 with consideration of temperature dependence is less than the value given in Ref. 3 by $7 \cdot 10^{-7}$ deg^{-1}. For glasses with low P_0 this is a considerable error.

Given in Table 2 are the values of $T^I_{r,\phi}$ and $T^{II}_{r,\phi}$ obtained from the data of Fig. 3, and the distributions of heat lens power over the cross section of the AE (see Fig. 2) as compared with results of Ref. 1 on determination of the "optimum temperature" $T^0_{r,\phi}$ (formula (3)). It can be concluded from a comparison of the results that the values of $T^0_{r,\phi}$ are closer to the values of $T^I_{r,\phi}$ corresponding to the zero value of lens power in the center of the AE.

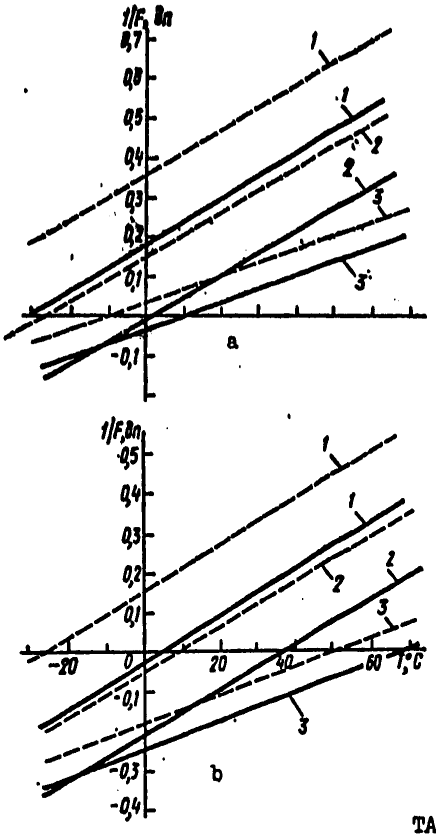

Fig. 3. Temperature dependence of heat lens power: $\Delta T = 28°C$; a) r-polarization; b) ϕ-polarization; 1--LGS-I; 2--GLS22; 3--LGS-M; $\xi = 0.5$ (broken line) and 0.82 (solid line)

∂n = diopters

TABLE 1

(5) Марка стекла	(1) Термооптические постоянные для $\lambda = 0{,}63$ мкм, 10^{-7} град$^{-1}$							
	Из выражений (8) и (9) (2)		Из выражений (6) и (7) (3)		Из аналитических выражений* [4] (4)		[3]**	
	P_0	Q_0	P_0	Q_0	P_0	Q_0	P_0	Q_0
(6) ГЛС22	—6	4,6	—7	4,5	—5	5,4	1	4
(7) ЛГС-И	—2,7	5,0	—3,7	5,2	—4	4,7		
(8) ЛГС-М	—6	5,5	—6,4	5,6	—6	5,8		

KEY: 1--thermo-optical constants for $\lambda = 0.63$ μm, 10^{-7} deg^{-1}
2--from expressions (8), (9)
3--from expressions (6), (7)
4--from analytical expressions* [Ref. 4]
5--Glass grade
6--GLS22
7--LGS-I
8--LGS-M

*P, Q calculated from thermal expansion, Young's modulus, Poisson's ratio and thermoelastic constants.

**Recalculated for $\lambda = 0.63$ μm using data for $W(\lambda)$ from Ref. 9.

TABLE 2

(1) Марка стекла	T^I, °C		T^{II}, °C		T^0, °C [1]	
	r	φ	r	φ	r	φ
(2) ЛГС-И	−25	5	−60	−35	—	—
(3) ГЛС22	2	42	−35	5	−25	4
(4) ЛГС-М	15	75	−15	40	—	—

KEY: 1--Glass grade
2--LGS-I
3--GLS22
4--LGS-M

Note. T^0 is recalculated for $\lambda = 0.63$ μm by means of expression (6); r, φ are the radial and tangential polarization respectively.

The problem of divergence of emission of a pulse-periodic laser is considerably complicated by the spherical aberration of the heat lens, and its examination requires a more complex approach than that used in Ref. 1. It can be concluded that with a reduction in θ while retaining optimum values of P_0 and Q_0 both the divergence of the radiation and its temperature dependence must decrease. The results of divergence measurement as a function of temperature for a number of glasses are shown in Fig. 4 (the measurements were made at a level of 25% of the total emission energy). The temperature behavior for GLS22 glass agrees with the data of Ref. 1; the divergence at the minimum is close to the diffraction limit. The value of the rate of change in divergence with temperature in the vicinity of 40°C for LGS-M glass is approximately 67% lower than for LGS-I and GLS22 glasses, which agrees with the ratio of the values of θ for these glasses.

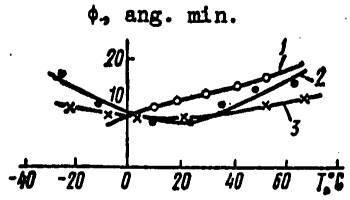

Fig. 4. Divergence as a function of temperature for glass grades LGS-I (1), GLS22 (2) and LGS-M (3)

Just how appreciable is the contribution that the value of θ makes to the power of the thermal lens induced in the AE of the laser in the pulse-periodic mode can be judged from the data of Table 3. It is only for GLS-1 with high P_0 that the contribution determined by θ is lower than P_0 and Q_0; for glasses with low P_0, which includes all athermal glasses, this contribution becomes decisive.

An investigation of the way that lasing depends on temperature (Fig. 5) has shown that maximum lasing energy occurs at a temperature that corresponds to the change of sign of the heat lens power for a radially polarized light beam, and the steepness of the drop increases with increasing θ. Thus our research leads to the following conclusions.

TABLE 3

(4) Марка стекла	1/f_1, дп (формула (6)) (1)	1/f_2, дп (формула (7)) (2)	(3) $\theta \cdot 10^7$, град$^{-1}$
(5) ЛГС-И	—0,15	0,33	0,14
(6) GLS22	—0,25	0,24	0,13
(7) ЛГС-М	—0,17	0,14	0,09
(8) GLS1	0,88	0,37	0,16 [2]

KEY: 1--$1/f_1$, diopters (formula (6))
2--$1/f_2$, diopters (formula (7))
3--$\theta \cdot 10^7$, deg^{-1}
4--Glass grade
5--LGS-I
6--GLS22
7--LGS-M
8--GLS-1

Note: r-polarization, $T_{surf} = 0°C$, $\Delta T \approx 28°$

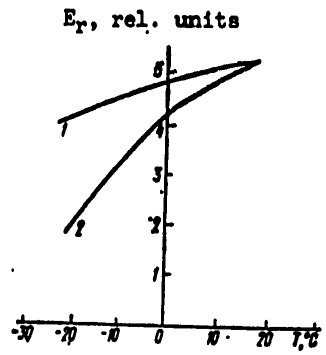

Fig. 5. Temperature dependence of lasing energy for glass grades LGS-M (1) and GLS22 (2)

1. The heat lens that arises under the influence of pumping in the AE of a solid-state laser in the pulse-periodic mode is determined by the thermo-optical constants P and Q, and also by the quantity $\theta = dP/dT$. Under steady-state thermal conditions with parabolic temperature distribution the lens formed by the contribution of P and Q is equivalent to a spherical lens, while the lens formed due to the contribution of θ is aspherical.

2. The temperature at which the power of the heat lens on the edge or in the center of the AE becomes zero depends on the pumping power, and therefore the glass cannot be characterized by a definite "optimum temperature."

3. By measuring the power of the heat lens and its temperature dependence for orthogonally polarized light beams we can find the values of the quantities P, Q and θ. It has been shown that disregarding the temperature dependence of P when measuring thermo-optical characteristics by the gradient method leads to systematic overstatement of the measurement results.

4. For athermal glasses, which have small values of the constants P and Q there is an increase in the role of the contribution of the aspherical lens determined by the quantity θ.

5. LGS-M glass, which has the minimum value of θ, has the weakest dependence of radiation energy and divergence on temperature.

REFERENCES

1. K. P. Vakhmyanin, A. A. Mak, V. M. Mit'kin, L. G. Popova, V. V. Raba, L. M. Soms, A. I. Stepanov, KVANTOVAYA ELEKTRONIKA, Vol 3, 1976, p 196.

2. O. S. Shchavelev, V. M. Mit'kin, V. A. Babkina, N. N. Bunkina, A. I. Stepanov, OPTIKO-MEKHANICHESKAYA PROMYSHLENNOST', No 1, 1975, p 30.

3. V. M. Mit'kin, O. S. Shchavelev, N. N. Bunkina, ZHURNAL PRIKLADNOY SPEKTROSKOPII, Vol 23, 1975, p 218.

4. A. A. Mak, V. M. Mit'kin, L. N. Soms, A. I. Stepanov, O. S. Shchavelev, OPTIKO-MEKHANICHESKAYA PROMYSHLENNOST', No 9, 1971, p 42.

5. Yu. A. Anan'yev, N. I. Grishmanova, ZHURNAL PRIKLADNOY SPEKTROSKOPII, Vol 12, 1970, p 668.

6. A. A. Mak, L. N. Soms, A. I. Stepanov, A. B. Sudakov, OPTIKA I SPEKTROSKOPIYA, Vol 30, 1971, p 1081.

7. A. K. Gromov, A. A. Izyneyev, Yu. L. Kopylov, V. B. Kravchenko, FIZIKA I KHIMIYA STEKLA, Vol 2, 1976, p 444.

8. Zernike, J. OPT. SOC. AMER., Vol 40, 1950, p 326.

9. V. V. Blazhko, M. M. Bubnov, Ye. M. Dianov, A. V. Chikolini, KVANTOVAYA ELEKTRONIKA, Vol 3, 1976, p 1151.

6610
CSO: 1870

PHYSICS

UDC 621.373.8.029.71

GASDYNAMIC PERTURBATIONS OF THE FLOW IN PULSE-PERIODIC CO_2 LASERS. I. CONVECTIVE REMOVAL OF HEATED GAS FROM THE DISCHARGE REGION

Moscow KVANTOVAYA ELEKTRONIKA in Russian Vol 6, No 1, Jan 79 pp 177-183

[Article by V. Yu. Baranov, V. G. Niz'yev and S. V. Pigul'skiy]

[Text] A Mach-Zender interferometer is used to study gasdynamic phenomena that lead to limitation of the pulse recurrence frequency in periodic CO_2 lasers. Experiments were done on a model facility in nitrogen, carbon dioxide and a laser mixture.

Introduction

The output parameters of a pulse-periodic carbon dioxide laser are determined first of all by the working efficiency of the electrode system in the case of isolated pulses, and secondly by the extent to which these parameters are retained when the laser operates at a high pulse recurrence frequency (prf). Quite significant advances have been made in the development of electrode systems for pulse lasers [Ref. 1, 2]: the specific output energy is 20-26 J/(l·atm) at an efficiency of 10-17%.

As far as pulse-periodic CO_2 lasers are concerned, to maintain maximum discharge parameters in an individual pulse it is necessary to work with a prf $f \ll f_0 = v_0/b_0$ (v_0 is the velocity of the gas flow, b_0 is the width of the working part of the electrodes along the flow) since only in this case can arcing be avoided. For instance in Ref. 3, 4 this frequency limitation is very great: $f_0/f = 10$. The attainment of a prf close to f_0 in Ref. 5 is not indicative since the specific output energy in this case did not exceed 2.5 J/(l·atm).

Problems of limitation of the prf were considered in particular in Ref. 6. Experiments were done on an electrode system with UV pre-ionization. The authors discuss the possible mechanisms of limitation of the average power for different energies W invested in the discharge in an individual pulse. At a low prf the power limitation is due to contraction of the discharge

with an increase in the input in an individual pulse above some limiting value W_0. Gasdynamic effects at such frequencies are insignificane.

In the other limiting case (very low energy inputs) the authors attribute the limitation of prf to the presence of a boundary layer on the electrodes. At intermediate values of W, the authors of Ref. 6 are of the opinion that a decisive part is played by the increase in size of the heated gas plug due to adiabatic expansion. Shock waves (SW) are mentioned in the work, but their role in prf limitation is not explained. Direct measurements of the degree of gas nonuniformity in the discharge region were not done in the research. Estimates on adiabatic expansion are given for a specific system with electrodes protruding into the flow. Calculations on boundary layers are done approximately without consideration of the actual trajectory of motion of the particles in the layer; the increase in energy release at the electrodes was not taken into consideration, and heat drift to the electrode was estimated only with respect to order of magnitude.

Ref. 7 discusses the possible influence of SWs arising in the gas channel after pulsed energy input. The limitation of the prf is associated with the entry of gas into the discharge region that has already been heated due to dissipation of energy on the front of SWs propagating upstream. Estimates of this effect are not given in the article, and indirect proofs can be interpreted in more than one way. It is shown in Ref. 8 in particular that gas heating upstream due to dissipative processes is negligible.

In Ref. 9 a numerical solution is found for equations of one-dimensional unsteady gasdynamics to determine the nature of establishment of a quasi-steady state in a space closed for perturbation with gas flow with periodic energy release. The main conclusion of the work is: at a prf close to f_0 we get a quasi-steady level of values of gas temperature and density in the working channel that differ from the undisturbed values by 10-30%. It should be stated that numerical methods of solving this problem have not yielded a physically clear solution. They are special in nature, and are applicable to evaluation of the influence of wave processes only on a specific installation.

Our research is devoted to the study of gasdynamic phenomena that take place in pulse-periodic lasers, and their effect on prf limitation.

General analysis of efficiency of pulse-periodic CO_2 lasers

The generally accepted physical parameters that characterize the efficiency of operation of a pulsed CO_2 laser are the specific radiation energy output and the laser efficiency. Since the radiation output depends on the energy input, and this process is isochoric in laser mixtures, it would be more accurate to refer the energy input, and hence the specific radiation energy output to the internal energy of the gas that is in the discharge region, this energy being equal to $p_0V/(\gamma-1)$, where p_0 is the pressure of the undisturbed gas, V is the volume of the discharge region and γ is the

adiabatic exponent. This effect becomes all the more significant since an important part in pulse-periodic lasers is played by gasdynamic effects in which a characteristic of intensity in isochoric energy input is the quantity $w = W/[p_0V/(\gamma - 1)]$.

Thus by analogy with pulsed CO_2 lasers it is suggested that two parameters be used for the characteristic of effectiveness of pulse-periodic lasers: the efficiency of the installation $\eta_{\text{п}}$ and the ratio of average emission power G to internal energy of the gas stream flowing through the discharge region in 1 s. This parameter can obviously be expressed as

$$g = G/[p_0 S v_0/(\gamma - 1)] = w_0 \eta_{\text{п}} [Wf/(W_0 f_0)], \qquad (1)$$

where v_0 is the velocity of gas flow in the middle of the channel, S is the cross sectional area of the flow in the discharge region, W_0 is the maximum value of invested energy in operation with isolated pulses; $w_0 = W_0/[p_0V/(\gamma-1)]$.

As can be seen from the given formula, the effectiveness of a pulse-periodic laser is determined first of all by the parameters w_0 and $\eta_{\text{п}}$ that characterize laser operation in isolated pulse conditions, and secondly by how much average power the electrode system can put into the gas in operation in the periodic mode as compared with $W_0 f_0$. Let us note that for the pulse recurrence rate where superposition of hot gas plugs does not take place, i. e. where the hot gas plug is totally removed from the discharge region by the next pulse, the laser efficiency $\eta_{\text{п}}$ is close to its value for operation in the isolated pulse mode. Thus in order to increase g it is essential to study the question of prf limitation, i. e. the relation

$$f/f_0 = \varphi(W).$$

Description of experimental facilities

Research was done on an installation with closed gas-pumping cycle (Fig. 1) with especially pure nitrogen in which the total content of impurities did not exceed 0.001%, commercial CO_2 and a laser mixture of $CO_2:N_2:He = 2:2:3$.

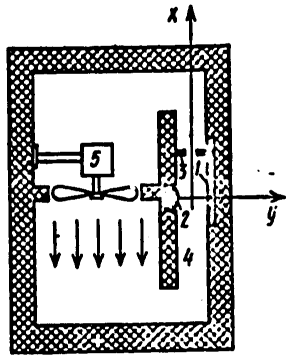

Fig. 1. Diagram of the experimental chamber: 1--anode; 2--cathode; 3--anode of auxiliary discharge; 4--gas channel; 5--blower

The gas pressure in the loop was 100 mm Hg. The gas flow in the discharge region was formed by a gas channel of constant cross section with flow length of 29 cm. Both ends of the channel were open, the electrode system was located in the center. The velocity of gas flow in the discharge region was 4 m/s, and a system with UV pre-ionization was used [Ref. 10]. The electrodes were mounted in the walls of the channel so that disturbance of the gas flow would be minimized. The width of the working part of the electrodes with respect to the flow was 1.1 cm, distance between them was 1.3 cm and length was 15 cm. An electric diagram of the facility is shown in Fig. 2.

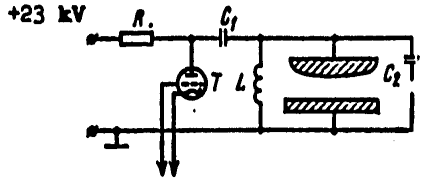

Fig. 2. Electric diagram of the facility: C_1--working capacitance 3.5 nF; C_2--capacitance of auxiliary discharge; T--TGI1-1000/25 thyratron; R--charging resistor; L--inductance

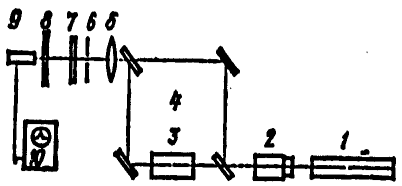

Fig. 3. Diagram of interferometer installation: 1--LG-36 laser; 2--collimator; 3--experimental chamber; 4--Mach-Zander interferometer; 5--lens; 6--diaphragm; 7--light filter; 8--screen with aperture; 9--FEU-29 photomultiplier; 10--S1-37 oscilloscope

To measure gas density, space and time interference patterns were obtained on a Mach-Zander interferometer. A Q-switched ruby laser was used for finding the space interference patterns. Emission pulse duration was 50 ns. In studying gasdynamic phenomena associated with periodic energy input, an LG-36 He-Ne laser was used (Fig. 3) as the source of emission. The laser output was converted by a collimator to a wide beam and sent to the input mirror of the interferometer. The ends of the chamber on the emission path were covered by optical glass so that the discharge gap and upstream and downstream parts of the channel fell into the field of view. The interference pattern in the discharge region was projected onto a screen by a lens. Light passing through an aperture 0.5 mm in diameter in the screen was incident on the cathode of the FEU-29 photomultiplier. With a change of gas density in the chamber there is a shift of the interference pattern, and the signal from the photomultiplier is registered on the S1-37 oscilloscope. By shifting the screen and the photomultiplier, the time change in gas density could be observed at any point of the discharge gap as well as upstream and downstream. To eliminate luminous interference from the discharge, a light filter was used as well as a diaphragm placed at the focus of the lens.

Pulse discharge in quiescent gas

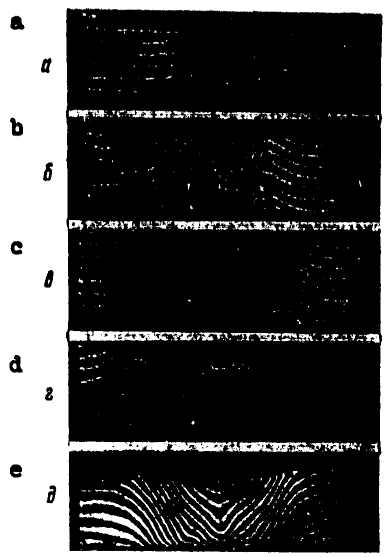

Fig. 4. Interference patterns of the discharge region taken 2 (a), 8 (b), 16 (c), 30 (d) and 500 μs (e) after a pulse discharge in CO_2. The size of the discharge in the direction of photography was 25 cm. $C_1 = 10$ nF.

Shown in Fig. 4 are interference patterns of gasdynamic perturbations in the discharge gap taken with different delay times relative to a pulse discharge in CO_2. On the interference patterns we can see the electrode SWs that indicate elevated energy release at the electrodes. From the rate of propagation of the electrode SW we can estimate the gas temperature in the electrode layer. According to estimates, at the cathode in nitrogen it may reach 1000 K, and the gas heating in the electrode layer in CO_2 is still higher.

Acoustic waves propagate to the sides of the discharge, their intensity in CO_2 being higher than in nitrogen. Energy release as heat in commercial CO_2, just as in the laser mixture that we used, takes place more rapidly than the propagation of gasdynamic perturbations to characteristic distances, and therefore with fair accuracy the size of the heated gas plug after expansion can be calculated by using the formulas of the adiabatic process:

$$b/b_0 = (1+w)^{1/\nu}, \qquad (2)$$

where b_0 and b are the dimensions of the heated gas plug before and after expansion. For instance in our case the characteristic size of the plug in CO_2 at $t \geq 100$ μs, $b = 2.3$ cm, and $w = 1.7$. Then from formula (2) we get $b_0 = 1.1$ cm, which is in good agreement with the size of the luminescent region in pulsed discharge.

Shown in Fig. 5 are the time dependences of change in gas density in the center of the discharge gap in CO_2, N_2 and the laser mixture in the absence of flow as determined from processing of time interference patterns. The reduction in gas density is due to expansion when heated during discharge or as a result of relaxation of the energy stored in the vibrational levels of molecular gases into heat. Restoration of the density to the original value can be attributed to heat drift to the electrodes.

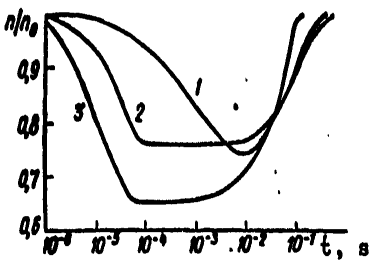

Fig. 5. Time change of gas density in the center of the discharge gap after a pulse discharge for N_2 (1), CO_2 (2) and the laser mixture (3)

Expansion of heated gas plug in the flow

As has already been mentioned, when a pulse-periodic CO_2 laser uses an electrode system that operates effectively in the pulse mode, the experimentally achieved frequency differs appreciably from f_0. In our case $f_0 \approx 360$ Hz. The dependence of the maximum attainable prf on the energy invested in an individual pulse as found on our setup is shown in Fig. 6.

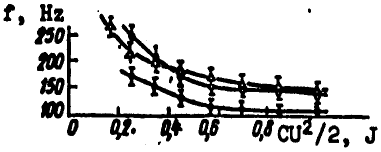

Fig. 6. Dependence of prf on energy invested in the discharge in an individual pulse: o--CO_2; •--N_2; Δ--laser mixture

It is readily seen that the prf limitation determined from formula (2) cannot explain the experimental results. For instance in CO_2 when $C_1U^2/2 = 0.9$ J, $w = 0.97$ and $b/b_0 = f_0/f = 1.68$, i. e. $f = 213$ Hz whereas the observed frequency $f = 140$ Hz (see Fig. 6). However we must also consider the fact that as the hot gas plug is carried off it continues to expand along the flow due to heat conduction.

Fig. 7. Typical oscillogram of signal from the photomultiplier after an isolated pulse in the presence of gas flow

Shown in Fig. 7 is a typical oscillogram of the signal from the photomultiplier where the observation point had coordinates $x = 13$, $y = 0$ mm (see Fig. 1). Fixed on the oscillogram is the passage of the hot gas plug through the observation point. The break in the center of the oscillogram corresponds to minimum gas density. Fig. 8 gives the profiles of gas density at different instants as determined from processing of time interference patterns. According to estimates,

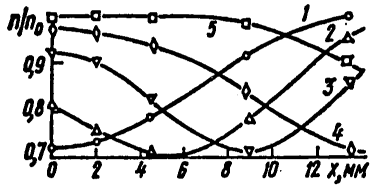

Fig. 8. Density profiles in a stream of N_2 ($y = 0$) for $t = 0.8$ (1), 1.6 (2) 2.6 (3), 3.7 (4) and 6 ms (5)

the coefficient of diffusion in N_2 and CO_2 is about 15 cm^2/s, which shows the turbulent nature of gas flow in the channel. For instance the Reynolds number in the case of N_2 is equal to $Re = v_0 h/\nu = 3700$, where $h = 1.3$ cm is the distance between the walls of the channel, ν is kinematic viscosity (for nitrogen $\nu = 0.4$ cm^2/s). As can be seen from Fig. 8, for the given energy input by the beginning of the next pulse in the middle of the gas channel the density becomes constant and equal to the undisturbed value over the entire extent of the discharge region, i. e. the prf limitation cannot be explained by adiabatic expansion of the heated gas plug and turbulent heat conduction along the flow.

Boundary layers

When gas flows near a wall, a boundary layer is formed in which the gas velocity varies from zero at the wall to the maximum at the surface of the layer. The rate of renewal of the mixture in the electrode layer was observed to be lower than in the center of the discharge gap in our experiments also (Fig. 9). The gas velocity at a distance of 1 mm from the electrode is approximately 2/3 of the flow velocity in the center of the discharge region. Measurements were made of gas density at a point with coordinates $x = 7$ mm, $y = 5$ mm. These measurements showed that at the limiting frequency of $f = 140$ Hz, by the time of the next pulse the gas density at the given point is 4% lower than the gas density in the center of the discharge gap. Such inhomogeneity of the gas density with respect to the width of the electrode may lead to arcing since it is known that an electrode system with UV pre-ionization must be carefully made for stable operation with special shaping of the electrodes to eliminate edge effects and also requires careful adjustment.

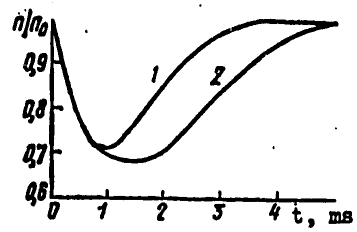

Fig. 9. Time change of density in the center of the discharge region (1) and at the electrode (2) ($x = 0$, $y = 5$ mm) for N_2

Estimates were made of the influence of inefficient renewal of the mixture in boundary layers [Ref. 11]. As the computational rate of gas exchange the authors took the velocity of a particle moving in the layer in a trajectory such that the time of its convective removal and the characteristic time of heat drift to the electrode are equal. The approximate formula for the case where the laminar layer is formed at distance "a" from the centers of the electrodes when $a \gg b$ takes the form

$$f_0/f = 1{,}96\,(b/b_0)(a/b)^{1/3}, \qquad (3)$$

where b is the dimension of the heated gas region established after equalizing of the pressure in the discharge region and that defined by formula (2).

Analogous calculations for a turbulent layer give the following expression:

where Re_a is the Reynolds number when the distance "a" is taken as the linear dimension.

An estimate by formula (4) for $C_1U^2/2 = 0.9$ J, $a = 14.5$ cm gives $f_0/f = 2.3$, i. e. $f = 156$ Hz with experimentally attainable frequency of $f = 140$ Hz. In more exact calculation it is necessary to solve an unsteady two-dimensional problem with consideration of increased energy release at the electrodes and heat conduction with respect to the flow, since comparatively small inhomogeneities of gas density may lead to arcing.

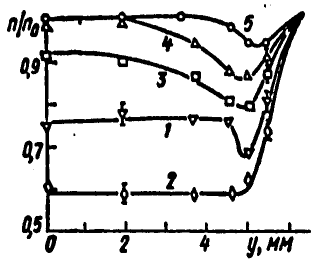

Fig. 10. Density profiles of the laser mixture across the flow at times $t = 0.5$ (1), 1.2 (2), 3.0 (3), 3.8 (4) and 6 ms (5). Isolated pulses, $x = 7$ mm.

Fig. 10 illustrates what we have said. It gives the profiles of gas density distribution along the y-axis for $x = 7$ mm at different times. The shape of the profile when $t = 0.5$ ms can be attributed to increased electrode heating of the gas. By time $t = 1$ ms the center of the heated gas plug is in the investigated cross section of the channel. At later times in the electrode region the gas is effectively cooled by heat drift to the electrode, and in the center of the discharge gap the hot gas plug is carried away by the flow at velocity v_0. Quite clear on Fig. 10 is the region where the recovery of gas density takes place at the minimum velocity.

In addition to the effects described above, acoustic waves arise in pulse-periodic energy input. As we will show in the second part of the article, under the conditions of our setup, density inhomogeneities associated with such waves are at least an order of magnitude less than those that arise in boundary layers. This is also emphasized by the fact that at a high prf in energy stressed modes the arc appears downstream on the electrode, which agrees with the data of Ref. 12. The inhomogeneities in gas density that arise in the discharge gap lead to inhomogeneities of the parameter E/n (E is equal to the ratio of the applied voltage to the distance between electrodes h). Thus under the conditions of our setup the density gradients in the boundary layers are responsible for the prf limitation.

REFERENCES

1. M. C. Richardson et al., IEEE L., QE-9, 1973, p 236.

2. R. Dumanchin, I. C. Farcy, Int. Quantum Electr. Conf., Kyoto, 1970.

3. R. Dumanchin,, LASER FOCUS, No 8, 1971, p 32.

4. R. Dumanchin, M. Michon et al., IEEE J., QE-8, 1972, p 163.

5. D. C. Hamilton, D. J. James, S. A. Rawsden, J. PHYS. E., Vol 8, 1975, p 849.

6. G. S. Dzakowic, S. A. Wutzke, J. APPL. PHYS., Vol 44, 1973, p 5061.

7. A. A. Vedenov, S. V. Drobyazko, V. N. Knizhnikov, V. B. Trundayevskiy, TEPLOFIZIKA VYSOKIKH TEMPERATUR, Vol 13, 1975, p 425.

8. V. Yu. Baranov, G. M. Klepach, D. D. Malyuta et al., TEPLOFIZIKA VYSOKIKH TEMPERATUR, Vol 15, No 2, 1977.

9. S. V. Golubev, A. S. Kovalev et al., DOKLADY AKADENII MAUK SSSR, Vol 225, 1975, p 1300.

10. N. H. Burnett, A. A. Ofenberger, J. APPL. PHYS., Vol 44, 1973, p 3617.

11. V. Yu. Baranov, V. V. Breyev, D. D. Malyuta, V. G. Niz'yev, KVANTOVAYA ELEKTRONIKA Vol 4, 1977, p 1861.

12. V. I. Kozlov, A. S. Korablev, PIS'MA V ZHURNAL TEKHNICHESKOY FIZIKI, Vol 3, 1977, p 24.

6610
CSO: 1870

PHYSICS

UDC 621.373.8.029.71

GASDYNAMIC PERTURBATIONS OF THE FLOW IN PULSE-PERIODIC CO_2 LASERS. II. ACOUSTIC WAVES

Moscow KVANTOVAYA ELEKTRONIKA in Russian Vol 6, No 1, Jan 79 pp 184-188

[Article by V. Yu. Baranov, B. Ya. Lyubimov, V. G. Niz'yev and S. V. Pigul'skiy]

[Text] The gas channel of a pulse-periodic CO_2 laser is considered as an acoustic resonator. Experimental and theoretical studies are done on acoustic oscillations in such a resonator, and on the influence that they have on limitation of pulse recurrence frequency. The results of numerical calculation are compared with experimental data.

Pulsed energy input to gas is accompanied by the arisal of acoustic waves. With sufficiently large energy inputs into a discharge, these waves may take on the nature of weak shock waves (SW) that propagate upstream and downstream from the discharge gap and are reflected from the ends of the gas channel. The authors of Ref. 1 relate the limitation of pulse recurrence frequency (prf) with heating of gas upstream and downstream due to energy dissipation on the SW front. However, the work does not give the corresponding estimates and experimental data. As shown in Ref. 2, gas heating due to SW dissipation is quite minor as a consequence of the fact that the SWs that arise are weak for typical energy inputs in laser systems.

On the facility described in the first part of this article we measured the gas temperature by thermocouples in the flow above the discharge region. Heating of the gas entering the discharge region was about 10 K at a flowrate of 4 m/s, specific energy input of 360 J/(l·atm) and pulse recurrence frequency of 120 Hz. Inhomogeneities of gas density on the width of the electrodes amounted to about 0.3%.

On the other hand, consideration should be taken of the fact that the gas channel of a laser is an acoustic resonator subjected to periodic external action. In our experiments, the channel forming the gas flow took the form

of a uniform acoustic open-ended cavity 29 cm long with the electrodes located in the center. Such a resonator has a spectrum of natural frequencies $\nu_m = mc/(2L)$, where c is the speed of sound, L is the length of the cavity, m = 1, 2, 3,... With consideration of the fact that the discharge acting as the source of perturbations takes place in the middle of the cavity, it can be concluded from general considerations that no oscillations corresponding to even m will be excited.

Besides, in our setup $f_0 < \nu_1$ ($f_0 = v/b_0$, v is the flow velocity, b_0 is the width of the working part of the electrodes), which in further analysis allows us to restrict ourselves to consideration of oscillation ν_1, since the effectiveness of excitation of oscillations of higher order is considerably lower. Oscillation ν_1 can also be excited with operation in the isolated pulse mode since frequencies that coincide with ν_1 or are multiples of it may be present in the Fourier expansion of the space-time function of energy input. The effectiveness of excitation of a standing wave, and consequently its amplitude are low in this case. The standing wave damps out in time as a consequence of dissipation of its energy on the ends.

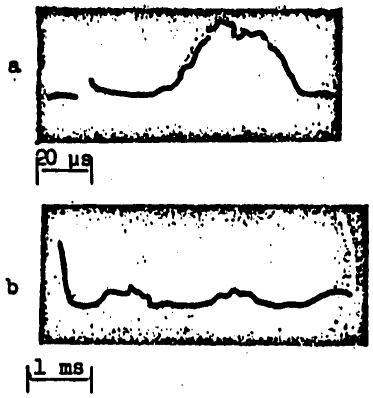

Fig. 1. Oscillograms of the waves of compression (a) and expansion (b) that arrive in the discharge region after pulsed energy input

Shown in Fig. 1a is an oscillogram that corresponds to the compression wave arriving at the point of observation after discharge in nitrogen. Subsequently waves of expansion and compression reflected from the ends arrive in the discharge region (Fig. 1b).

With periodic energy input, resonant excitation of oscillation ν_1 is possible in the case where $\nu_1/f = N$ (N is an integer). This case corresponds to the arrival of a compression wave in the discharge region. The amplitude of oscillation ν_1 will be the greater, the closer N is to unity (Fig. 2). When $\nu_1/f = N + \frac{1}{2}$, the effectiveness of excitation of standing waves is minimum. This can be clearly seen in Fig. 3. When the pulse recurrence frequency is such that the next pulse corresponds to arrival of an expansion wave in the discharge region, no oscillations of gas density are observed in the discharge gap during the time between pulses. On the other hand if the next pulse arrives at the

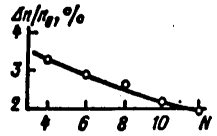

Fig. 2. Amplitude of a standing wave in nitrogen as a function of N

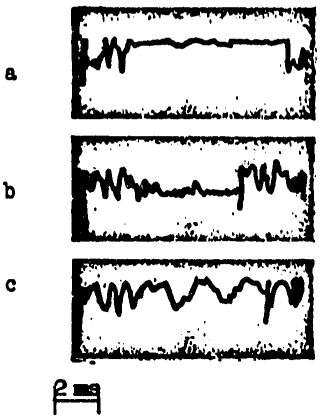

Fig. 3. Oscillograms of signals from the photomultiplier for cases where the next pulse occurs at the instant of arrival of the 5-th (a) and 4-th (b) expansion waves, and also the 4-th compression wave (c) in the discharge gap in CO_2

instant when a compression wave is in the discharge gap, a standing wave will also be effectively excited, and oscillations of the gas density will be observed in the discharge gap. The damping of standing waves with time is illustrated by Fig. 4.

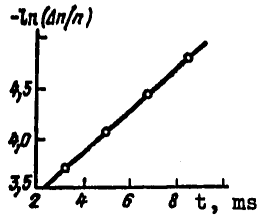

Fig. 4. Damping of a standing wave with time

Theoretical model

Small longitudinal oscillations of the gas in the absence of an electric discharge in the chamber are described in the linear approximation by the system of equations

$$\frac{\partial v}{\partial t}+v_0\frac{\partial v}{\partial x}=-\frac{1}{\rho_0}\frac{\partial p}{\partial x},$$

$$\frac{\partial \rho}{\partial t}+v_0\frac{\partial \rho}{\partial x}+\rho_0\frac{\partial v}{\partial x}=0,$$

$$\rho_0 T_0\left(\frac{\partial S}{\partial t}+v_0\frac{\partial S}{\partial x}\right)=Q, \qquad (1)$$

where v, ρ, p, S are the perturbed values of velocity, density, pressure and entropy of the flow, v_0, ρ_0, T_0 are corresponding undisturbed values. The quantity Q denotes the power invested per unit of gas volume. By introducing the velocity potential $v=\partial\Phi/\partial x$, system (1) can be reduced to a single equation

$$\left(\frac{\partial}{\partial t}+v_0\frac{\partial}{\partial x}\right)^2\Phi-c^2\frac{\partial^2\Phi}{\partial x^2}=\frac{Q}{\rho_0 c_v}, \qquad (2)$$

where c is the speed of sound in the gas, $c_v=1/(\gamma-1)$, γ is the adiabatic exponent.

The influence of the open ends of the cavity reduces to two effects: some reduction of natural frequencies, which can be accounted for by a slight increase in the length of the cavity by an amount of the order of h (the height of the channel), and emission from the open end of the waveguide.

Before going on to analysis of the spectrum of vibrations in the channel, we derive a system of eigenfunctions for the free vibrations in an acoustic resonator with flow. Equation of potential (2) must be solved for $Q=0$ with boundary condition $p=0$ when $x=0$, L, which when $v_0\neq 0$ takes the form

$$\frac{\partial \Phi}{\partial t} + v_0 \frac{\partial \Phi}{\partial x}\Big|_{x=0,L} = 0.$$

Assuming that the eigenfunctions are proportional to $e^{-i\omega t}$, we find ($M = v_0/c$)

$$\omega_n = (\pi n/L)(1-M^2) = 2\pi v_0 n(1-M^2),$$

i. e. the natural frequencies of the cavity are somewhat lower than in the case of a quiescent gas.

Let us now consider impact excitation of the cavity, disregarding gas flow (in our case $M \gtrsim 10^{-2}$). Let us find the Green's function for concentrated periodic excitation with more general boundary conditions that include both radiation and reactive effects on the free end. In the spectral representation we introduce the boundary conditions: at $x=0$ $(i\omega\Phi+c\alpha)(\partial\Phi/\partial x)=0$; at $x=L$ $(i\omega\Phi-c\alpha)(\partial\Phi/\partial x)=0$.

In the general case $\alpha = \alpha(\omega)$. It can be readily seen that for a traveling wave the coefficient of reflection from the end for such boundary conditions takes the form $z(\omega) = (\alpha - 1)/(\alpha + 1)$.

When $\alpha = 1$, the acoustic impedance z vanishes, which corresponds to total emanation of vibrations from the volume, and the absence of reflected waves. The next characteristic case: $\alpha = 0$, which corresponds to $z = -1$, i. e. total reflection from the open end takes place. When $\alpha \gg 1$, $z=1$ (typical of the closed end). We can make certain that the natural oscillations have real frequencies and do not damp out if $|z| = 1$, and the influence of the ends reduces to phase shifts and a change in the spectrum of oscillations. In the general case the natural oscillations are found from the condition $z^2 \exp(-2i\omega L/c) = 1$. By using $z = z(\omega)$ we can study an extensive class of models while remaining within the framework of the linear approximation, in particular we can describe the change in pulse shape with reflection from the end, and use a model to account for the process of nonlinear change in the wave as it propagates in the channel. Formally, $z(\omega)$ is the Fourier transform of the signal reflected from the boundary if the incident signal took the form of a δ-function.

Among the specific one-parameter models of $z(\omega)$, mention should be made of the model

$$z(\omega) = -1/(1 + i\omega/\omega_0). \qquad (3)$$

This impedance has all the necessary properties: at low frequencies $z(0) = -1$; at high frequencies reflection is low since $z(\omega) \sim -1/\omega$. By using (3), we can find that with the n-th reflection of a δ-shaped pulse we get a signal $(\omega_0 t)^{n-1} e^{-\omega_0 t}/n!$

The Green's function -- response to the instantaneous action at a point -- is most simply constructed on the basis of a quantitative examination of the receiver and source, which are located in the center of the channel at an equal distance from the open ends. After an instantaneous discharge

has taken place, the pressure distribution in the channel can be described by a δ-function with amplitude Q_0. In accordance with the particulars of acoustic analysis, the signal is split into two signals with half amplitude moving at the speed of sound toward opposite ends of the channel. In the Fourier representation, these signals have the shape of z. After reflection and return to the point of observation as a result of repeated passages the Fourier transform of the signal at the observation point acquires the form

$$z\exp(-i\omega L/c)+z^3\exp(-2i\omega L/c)+z^5\exp(-3i\omega L/c)+\ldots$$

The sum of this series is $z\exp(-i\omega L/c)/[1-z\exp(-i\omega L/c)]$.

Carrying out Fourier transformation, we find

$$p(t)=Q_0\int_{-\infty}^{\infty}\frac{z(\omega)\exp(-i\omega L/c)}{1-z(\omega)\exp(-i\omega L/c)}\exp(i\omega t)\,d\omega.$$

This expression describes time changes of pressure in the center of the channel. The original signal is lacking in this formula: it can be readily accounted for by addition to p(t).

With periodic action of short pulses repeating in time τ, the pressure by instant $t<\tau$, i. e. before the moment of arrival of the next pulse, is defined as

$$p(t)=Q_0\int_{-\infty}^{\infty}\frac{z(\omega)\exp(-i\omega L/c)}{1-z(\omega)\exp(-i\omega L/c)}\cdot\frac{\exp(i\omega t)}{1-\exp(i\omega\tau)}\,d\omega. \qquad (4)$$

This formula enables us to analyze both resonant effects and effects of accumulation in the case of steady-state periodic action. If it is necessary to know the cumulative effects by the time of arrival of the next pulse, then in (4) we must set $t=0$ or $t=\tau$, which is equivalent in virtue of the periodicity of the phenomenon. To account for the velocity of the flow, it is sufficient to substitute $(L/c)(1-M^2)^{-1}$ for L/c in the exponential functions. Integral (4) is easy to calculate by writing it as a series in terms of the residues at the poles of the integrand. The results of calculation at time $t=\tau$ are shown in Fig. 5. The calculated curve agrees qualitatively with experimental results.

Conclusions

Thus in the case of pulse-periodic energy input, depending on the prf, oscillations of gas density may be present or absent in the discharge gap, which is due to excitation of a standing wave in the acoustic resonator, or the absence of such a wave. However, the amplitude of the oscillations of gas density at the crest of the standing wave does not exceed 4% (see Fig. 2), which creates inhomogeneities of gas density of no more than 0.25% on the width of the electrode. Such inhomogeneities cannot lead to limitation of the prf. Therefore, as has already been stated in the first part of the article, the authors attribute prf limitation to inefficient renewal of the mixture in the electrode layers.

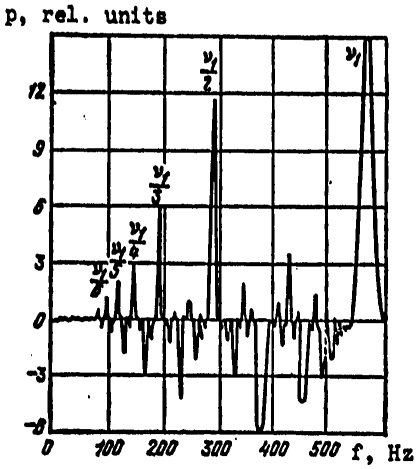

Fig. 5. Dependence of pressure in the discharge region on prf as calculated from formula (4) at $t = \tau$

However, if the natural frequency of the acoustic resonator in the pulse-periodic mode falls within the working range of the prf, or if N is equal to a small integer, the amplitude of the stimulated standing wave may be great, and the inhomogeneities of gas density thus set up may lead to arcing. This should be taken into consideration when designing the gas channel of a pulse-periodic CO_2 laser.

REFERENCES

1. A. A. Vedenov, S. V. Drobyazko, V. N. Knizhnikov, V. B. Turundayevskiy, TEPLOFIZIKA VYSOKIKH TEMPERATUR, Vol 13, 1975, p 425.

2. V. Yu. Baranov, G. M. Klepach, D. D. Malyuta et al., TEPLOFIZIKA VYSOKIKH TEMPERATUR, Vol 15, 1977, p 972.

6610
CSO: 1870

PHYSICS

UDC 621.378.33

OPTIMIZING A 10 kW CLOSED-CYCLE CO_2 PROCESS LASER

Moscow KVANTOVAYA ELEKTRONIKA in Russian Vol 6, No 1, Jan 79 pp 204-209

[Article by G. Abil'siitov, L. I. Antonova, A. V. Artamonov, V. S. Golubev, S. V. Drobyazko, Yu. A. Yegorov, N. I. Natsuro, A. V. Kazhidub, F. V. Lebedev, Yu. M. Senatorov, Ye. M. Sidorenko, V. V. Sumerin, V. B. Turundayevskiy and V. M. Frolov]

[Text] A report on optimization of the electro-optical system, the composition and degree of renewal of the working mixture of a closed-cycle CO_2 process laser, resulting in an increase in output power of the facility to 10 kW with overall efficiency of the order of 8%.

1. An earlier paper [Ref. 1] told of the development of a steady-state fast-flow closed-cycle CO_2 process laser with emission power of 6 kW in which a self-maintained transverse DC discharge was used for excitation of the active medium, and emission was stimulated in a single-pass unstable cavity located in direct proximity to the discharge chamber. As pointed out in Ref. 1, such an electro-optical arrangement has fairly low efficiency since the length of the discharge chamber, which is limited because of relaxation processes, does not permit attainment of high specific (per unit of mass) energy inputs W_g, and the concomitant low gain of the medium in the cavity for the actually realizable transparency of the latter (20-30%) does not permit efficient transformation of the stored vibrational energy of molecules into emission.

This flaw can be almost totally eliminated by using an electro-optical laser arrangement with a combined multiple-pass cavity [Ref. 2]. In the first place, this obviates the limitations imposed by collisional relaxation, and the necessary values of W_g can be realized by increasing the length of the chamber; in the second place, with an increase in the number of passes there is an increase in the optical length of the cavity, enabling operation with greater transparency of the optical system. Naturally a large number of passes in the cavity leads to an increase in the number of elements in the optical arrangement, increases the energy losses on the mirrors and

imposes higher requirements on the construction of adjustment members. According to preliminary estimates, use of a combined cavity arrangement could increase electro-optical efficiency η_{eo} (the fraction of energy supplied to the positive discharge column that is converted to emission) by a factor of 1.5-2.

This paper gives the results of experimental studies done on a fast-flow closed-cycle gas-discharge laser (FGL) with a combined multiple-pass electro-optical system and increased electrode spacing to optimize working conditions and check out the feasibility of increasing η_{eo}. In addition, this paper gives the results of chemical analyses of the working mixture and discusses problems common to process lasers: the necessary rate of renewal of the mixture and the way that this rate depends on the composition of the working gas.

2. The investigated laser was designed around the gasdynamic channel of the process laser described in Ref. 1, differing only in the geometry and design of the electro-optical module. The flow length of the discharge zone was 350 mm, and the width along the optical axis was 1300 mm, the distance between the cathode plate and the anode being 60 mm. The anode was a solid water-cooled stainless steel plate. The cathode plate was made up of copper cathode elements [Ref. 3]. A ballast resistor was connected in the electric circuit of each cathode with value increasing toward the end of the discharge chamber, reaching 20 kΩ. To ensure discharge ignition and improve discharge stability [Ref. 4] a preionizer was installed at the inlet to the discharge chamber fed by DC voltage from a separate source and enabling a considerable increase (up to 30%) of the maximum current in the discharge chamber.

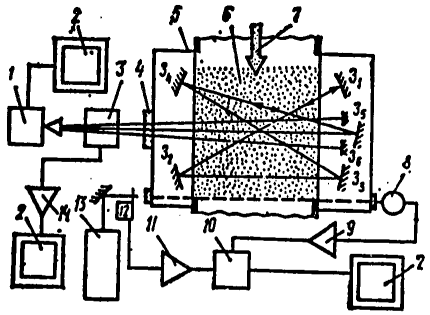

Fig. 1. Optical system of the laser: 3_1-3_4--cavity mirrors; 1--calorimeter; 2--chart recorder; 3--flow-through power sensor; 4--single-crystal KCl window; 5--discharge chamber housing; 6--pumping zone; 7--inflow of working mixture; 8--photoresistor; 9, 11, 14--amplifiers; 10--synchronous detector; 12--modulator; 13--test laser

The optical arrangement of the laser is given in Fig. 1. The system is made up of six cooled mirrors and includes an unstable confocal four-pass cavity

with rated transparency of 75% and a single-pass amplifier. The use of mirrors 120 mm in diameter and extraction of emission by using a rotating flat mirror with central rectangular coupling aperture (25 x 45 mm) fills most of the discharge zone with radiation. Emission is coupled out of the facility through a single-crystal KCl window.

Measurements were made of the electric parameters of the discharge, the gasdynamic parameters of the loop, the gain of the active medium on the axis of the cavity and at the output from the discharge chamber, the parameters of emission and the composition of the gas mixture. The electric and gasdynamic parameters were measured by conventional methods. The gain K_0 was measured in the arrangement shown in Fig. 1 by a technique involving the transmission of a test laser signal through the active medium. The emission power of the laser was determined by a special quick-response flow-through sensor, and also calorimetrically.

Gas chromatography was used to analyze the gas mixture for components of CO_2, CO, O_2, N_2 and H_2. The amount of water vapor was determined from the dew point and the partial pressure of atmospheric air in the loop with measurement of the humidity of the air. The total concentration of nitrogen oxides ($NO + NO_2$) was determined by titration. The CO_2 concentration was also continuously measured by an OA-2209 gas analyzer. The initial N_2 and air concentrations were determined from the corresponding partial pressures.

3a. When a working mixture of N_2 + air + CO_2 was used the installation worked in the steady state with the following volumetric concentration of components: $X_{N_2} = 0\text{-}0.8$, $X_{air} = 0.2\text{-}0.95$, $X_{CO_2} = 0\text{-}0.05$. The static pressure at the inlet to the discharge chamber was maintained at 25 mm Hg. The degree of renewal γ (ratio of the rate of evacuation of the loop to the flowrate of gas through the discharge chamber) remained constant at 0.4%.

The maximum electric power released in the positive discharge column in the absence of lasing was $W_0 \approx 70$ kW. In the presence of lasing it dropped by 10-15%. The volumetric energy input jE increased downstream by 50%, and its average value with respect to the volume of the discharge chamber did not exceed 2.5 W/cc.

The gas flowrate through the discharge chamber at maximum values of W_g was $g = 260$ g/s, and values of W_g reached about 240 J/g. The gas velocity with passage through the discharge zone increased due to heating from 90 to 150 m/s and its temperature rose from 290 to 420 K.

The time of continuous laser operation at a given power level was at least 1 hour. The time change in lasing power after the elements of the optical system had reached thermal conditions was no more than 1 kW. The luminous flux was coupled out of the facility in the form of a rectangular frame uniformly filled with radiation. The beam divergence and its spectral makeup were not studied in this research.

Maximum output emission power W was reached at maximum values of W_g, and amounted to (10 ± 1) kW, which corresponds to a specific luminous energy output of w = 35-40 J/g, and an electro-optical efficiency η_{eo} = 15%. The overall efficiency η of the laser (without consideration of energy expenditures on circulation and losses in the power supply) was 8%.

A comparison of the given laser characteristics with those found under analogous gasdynamic conditions in the case of a spaced electro-optical arrangement [Ref. 1] (where $\langle jE \rangle = 5$ W/cm^2, $W_g = 150$ J/g, W = 6 kW, $\eta_{eo} = 8\%$, $\eta = 5\%$, w = 12 J/g) shows that increasing the interelectrode gap and combining the discharge and cavity zones, despite a reduction in $\langle jE \rangle$, increased W_g by a factor of 1.5, doubled η_{eo} and raised the emission output per unit of gas by a factor of 3-4. The output emission of such a laser is more uniformly distributed, and the emission power density at the output aperture (~300 W/cm^2) is two-thirds of the corresponding value (500 W/cm^2) for a laser with a spaced system. All this is a good recommendation for the use of a combined electro-optical system in making CO_2 process lasers with power level of 10 kW.

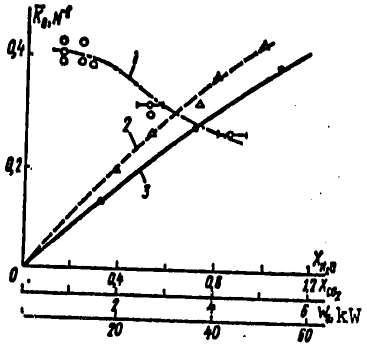

Fig. 2. Relations for the mean value of weak-signal gain on the optical axis of the cavity as a function of the concentration of water (1), carbon dioxide (2) and invested electric power (3)

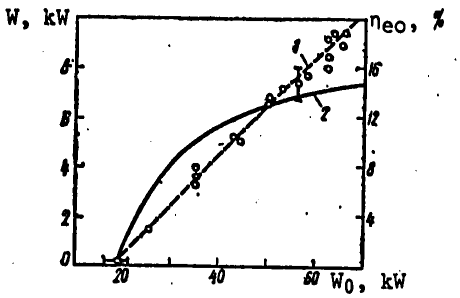

Fig. 3. Output power (1) and electro-optical efficiency of the laser (2) as related to the invested electric power

3b. Typical results of optimization of the average value of $\bar{K}_0$ along the optical axis of the cavity with respect to concentrations of water and carbon dioxide are shown in Fig. 2. The optimum concentration of CO_2 in the mixture that ensures a value of $\bar{K}_0 \approx 0.4$ m^{-1} (without noticeable impairment of W_0) was 5%, and the optimum value of X_{H_2O} is related to X_{CO_2} by the expression $(X_{H_2O})_{opt} = (3\text{-}5) \cdot 10^{-2} X_{CO_2}$.

Typical curves for emission power W, η_{eo} and $\bar{K}_0$ as functions of W_0 at the optimum values of X_{CO_2} and X_{H_2O} are shown in Fig. 2 and 3. The nearly linear behavior of $W(W_0)$ and the rise in $\eta_{eo}(W_0)$ show the advisability of

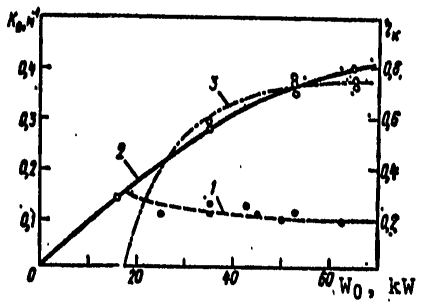

Fig. 4. Gain at the output of the discharge chamber (1, 2) and cavity efficiency $\eta_K = 1 - K_0(W)/K_0(0)$ (3) as functions of invested power with (1) and without (2) lasing.

further increasing the energy investment in the discharge, and allow us to hope for some improvement in η_{eo} when W_0 is increased.

The effectiveness of the optical arrangement used can be judged from the relations given in Fig. 4 for the gain of the medium K_0 at the output of the discharge chamber as a function of the power investment with and without lasing. When stimulated emission begins, K_0 drops to values close to the threshold levels, and decreases with increasing power investment. An estimate shows that no less than 30% of the vibrational energy stored in the discharge zone is coupled out of the cavity, which is in good agreement with the energy balance defect found on the basis of measurement of the translational temperature of gas at the output of the discharge cavity and the total energy input to the discharge cavity. This energy transfer is in all probability due to the nonoptimum transparency of the cavity.

3c. According to studies of the chemical composition of the mixture in steady-state operation for an initial mixture of $CO_2:N_2:air = 1:9:10$, the loop contains less than 10^{-2}% hydrogen, ~10^{-3}% nitrogen oxides, ~10% oxygen, ~5% CO_2, and the steady degree of dissociation of CO_2 $\alpha = X_{CO}/(X_{CO} + X_{CO_2})$ in optimum conditions is ~7%. Such concentrations of nitrogen oxides and hydrogen do not have any appreciable effect on the balance of the major gas components or relaxation processes. To explain the observed values of α, its value was theoretically calculated for typical experimental conditions with consideration of partial renewal of the mixture. The presence of water vapor reduces the steady degree of dissociation of carbon dioxide; however, the catalytic effect of H_2O at an initial concentration of O_2 ~ 10% is slight. Estimates show that the ratio of reaction rates $CO + O + M \rightarrow CO_2 + M$ and $CO + OH \rightarrow CO_2 + H_2$ is equal to 60, and therefore only the following processes were considered in calculations:

$CO_2 + e \rightarrow CO + O + e$,	$k_1 = 7.2 \cdot 10^{-11}$ cm^3/s [Ref. 5];
$O_2 + e \rightarrow O + O + e$,	$k_2 = 6 \cdot 10^{-11}$ cm^3/s [Ref. 6];
$CO + O + M \rightarrow CO_2 + M$,	$k_3 = 9.6 \cdot 10^{-35}$ cm^6/s [Ref. 7];
$O + O + M \rightarrow O_2 + M$,	$k_4 = 1.1 \cdot 10^{-33}$ cm^6/s [Ref. 8].

The value $\alpha \approx 5\%$ calculated for $X_{O_2} = 0.1$ and $\gamma = 0.4\%$ agrees quite satisfactorily with experiment. We should note the weak dependence of $\alpha(\gamma)$ when oxygen is present in the working mixture. According to calculations, a change of γ from 0.4 to 0.1% increases α from 5 to only 7.5%, and without renewal ($\gamma = 0$), $\alpha = 10\%$. The calculated values of α increase considerably

when there is no oxygen in the initial mixtures. For instance for a typical laser mixture N_2:He:CO_2 = 1:1:0.1 when $\gamma = 0.3\%$ $\alpha \approx 20\%$ and drops considerably with an increase in the renewal rate. These estimates explain the high values of $\alpha \approx 24\%$ observed at values of $\gamma \approx 0.3\%$ in the case of oxygen-free helium laser mixtures [Ref. 10], and show that the use of atmospheric air in a laser mixture not only eliminates the dependence on costly helium, but reduces requirements for the rate of renewal of the mixture, improving the economy of the process laser.

On the other hand, oxygen plays a negative role in the plasma of the CO_2 laser [Ref. 9], and therefore the problem of the optimum amount of oxygen in a closed loop must be studied in more detail.

3d. According to our experiments, the value of $\overline{K}_0$ after energizing the discharge falls within 2-3 minutes to a level of 85-90% of the initial value, and then changes only slightly. The degree of dissociation of CO_2 also behaves in a similar way: the value of α rises to a steady value within 2-3 minutes. The time required for α to reach a steady level corresponds to the rates of the mentioned reactions and the degree of renewal of the mixture. The time correlation of $\overline{K}_0$ and α suggests that the mechanism responsible for the drop in $\overline{K}_0$ is dissociation of CO_2, which leads to a reduction in the concentration of CO_2 and appearance of CO and O_2; however, the observed decrease in $\overline{K}_0$ exceeds the amount that one should expect on the basis of the measured change in CO_2 concentration alone.

4. The results given in this work graphically show the advantages of a combined electro-optical arrangement in a CO_2 process laser, and demonstrate the high effectiveness of using such an arrangement in closed-cycle lasers with emission power level of the order of 10 kW. It should be noted that there are data in the literature on attainment of a power of 10-20 kW with an efficiency of the order of 15-20% when multiple-pass amplification arrangements are used (9-17 passes) [Ref. 2, 11, 12]. However, all these results have been obtained on helium mixtures and with the use of more complicated (from the technical standpoint) excitation methods.

Our experiments have shown that the chemical processes taking place in a laser may have an appreciable effect on altering its characteristics. In particular, the dissociation of CO_2 leads to a reduction of gain.

The use of an N_2-air-CO_2 working mixture with optimum amounts of CO_2 and H_2O can eliminate the use of costly and scarce hleium in process laser facilities and reduce the required degree of renewal, and hence the expenditure of all gas components used.

The proposed laser has high output emission power (about 10 kW) and efficiency (about 8%) with small overall dimensions (2 x 2 x 2 m without the systems for supply and renewal of the medium), does not require helium for operation, and may find extensive application in scientific research and production.

REFERENCES

1. A. V. Artamonov, Yu. A. Yegorov, A. V. Kazhidub, N. I. Katsuro, F. V. Lebedev, Ye. M. Sidorenko, V. V. Sumerin, V. M. Frolov, KVANTOVAYA ELEKTRONIKA, Vol 5, 1978, p 920.

2. A. E. Hill, AIAA PAPER No 71-65, 1965.

3. G. D. Myl'nikov, A. P. Napartovich, FIZIKA PLAZMY, Vol 1, 1975, p 892.

4. A. I. Ivanchenko, R. I. Soloukhin, G. N. Fidel'man, Yu. A. Yakobi, "Gazovyye lazery" [Gas Lasers], Novosibirsk, Nauka, 1977.

5. A. L. S. Smith, I. M. Austin, J. PHYS. D: APPL. PHYS., Vol 7, 1974, p 314.

6. D. I. Slovetskiy, Doctoral Dissertation, Institute of Petrochemical Synthesis imeni A. V. Topchiyev, Academy of Sciences USSR, 1977.

7. V. N. Kondrat'yev, SOOBSHCHENIYA PO KINETIKE I KATALIZU, Vol 1, 1974, p 7.

8. "Fizicheskaya khimiya bystrykh reaktsiy" [Physical Chemistry of Fast Reactions], Moscow, Mir, 1976.

9. A. L. S. Smith, T. H. Bett, P. G. Browne, IEEE J., QE-11, 1975, p 335.

10. S. S. Vorontsov, A. I. Ivanchenko, R. I. Soloukhin, A. A. Shelepenko, ZHURNAL PRIKLADNOY TEKHNIKI I TEKHNICHESKIY FIZIKI, No 3, 1977, p 6.

11. C. O. Brown, J. W. Davis, APPL. PHYS. LETTS., Vol 21, 1972, p 480.

12. LASER FOCUS, No 10, 1976, p 16.

6610
CSO: 1870

PHYSICS

UDC 621.37:536.4

CONCERNING THE BEHAVIOR OF METAL ABSORPTIVITY WITH EXPOSURE TO LASER RADIATION

Moscow KVANTOVAYA ELEKTRONIKA in Russian Vol 6, No 1, Jan 79 pp 210-217

[Article by A. I. Korotchenko, A. A. Samokhin and A. B. Uspenskiy, Physics Institute imeni P. N. Lebedev, Moscow]

[Text] To calculate the temperature of an irradiated surface T(t), experimental data are used on the behavior of absorptivity A(t) of a copper target during the action of a laser monopulse. From the functions A(t) and T(t) the authors determine the temperature dependence of absorptivity A(T) in the range of 300-6000 K for emission with wavelength of 1.06 μm. The possibilities and limitations of this kind of method of determining A(T) are discussed.

Under normal conditions the reflectivity R of many metals is close to unity. When intense optical radiation acts on the metal, the temperature of the irradiated surface increases, which is usually accompanied by a reduction of R. Since the relative change in absorptivity $A = 1 - R$ may be considerable in this case, the given effect must be taken into consideration in analysis of the interaction of intense radiation with metals [Ref. 1-3].

The reflectivity of metals under the action of laser radiation has been experimentally studied in many papers (see Ref. 1-7 and the references cited there); however, very little is known as yet on the behavior of reflectivity in the high-temperature region. Usually in experiments the time change of absorptivity A(t) is measured, and the temperature T_0 of the exposed surface remains unknown. In this research, the experimental curve for A(t) from Ref. 5 is used to calculate the surface temperature of a copper target, and the resultant function A(T) is analyzed. In addition, an examination is made of the behavior of optical parameters in the case of a transition of metal-dielectric type where the action of intense radiation on the metal may lead to an increase in reflectivity.

In Ref. 5, measurements were made of the relation A(t) when a copper target was exposed to a laser monopulse ($\lambda = 1.06$ μm) with peak intensity of $I_p = 320$ W/cm^2 and duration of 60 ns at half power. The behavior of absorptivity A(t) is shown on Fig. 1 (1). In the interval $t_1 \leq t \leq t_2$, A(t) increases to $A_m = 0.37$, and remains on this level until $t = t_3$, after which a rapid drop is observed in A(t). As was noted earlier in Ref. 8, the estimate of the surface temperature given in Ref. 5 (1573 K at $t = t_2$) is very understated, and therefore the conclusion of Ref. 5 on lack of agreement between the observed behavior of A(t) and calculations by the Drude model [Ref. 9] needs more analysis.

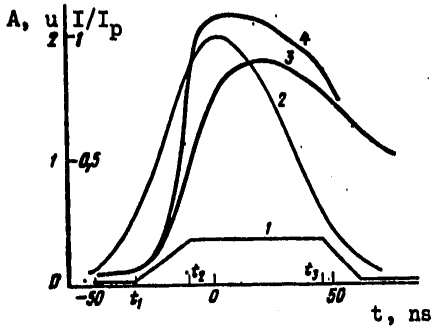

Fig. 1. Time behavior of absorptivity (1), incident intensity (2) and surface temperature at $\chi = \chi_0$ (3) and $\chi = \chi_1$ (4)

In the investigated range of intensities the maximum value of T may exceed the normal boiling point T_K (2860 K for copper [Ref. 10]), i. e. the role of vaporization in the energy balance of interaction of the radiation with the target is not small, generally speaking. We will describe the dynamics of heating and vaporization of the irradiated target within the framework of a one-dimensional equation of heat conduction in a region with a moving boundary coincident with the vaporization front. The corresponding boundary value problem takes the form

$$c\left(\frac{\partial T}{\partial t} - v\frac{\partial T}{\partial x}\right) - \frac{\partial}{\partial x}\left(\varkappa\frac{\partial T}{\partial x}\right) = 0,$$

$$\varkappa\frac{\partial T_0}{\partial x} = qv - AI; \quad T(t, \infty) = T(0, x) = T(0), \qquad (1)$$

where c and q are the specific heat and the heat of vaporization of a unit of volume of the target substance respectively, $\kappa = \chi c$ is the coefficient of heat conduction. The velocity of motion of the vaporization front v is determined by the formula

$$v = (p_н/\rho)(M/2\pi kT_0)^{0,5}; \quad p_н = p_к \exp[13{,}5(1 - T_к/T_0)]. \qquad (2)$$

The relation $p_H(T_0)$ for saturated vapor pressure as a function of surface temperature that is used in (2) agrees with the estimated values of critical parameters for copper ($p_{cr} = 7500$ bars, $T_{cr} = 8400$ K [Ref. 11]).

As can be seen from (2), the boundary value problem (1), (2) is nonlinear even at fixed values of the thermophysical parameters, and it can be solved only by numerical methods. In accounting for melting, equations (1), (2) must be supplemented by the relations on the solid [тв]-liquid [ж] phase boundary $x = x_1$:

$$\varkappa\frac{\partial T}{\partial x}\Big|_{ж} = -(v_1 + v)q_1 + \varkappa\frac{\partial T}{\partial x}\Big|_{тв}; \quad T(x_1) = T_1, \qquad (3)$$

where q_1 and T_1 are the latent heat and melting point respectively, v_1 is the velocity of motion of the melting front relative to the vaporization front $x = 0$.

The nonlinear boundary value problem (1)-(3) was numerically solved on the BESM-6 computer using an implicit four-point finite-difference scheme. The absorptivity A(t) in accordance with Ref. 5 was approximated by a piecewise-linear function (curve 1, Fig. 1) with initial value $A_0 = 0.03$. The intensity of the incident radiation was assigned in the form of an asymptotic gaussian curve $I(t) = I_p \exp(-t^2/\tau^2)$ with $\tau = 31$ ns when $t \leq 0$ and $\tau = 41$ ns when $t > 0$ (curve 2, Fig. 1). The following values were used for the thermophysical parameters of copper: $q = 23.4$, $q_1 = 428$ J/cm^3, $T_1 = 1356$ K, $q/cT_K = 3.5$, $\rho = 8.9$ g/cm^3, $M = 1.07 \cdot 10^{-22}$ g. In the general case the thermal diffusivity χ was not considered constant.

Let us first consider the dynamics of heating of a target with constant thermal diffusivity $\chi = \chi_0 = 1$ cm^2/s and zero heat of fusion. The bahavior of the dimensionless surface temperature $u = T_0/T_K$ for such a case is shown in Fig. 1 (2). The calculated function u(t) together with A(t) defines the temperature dependence of the coefficient of absorption A(u) in parametric form shown in Fig. 2 (1). This dependence is quite sharp. For slight

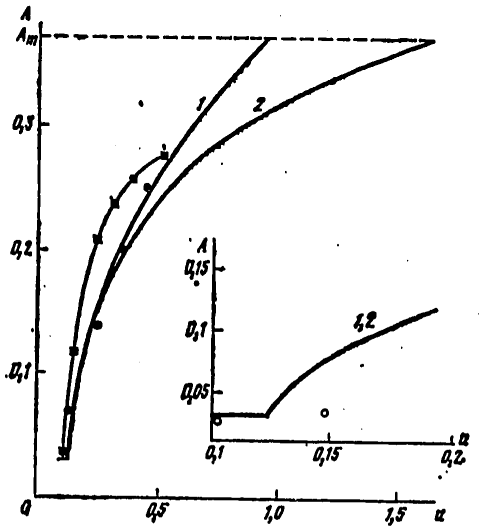

Fig. 2. Temperature dependence of absorptivity at $\chi = \chi_0$ (1), $\chi = \chi_1$ (2), and also from data of Ref. 9 (black circles), Ref. 12 (white circles) and Ref. 14 (black squares).

excesses of u over the initial value $u_0 = 0.1$ the rate of change of the coefficient of absorption with temperature reaches a value of $dA/du \approx 3$.

On the average in the interval $u \leq u_1 = T_1/T_K$ this rate is equal to $\Delta A/\Delta u = 0.4$. Such behavior of A(u) agrees basically with the results of calculations in the Drude model [Ref. 9] (see Fig. 2).

However, experimental studies of the optical characteristics of copper at temperatures considerably below T_0 [Ref. 12, 13] do not show a similar sharp change in the coefficient of absorption. In Ref. 12, measurements were made of the real n and imaginary k parts of the complex index of refraction of copper for T = 77, 293 and 423 K and different light quantum energies. The values of dA/du calculated from the results of Ref. 12 in the interval of 293-423 K are respectively 0.16 and 0.13 at $\hbar\omega = 1.14$ and 1.76 eV. The temperature dependence of the coefficient of absorption of copper given in Ref. 13 on the frequency of the He-Ne laser yields $dA/du \approx 0.2$. These values of dA/du differ appreciably from the results of calculation by the Drude model [Ref. 9] in this temperature range.

In the Drude theory the complex permittivity

$$\varepsilon = (n + ik)^2 = 1 - \frac{\omega_p^2}{\omega^2 + \omega_c^2}\left(1 - i\frac{\omega_c}{\omega}\right) \qquad (4)$$

depends on the frequency of the electromagnetic field ω and two "material constants" -- the collision rate ω_c and the plasma frequency ω_p. If the real behavior of $\varepsilon(\omega)$ differs from dispersion formula (4) with constant values of ω_c and ω_p, then in a strict sense the description of such a situation transcends the limits of the Drude theory. Nonetheless, formula (4) is often suggested for use in just such situations, assuming for instance that ω_c depends on the frequency ω of the external field. A reduction in ω_c may weaken the temperature dependence of the coefficient of absorption; however, there is no adequate justification for using the static value of ω_c in formula (4) on optical frequencies, as is suggested in Ref. 13.

In Ref. 9 the temperature dependence of optical characteristics of copper was determined by formula (4) in which ω_p was taken as constant, and the collision frequency ω_c was given by the expression

$$\omega_c(T) = \frac{\omega_c(300\text{K})\, f(T)}{f(300\text{K})}; \quad f(T) = T^5 \int_0^{\theta/T} \frac{z^4}{e^z - 1}\, dz, \qquad (5)$$

where θ is the Debye temperature. Without going into any detail on the question of applicability of such a model to the case under consideration, let us note that the values of the parameters ω_c (300 K) $= 2.49 \cdot 10^{14}$ s^{-1} and $\omega_p = 1.03 \cdot 10^{14}$ s^{-1} for copper in Ref. 9 differ appreciably from the values $\omega_c = 1.7 \cdot 10^{14}$ s^{-1} and $\omega_p = 1.2 \cdot 10^{16}$ s^{-1} implied by formula (4) and the results of Ref. 12 for $\hbar\omega = 1.14$ eV and T = 293 K. Besides, the relative rate of change in collision frequency $d \ln \omega_c / d \ln T = 0.7$ obtained from the data of Ref. 12 is considerably less than the corresponding value from Ref. 9.

The behavior of the coefficient of absorption A(u) on the initial temperature section found in our calculations is shown in Fig. 2 in the inset where the scale along the u-axis is stretched out. Also shown in the figure are the

results of Ref. 12 for $\hbar\omega = 1.14$ eV. The strictly zero value of dA/du in the region $u \leq 0.124$ and the subsequent break in the curve for A(u) are due to the piecewise-linear approximation of the function A(t), which is an admitted simplification. Nevertheless, this kind of behavior of A(u) is a qualitative indication of the considerable change in the quantity dA/du on the initial heating stage. With consideration of this circumstance it can be assumed that the problem of discrepancy with data of Ref. 12 will be explained with more detailed measurement of the relation A(t) in laser experiments.

A rapid increase in the coefficient of absorption when a copper target is exposed to millisecond laser pulses with wavelength of $\lambda = 0.69$ μm and intensity $I \leq 0.1$ MW/cm^2 is also reported in the recent research of Ref. 14 (see Fig. 2). However, this paper does not give the relation of the coefficient of absorption A(t) from which the curve for A(u) was reconstructed, and there are no indications of any peculiarities in the initial heating stage. The knee of the curve for A(u) in the vicinity of $u = u_1$ is attributed in Ref. 14 to the possibility of beginning of melting, which was not considered in calculating the function u(t). The thermophysical parameters of copper were taken as constant in Ref. 14.

Our calculations imply that melting has little influence on the behavior of u(t) since the latent heat of fusion $q_1/cT = 0.15$ is relatively low. Besides, some retardation in the growth of u(t) due to melting may be compensated by a reduction of thermal diffusivity in the molten metal. The reduction in thermal diffusivity with increasing temperature leads to acceleration of surface heating, which corresponds to smoothing of the relation A(u) for a predetermined function A(t). The necessity of accounting for the reduction in χ with temperature is also shown by the sharp change in A(u) with attainment of the maximum value of $A_m = 0.37$ (curve 1, Fig. 2) that results with the assumption of a constant value of $\chi = \chi_0$.

The thermal diffusivity of copper in the solid state decreases by a factor of approximately 1.5 with a change from room temperature to T_1 [Ref. 10]. There is almost no information on the change in thermal diffusivity of molten copper with temperature. For example let us represent the relation $\chi(u)$ in the form

$$\chi(u) = [1, 2 \exp(-2u) + 0,1]\chi_0 \equiv \chi_1. \qquad (6)$$

The relations u(t) and A(t) for this case are shown in Fig. 1 (4) and 2 (2). As a consequence of acceleration in the rise of u(t), the curve A(u) approaches the maximum value of A_m more smoothly than in the case $\chi = \chi_0$. In this connection, the small change in A(t) after reaching the maximum is due to weakening of the temperature dependence of the coefficient of absorption A(t) at high temperatures $u \geq 1.5$. It can also be seen from a comparison of curves 1 and 2 in Fig. 2 that when $u \geq u_1$ the temperature dependence $\chi(u)$ has a relatively weak influence on the quantity A(u). Let us note that in this temperature region when the thermophysical coefficients are constant an analytical expression can be found for u(t) if A(t) and I(t) are given in polynomial or piecewise-polynomial form [Ref. 8].

The behavior of A(u) discussed up to this point has corresponded to the front of the curves for u(t). The temperature dependence A(u) found similarly on the descent of the u(t) curves differs considerably from that described above, the "hysteresis" being particularly great for the case $\chi = \chi_0$. Formally, this circumstance is caused by the very rapid reduction of absorptivity A(t) on the trailing edge of the emission pulse. At present it is difficult to draw any definite conclusions on the causes of such behavior of A(u) that may be due for instance to inaccuracy in the measurement of A(t) (in Ref. 5 there is only a single experimental point over the entire descent section of curve A(t)).

The results found above show the possibilities and disadvantages of the method of determining the temperature dependence of the coefficient of absorption A(u) from the laser curve of A(t). In the high temperature region where it is no longer possible to ignore the change in thermophysical parameters, it becomes necessary to get additional data on the behavior of the temperature of the irradiated surface u(t). When $u \gtrsim 1$ the required information can be obtained simultaneously with A(t) by measuring the recoil pressure p(t), which is approximately half the saturated steam pressure $p(t) = 0.5p_H[u(t)]$.

In view of the sharp dependence of p_H on u, the recoil pressure is quite sensitive to change in surface temperature. In accordance with formula (2) a recoil pressure of $p \approx 200$ bars corresponds to the maximum temperature when $\chi = \chi_0$ ($u_m = 1.8$, curve 3, Fig. 1), whereas the maximum recoil pressure in the case of decreasing thermal diffusivity $\chi = \chi_1$ (at $u_m = 2.17$, curve 4, Fig. 1) reaches 720 bars. By the instant that curve A(t) reaches the horizontal section, the recoil pressure in these cases is equal to 0.3 and 100 bars respectively.

The pattern of interaction of intense radiation with the target becomes more complicated when an absorbing plasma layer develops over the surface. The presence of such a layer precludes identification of the measured value of A(t) with absorptivity of the target surface. For this reason it is necessary to monitor the instant of development of the plasma in the experiment.

The influence of the plasma layer may be particularly strong if the electron concentration exceeds the characteristic value $n_p = \omega^2 m/4\pi e^2$, where e and m are the charge and mass of the electron. For neodymium laser radiation $n_p = 10^{21}$ cm^{-3}. Under conditions of developed vaporization the concentration of atoms at the surface of a copper target reaches such a value at T = 6400 K. The appearance of a plasma layer limits applicability of the method of determining the temperature dependence of the absorption coefficient of metal A(u) from the experimental curve for A(t). Nevertheless, this method enables a considerable advance into the still unstudied region of temperatures of molten metals. In this connection, for pulse heating of metal it is apparently advisable to use optical radiation with shorter wavelengths, which may lead to considerable displacement of the boundary of plasma development.

Let us now consider some peculiarities in the behavior of the coefficient of reflection that may occur in the case of a metal-dielectric transition. Numerical calculation [Ref. 15] shows that in the transcritical vaporization state when $p > p_{cr}$ and there are no phase boundaries, there may be a thin dielectric interlayer between the plasma and metal that has no appreciable influence on the general pattern of interaction of radiation with the metal. The problem of dielectrization of molten metal in the subcritical region that has been discussed in the literature for more than thirty years now has not yet been finally solved. It was assumed in Ref. 16-18 that such a transition occurs fairly smoothly, and therefore one can disregard interference effects associated with the development of additional interfaces in the exposed material.

If the metal-dielectric interface is not smooth, interference effects cannot be disregarded. Direct manifestation of such effects is possible, of course, only when there is fairly uniform distribution of intensity over the exposure spot. Just as in the case of analysis of the behavior of A(u) given above, this permits us to restrict ourselves to consideration of the one-dimensional pattern of the process.

The transition region on the metal-dielectric interface can be considered optically sharp if its characteristic dimension h is small compared with the wavelength of radiation in the medium ($h \ll \lambda$). For the visible range, this means that $h < 0.1$ μm. Since the scale of the drop in the temperature profile in front of the transition interface in the quasi-steady state is determined by the speed of motion of this interface v_2 and the thermal diffusivity of the material χ, the relative change in temperature in the region of the transition is given by the relation $\Delta T/T_2 \approx hv_2/\chi$. At a transition temperature $T_2 \approx 5 \cdot 10^3$ K, $v_2 \approx 10$ m/s, $\chi = 0.1$ cm^2/s and $h = 10$ nm, we get $\Delta T \approx 50$ K. Thus at constant pressure if the temperature width of the metal-dielectric transition does not exceed a few tens of degrees, and the time required for such a transition is fairly short ($t < h/v_2$), the metal-dielectric interface may be optically sharp.

The reflectivity of a metal with optical constants n_3 and k_3 having a transparent dielectric film on its surface with index of refraction n_2 and thickness L is given by the well-known expression [Ref. 9]

$$R = |[r_{12} + r_{23}\exp(2i\psi)]/[1 + r_{12}r_{23}\exp(2i\psi)]|^2,$$
$$r_{23} = (n_2 - n_3 - ik_3)/(n_2 + n_3 + ik_3) \equiv \rho\exp(i\varphi_{23}),$$
$$\psi = 2\pi n_2 L/\lambda, \quad r_{12} = (1 - n_2)/(1 + n_2). \qquad (7)$$

For given optical parameters the reflectivity changes periodically depending on the thickness of the dielectric layer. For the maximum R_M and minimum R_m values of reflectivity we have

$$R_M = (r + \rho)^2/(1 + \rho r)^2; \quad R_m = (r - \rho)^2/(1 - \rho r)^2; \quad r = |1 - n_2|/|1 + n_2|. \qquad (8)$$

The quantity R_M may exceed by a great amount that of the metal R_3 on the vacuum interface

$$R_3 = 1 - 4n_2/[(n_2 + 1)^2 + k^2]. \qquad (9)$$

When $n_2 = 4$, $n_3 = 1$, $k_3 = 3$, we have from (8) and (9) $R_M = 0.85$, $R_m = 0.05$ and $R_3 = 0.7$, i. e. in this case the absorptivities $A_M = 0.15$ and $A_3 = 0.3$ differ by a factor of 2. If $n_3 \ll n_2$, we can get the following expression for the ratio of absorptivities A_3/A_M from (8) and (9):

$$A_3/A_M = (n_2^2 + k_3^2)/[(n_3+1)^2 + k_3^2], \qquad (10)$$

which is valid when $n_2 > 1$ in the approximation that is linear with respect to $1 - \rho$.

Since $\mathrm{Im}\, r_{23} < 0$, then $-\pi < \phi_{23} < 0$, and the first maximum of reflectivity is reached at a film thickness such that $2\psi = \pi + |\phi_{23}|$. For the case of optical constants considered above, we find $L = (\pi + 1)\lambda/4\pi n_2 \approx 0.08\lambda$. The time for reaching this maximum after formation of the dielectric layer is equal in order of magnitude to $t = 1/v_2 \approx 6$ ns at $\lambda = 0.7$ μm and $v_2 = 10$ m/s. Let us recall that the velocity of motion of the metal-dielectric interface $v_2 = I_2/W_2$ is determined by the ratio of the intensity I_2 of emission absorbed on this interface to the change in enthalpy $W_2 \approx cT_2 + q_2$ that is related to the heating of the target and the latent heat of the transition q_2 if the latter differs from zero. When $W_2 \geq 10$ kJ/cm^3, an absorbed intensity of $I_2 \geq 10$ MW/cm^2 corresponds to velocity $v_2 = 10$ m/s.

Formula (7) also implies that for $L \leq |\phi_{23}|\lambda/4\pi n_2 = 0.02\lambda$ the reflectivity drops with increasing L, i. e. growth of the dielectric film on the metal surface initially leads to a reduction in R. However, it should be borne in mind that in the case of small L the behavior of reflectivity is not described by formula (7), since the dielectric film initially arises beneath the surface of the target, and the optical thickness of the outer metal layer is not small enough to be disregarded [Ref. 17]. Subsequent expansion of the dielectric region leads to a rapid reduction in thickness of the metal surface layer.

The oscillating behavior of reflectivity is accompanied by fluctuations of velocity v_2 that influence primarily the recoil pressure p(t). The value $p = p_0 + \Delta p$ registered by the pressure sensor differs from pressure p_0 on the surface of the target by an amount Δp due to the dynamics of thermal expansion of the material in the heat-affected zone. For ordinary metals the ratio $\Delta p/p_0$ is small; however, after the metal-dielectric transition, when v_2 becomes greater than v, and the increase in p_0 is abruptly retarded, the difference between p and p_0 increases considerably [Ref. 20]. In the quasi-steady state for the pressure differential we get

$$\Delta p = (\rho v_2)^2(\rho_2^{-1} - \rho^{-1}), \qquad (11)$$

where ρ_2 and ρ are the densities of the material on the transition front and far from it respectively. In contrast to the quasi-steady state of vaporization of ordinary metal, the quantity Δp depends quadratically on the intensity of the incident radiation I and the coefficient of absorption A. When $\rho_2 \leq 0.8\rho$, the fluctuation amplitude Δp corresponding to a change in velocity v_2 in the range of 10-100 m/s amounts to several hundred bars, which can be readily detected in measurement of the recoil pressure p(t).

REFERENCES

1. S. I. Anisimov, Ya. A. Imas, G. S. Romanov, Yu. V. Khodyko, "Deystviye izlucheniya bol'shoy moshchnosti na metally" [Action of High-Intensity Radiation on Metals], Moscow, Nauka, 1970.

2. A. A. Uglov, FIZIKA I KHIMIYA OBRABOTKI MATERIALOV, No 5, 1974, p 3.

3. G. R. Levinson, V. I. Smigla, KVANTOVAYA ELEKTRONIKA, Vol 3, 1976, p 1637.

4. J. F. Ready, IEEE J., QE-12, 1976, 137.

5. T. E. Zavecz, M. A. Saifi, M. Notis, APPL. PHYS. LETTS, Vol 26, 1975, p 165.

6. Yu. I. Dymshits, ZHURNAL TEKHNICHESKOY FIZIKI, Vol 47, 1977, pp 532, 1563.

7. A. P. Gagarin, I. N. Ivanova, M. N. Libenson, S. D. Pudkov, ZHURNAL TEKHNICHESKOY FIZIKI, Vol 47, 1977, 1523.

8. A. A. Samokhin, KRATKIYE SOOBSHCHENIYA PO FIZIKE, Physics Institute imeni P. N. Lebedev, Vol 12, 1976, p 12.

9. K. Ujihara, J. APPL. PHYS., Vol 43, 1972, p 2376.

10. I. K. Kikoin, ed., "Tablitsy fizicheskikh velichin" [Tables of Physical Quantities], Moscow, Atomizdat, 1976.

11. V. Ye. Fortov, A. N. Dremin, A. A. Leont'yev, TEPLOFIZIKA VYSOKIKH TEMPERATUR, Vol 13, 1975, p 1072.

12. P. R. Johnson, R. W. Cristy, PHYS. REV. Vol 811, 1975, p 1315.

13. S. D. Pudkov, ZHURNAL TEKHNICHESKOY FIZIKI, Vol 47, 1977, p 649.

14. P. W. Chan, Y. W. Chan, H. S. Ng, PHYS. LETTS, 61A, 1977, p 151.

15. S. I. Anisimov, V. A. Gal'burt, V. I. Fisher, PIS'MA V ZHURNAL TEKHNICHESKOY FIZIKI, Vol 1, 1975, p 321.

16. V. A. Batanov, F. V. Bunkin, A. M. Prokhorov, V. B. Fedorov, ZHURNAL EKSPERIMENTAL'NOY I TEORETICHESKOY FIZIKI, Vol 63, 1972, p 586.

17. R. V. Karapetyan, A. A. Samokhin, KVANTOVAYA ELEKTRONIKA, Vol 1, 1974, p 2053.

18. B. M. Kozlov, A. A. Samokhin, A. B. Uspenskiy, KVANTOVAYA ELEKTRONIKA, Vol 4, 1977, p 524.

19. L. D. Landau, Ye. M. Lifshits, "Elektrodinamika sploshnykh sred" [Electrodynamics of Continuous Media], Moscow, Fizmatgiz, 1959.

20. A. I. Korotchenko, A. A. Samokhin, FIZIKA I KHIMIYA OBRABOTKI MATERIALOV, No 6, 1978, p 3.

6610
CSO: 1870

PHYSICS

UDC 621.375.826

ON THE POSSIBILITY OF USING RESONANTLY EXCITED MEDIA FOR WAVEFRONT REVERSAL

Moscow KVANTOVAYA ELEKTRONIKA in Russian Vol 6, No 1, Jan 79 pp 218-224

[Article by A. N. Orayevskiy, Physics Institute imeni P. N. Lebedev, Academy of Sciences USSR, Moscow]

[Text] An analysis is made of the properties that a resonantly excited medium must have to use it for the basis of wavefront-reversing "mirrors." In the absence of saturation with respect to the signal to be reversed, the absorption cross section on this frequency should be considerably less than the cross section on the frequency of the reversed wave. Under conditions of strong saturation it is preferable to use materials with narrow spectral lines. To use a "reversing mirror" to compensate the distortions of the amplified wavefront, the required contrast of the reversed wave depends on the passband and gain of the amplifier.

The recently discovered phenomenon of reversal (reproduction) of the wavefront in stimulated Mandelstam-Brillouin scattering [Ref. 1] is of great interest from the standpoint of possible applications in experimental techniques and in practice. In Ref. 2 it was also shown that stimulated Raman scattering can be used for these purposes*. The problem arises as to whether it is only the substances that are active in the sense of stimulated Mandelstam-Brillouin scattering [SMBS] and stimulated Raman scattering [SRS] that can be used to make a "reversing mirror." Might not the resonantly pumped active media extensively used for making lasers be applied for this purpose as well?

SMBS has the following peculiarities that are essential for wavefront

*I would like to take this opportunity to propose a new term for "combination scattering," which is called the "Raman effect" outside of the USSR. To eliminate the difference in names of the same effect while maintaining the proper priority of discovery, I would like to suggest that this type of scattering be called the RAMAL effect [RAman-MAndelstam-Landsberg].

reversal: 1) the gain of a medium that is active for SMBS is much greater than unity; 2) the frequency ω_L of the radiation to be reversed is close to the frequency ω_S of the reversed signal, so that $(\omega_L-\omega_S)/\omega_L \ll 1$; 3) the gain of the active medium is linearly dependent on the intensity I_L of the pumping radiation (which is to be reversed). Let us examine to what extent the same conditions can be met if resonantly excited laser media are used.

For the sake of simplicity of our considerations, we will have in mind the scheme of levels depicted in Fig. 1. Let an inverse population be set up on frequency $\omega_S < \omega_L$ with pumping by laser emission of frequency ω_L. In the steady state with very rapid establishment of equilibrium between levels 0 and 1 the gain on frequency ω_S is

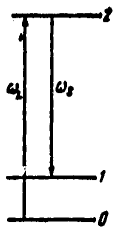

Fig. 1. Scheme of discrete levels for creating an active medium by optical pumping

$$\alpha = \sigma_{21}(N_2 - N_1) = \sigma_{21}N_0\left[\frac{\sigma_{20}\tau I_L(r,t)}{1+\sigma_{20}\tau I_L(r,t)} - e^{-\Delta}\right], \quad (1)$$

where σ_{21} and σ_{20} are the cross sections of induced transitions between levels with the corresponding subscripts, N_0 is the number of particles on level 0, τ is the time of relaxation of level 2, $I_L(r,t)$ is the intensity of the radiation to be reversed, $\Delta=(\hbar/kT)(\omega_L-\omega_S)$. It is assumed that because of rapid relaxation processes $N_1=N_0e^{-\Delta}$. To ensure positiveness of α and its linear dependence on I_L it is necessary that

$$\sigma_{20}\tau I_L > e^{-\Delta}; \quad (2)$$

$$\sigma_{20}\tau I_L \ll 1. \quad (3)$$

Condition (3) means absence of saturation, and hence independence of N_0 from I_L.

For the sake of definiteness, we will consider condition (3) satisfied if

$$\sigma_{20}\tau I_L = 0{,}1. \quad (4)$$

Then (2) implies that

$$\omega_L - \omega_S \geq (kT/\hbar)\ln 10. \quad (5)$$

The total amplification G on frequency ω_S under conditions (2) and (3) can be approximately found from the relation

$$G = \exp\left[\int \alpha(\xi)\,d\xi\right], \quad (6)$$

where

$$I_L(r,t) = I_0(\vec{\rho},t)\exp\left[-\sigma_{20}N_0\xi\right], \quad (7)$$

$I_0(\vec{\rho},t)$ is the intensity of the radiation to be reversed that is incident on the "mirror," ξ is the coordinate lengthwise of beam propagation, $\vec{\rho}$ is a coordinate in the plane perpendicular to this direction, Integration in (6) is done within limits of the positive value of α. From (6) and (7) it follows that

$$G = \exp\left[\sigma_{21}\tau(I_0 - I_\Pi)\right], \quad (8)$$

where $I_n=(1/\sigma_{s0}\tau)e^{-\Delta}$. Thus, $G\gg1$, if the quantity $\sigma_{21}\tau I_0$ is sufficiently large.

It follows from Ref. 1, 2 that it is necessary to achieve $G\sim e^{20}-e^{25}$ for good reproduction of the wavefront. We summarize the conditions in the table. Relation (в′) is implied by (в) and the fact that for good reproduction of the wavefront the mismatch $(\omega_L-\omega_s)/\omega_L\geq0.1$ is practically applicable [Ref. 2].

(1) Математическое выражение условия		(2) Практически приемлемый числовой эквивалент	
$\sigma_{21}\tau/_0\gg1$ $\sigma_{20}\tau/_0\ll1$	(а)	$\sigma_{21}\approx200\sigma_{20}$ $\sigma_{20}\tau/_0\approx0,1$	(а′)
$\omega_L-\omega_s>\frac{kT}{\hbar}\ln\left(1+\frac{1}{\sigma_{20}\tau/_0}\right)$	(б)	$\omega_L-\omega_s\approx3\frac{kT}{\hbar}$	(б′)
$\omega_L\gg\frac{kT}{\hbar}\ln\left(1+\frac{1}{\sigma_{20}\tau/_0}\right)$	(в)	$\omega_L\gtrsim20\frac{kT}{\hbar}$	(в)′

KEY: 1--Mathematical expression of the condition
2--Practically applicable numerical equivalent

What kinds of materials satisfy the relations given in this table?

These relations can be met in molecular systems consisting of simple molecules. In the case of rapid rotational relaxation the effective cross section of absorption in a molecule for a rotational-vibrational R or P transition is defined by the formula

$$\sigma_J=\sigma_0\frac{2J+1}{\Sigma}\exp\left[-\frac{E_{0J}}{kT}\right].$$

Here σ_0 is the cross section of the transition $v=0,\ J\to v=1,\ J\pm1$; Σ is the statistical sum of the molecule; E_{vJ} is the rotational energy of the initial state, which is an increasing function of the rotational moment $\hbar J$ (J is an integer). The radiative transition can be shifted toward lower J to satisfy the relation $\sigma_J^{abs}\ll\sigma_J^{rad}$. Most suitable for this purpose are molecules with large rotational constants such as hydrogen halides, ammonia and so forth. The necessary conditions: the duration of the pulse to be reversed and the time of rotational relaxation must be shorter than the time of vibrational-rotational relaxation, since the latter distorts the linear dependence of the inverse population on the intensity of the signal to be reversed.

One can use the transfer of energy from molecules excited on frequency ω_L with relatively small cross section of excitation of molecules with a larger cross section of the radiative transition.

As we see, materials can be selected that satisfy the conditions of the table. However, these conditions considerably restrict the the possibilities of using the reversal effect due to resonantly pumped media. In particular, when wavefront reversal is used to compensate inhomogeneities of the active medium of an amplifier it is necessary that frequencies coincide within the limits of the amplification linewidth. For instance for neodymium glass we must have $\omega_L - \omega_s < 10^2$ cm^{-1}. Gases require even closer agreement of frequencies. Besides, the conditions of the table permit us to use the reversal effect only in the wavelength range of $\lambda \gtrsim 3.2$ μm. These restrictions would be removed in the case of strong saturation if the requirement for linear dependence of gain on the intensity of the signal to be reversed could be avoided. Actually, when $\sigma_{20}\tau I_0 \gg 1$, relation (6) of the table takes the following form:

$$\omega_L - \omega_s \geq \frac{kT}{\hbar}\frac{1}{\sigma_{20}\tau I_0}. \qquad (9)$$

At a saturation parameter of 10-100, both frequencies may fall within an amplification linewidth of 2-20 cm^{-1}, and the long-wave boundary of reproduction is moved into the far infrared region.

One question remains: is reproduction possible with pumping by a saturating signal? Generally speaking, saturation, in smoothing out the gain dependence of intensity should lead to distortion of the reproduced wavefront. However, we can point out a case where saturation will not interfere with the reproduction process.

Let us represent the wave to be inverted $E_L(\vec{\rho},\xi)$ in the form

$$E_L(\vec{\rho},\xi) = \sum_q C_q(\xi)\, e^{-iq\vec{\rho}}, \qquad (10)$$

Let us assume, following Ref. 1, 2, that the quantities C_q are uncorrelated, so that

$$\langle C_{q'} C^*_{q''}\rangle = |C_{q'}|^2 \delta(q'-q''), \qquad (11)$$

and with this premise calculate the gain on frequency $\omega_s < \omega_L$. For the sake of simplicity we do the calculation for the system of levels shown in Fig. 2. We will assume equilibrium distribution by energy levels in band 2.

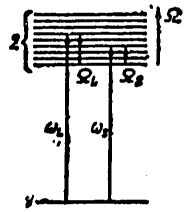

Fig. 2. Scheme of levels assumed for calculating reversal of a saturating emission pulse

The sought amplification factor α is given by the relation

$$\alpha = \sum_{\Omega} \sigma(\Omega_s, \Omega) N_2(\Omega) - \sigma_s N_1, \qquad (12)$$

where $\sigma(\Omega_s, \Omega)$ is the cross section of absorption from level 1 to level 2, Ω under the influence of emission of frequency ω_s, $\sigma_{s,L} = \sum_{\Omega} \sigma(\Omega_{s,L}, \Omega)$.

To determine $N_2(\Omega)$ we use the well known quasi-steady relations between the field, the number of particles and polarization of the medium P_L [Ref. 3, 4]:

$$\left.\begin{aligned} P_L &= i\frac{c}{8\pi}\frac{\sigma_L}{\omega_L}\left[N_2 e^{-\hbar\Omega_L/kT}a - N_1\right]E_L; \\ N_2 &= i\frac{\tau}{4\hbar}\left[E_L^* P_L - E_L P_L^*\right] + N_2^{(0)}; \\ N_1 &= -i\frac{\tau}{4\hbar}\left[E_L^* P_L - E_L P_L^*\right] + N_1^{(0)}; \\ N_2(\Omega) &= N_2 g(\Omega)\, e^{-\hbar\Omega/kT}, \end{aligned}\right\} \qquad (13)$$

where $N_2^{(0)}$ and $N_1^{(0)}$ are the equilibrium populations of the respective energy states (in the optical band $N_2^{(0)} \approx 0$); $a = \frac{1}{\sigma_L}\sum_{\Omega} g(\Omega_L - \Omega)\, e^{-\hbar\Omega/kT}\sigma(\Omega)$; the rest of the symbols are the standard ones.

We will also represent the polarization P_L and the reversed wave E_s in the form of a Fourier expansion with respect to "transverse" coordinates:

$$P_L\left(\vec{\rho}, \xi\right) = \sum_q P_q(\xi)\, e^{-iq\vec{\rho}}; \quad E_s\left(\vec{\rho}, \xi\right) = \sum_q S_q(\xi)\, e^{-iq\vec{\rho}}. \qquad (14)$$

To solve the formulated problem it is necessary to find the averaged gain $\langle\alpha_q\rangle$ for the Fourier components of the reversed wave:

$$\langle\alpha_q\rangle = (\alpha E_s)_q S_q^* / \langle S_q S_q^*\rangle, \qquad (15)$$

where

$$(\alpha E_s)_q = \int \alpha E_s e^{i\vec{q}\vec{\rho}}\, d\vec{\rho}. \qquad (16)$$

Calculation of $\langle\alpha_q\rangle$ consists in substituting (10) and (14) in (13) and calculating $\langle\alpha_q\rangle$ with consideration of relation (11). As a result of the calculation we get

$$\langle\alpha_q\rangle = \sigma_s N_1^{(0)}\left\{\frac{1/2\sigma_L\tau/I_L a e^{-\hbar\Omega_s/kT}}{1+(1+b)\sigma_L\tau/I_L}\left[1 + \frac{\langle C_q S_q^*\rangle}{I_L\langle|S_q|^2\rangle}\sum_{q'}\langle C_{q'}^* S_{q'}\rangle + \langle C_{q'} S_{q'}^*\rangle\right] - \frac{b}{1+b}\right\}, \qquad (17)$$

where $I_L = \sum_q \langle|C_q|^2\rangle$; $b = a e^{-\hbar\Omega_L/kT}$. For the reversed wave, i. e. the wave completely correlated with the one to be reversed, $S_q = \text{const}\cdot C_q$ and the expression in brackets in (17) is equal to 2. For waves that are not correlated with the incident wave, $\langle S_q C_q^*\rangle = 0$, and this expression is equal to 1.

Thus with the assumptions that have been made, the gain for the reversed wave will be greater than for other waves regardless of the degree of saturation. This result is obtained with condition (11) that denotes uniform distribution of intensity with respect to transverse coordinates. Such intensity distribution can be achieved for instance by multiple reflection of the wave in a waveguide system [Ref. 1, 5].

In the limit of strong saturation ($\sigma_L \tau I_L \gg 1$) we have

$$\langle \alpha_q \rangle_{кор} = \frac{b}{1+b} \sigma_s N_1^{(0)} (e^{\Delta} - 1); \quad (18a)$$

$$\langle \alpha_q \rangle_{нк} = \frac{b}{1+b} \sigma_s N_1^{(0)} \left(\frac{1}{2} e^{\Delta} - 1 \right). \quad (18б)$$

[The index кор stands for "correlated," and нк -- for "uncorrelated]. The most favorable case is where $\langle \alpha_q \rangle_{кор} > 0$, and $\langle \alpha_q \rangle_{нк} < 0$. This cannot be realized throughout the entire frequency interval since only those mismatches are possible where $e^{\Delta} > 2$ and $\langle \alpha_q \rangle_{нк} > 0$. However, for sufficiently narrow lines, a situation can be realized such that near resonance $\langle \alpha_q \rangle_{нк} < 0$, while far from resonance σ_s becomes small, so that amplification on these frequencies is insignificant.

Let us consider the requirements imposed on gain in this case. The frequency mismatch necessary to achieve amplification on uncorrelated waves is

$$\omega_L - \omega_s^{нк} > (kT/\hbar) \ln 2. \quad (19)$$

he maximum attainable gain is

$$\langle \alpha_q \rangle_{нк} = \frac{1}{2} \frac{b}{1+b} \sigma_s^{нк} N_1^{(0)} e^{\Delta}, \quad (20)$$

$\sigma_s^{нк}$ being taken for frequencies defined by relation (19). The amplification $\langle \alpha_q \rangle_{кор}$ for resonant frequencies is

$$\langle \alpha_q \rangle_{кор}^{рез} \approx \frac{b}{1+b} \sigma_s N_1^{(0)} \frac{\hbar}{kT} (\omega_L - \omega_s^{кор}). \quad (21)$$

For instance, requiring an increase in $\langle \alpha_q \rangle_{кор}^{рез}$ over $\langle \alpha_q \rangle_{нк}^{max}$ by a factor of 2-3, we can find the parameters that must be satisfied by the material of a reversing active medium.

Let us assume that the line is uniformly broadened. Then $a = 1$,

$$\sigma_s = \sigma_0 \frac{(\Delta\omega)^2}{(\omega_s - \omega_0)^2 + (\Delta\omega)^2}. \quad (22)$$

When ω_L is selected near the resonant transition frequency ω_0 within the limits of linewidth $\Delta\omega$ (or several linewidths) and, assuming $\Delta\omega \ll kT$, we have for $\sigma_s^{нк}$ in accordance with (19) and (22)

$$\sigma_s^{нк} \approx \sigma_0 [\Delta\omega/(\omega_0 - \omega_s^{нк})]^2.$$

Then the condition $\langle \alpha_q \rangle_{кор}^{рез} = 2 \langle \alpha_q \rangle_{нк}^{max}$ leads to the situation

$$\omega_L - \omega_s^{кор} \sim \hbar (\Delta\omega)^3 / kT. \quad (23)$$

If $\Delta\omega \approx 1$ cm^{-1}, then $\omega_L - \omega_s^{кор} \sim 0.01$ cm^{-1} at room temperature.

The contrast of the reversed wave depends on gain $G = e^{\langle \alpha_q \rangle_{кор} L}$ (L is the effective length of the active region excited by the wave E_L to be reversed). In the case of strong saturation L is determined by the pulse energy density of the wave to be reversed ε and the density of absorbing particles $N_1^{(0)}$

$$L \approx \frac{1}{2} \frac{\varepsilon}{\hbar\omega_L} \frac{1}{N_1^{(0)}}.$$

For a contrast of the order of 10^5 it is necessary that

$$\frac{1}{2} \langle \alpha_0 \rangle_{\text{нор}} \frac{\varepsilon}{\hbar\omega_L} \frac{1}{N_1^{(0)}} \geq 10, \qquad (24)$$

which determines the minimum pulse energy ε.

However, the contrast required depends to a considerable extent on the job to be done by the reversing mirror. For instance to compensate distortions in an amplifier with high gain it is sufficient to require the necessary contrast only for frequencies that fall within the amplification band, and not worry about what happens to the response on frequencies far removed from resonance. In this case, in virtue of (19) we may not be bothered by the contrast of the reversed wave with respect to waves that are not correlated with it.

Diffusion processes that are most essential for gases will distort the spatial structure of the gain in the reversing mirror, and hence will be detrimental to conditions of reversal (reproduction) of the wavefront. This imposes obvious limitations on the maximum duration of the reproduced pulse and on the degree of reproduction of the microstructure of the wavefront. In this connection, the speed of formation of the reversed wave is important.

Reports recently appeared in the literature in which an analysis was made of the possibility of making reversing mirrors by using different nonlinear effects. In Ref. 6, 7 it is shown that suitable materials for this purpose have rather well-developed nonlinear susceptibility. The author of Ref. 8 presents successful experiments on the use of parametric resonance for wavefront reversal. However, the methods described in Ref. 6-8 for making a reversing mirror require an additional (auxiliary) source of emission. In the presence of one or more auxiliary emission waves, many nonlinear effects may be used for wavefront reversal. Such "active reversing mirrors" may have certain advantages over the "passive mirrors" discussed in Ref. 1, 2, and also in our article. One of the advantages is the possibility of getting a reversed wave with frequency coinciding accurately with that of the wave before reversal ($\omega_L = \omega_s$). However, the necessity of auxiliary radiation makes active mirrors very complex devices.

Of interest in this connection is the possibility of using coherent spontaneous emission (and the related photon echo) in systems with extent much greater than a wavelength. The particulars of coherent spontaneous emission of extended systems are considered in Ref. 9. An analysis of formula (91) in this article shows that the maximum intensity of coherent spontaneous emission must be observed in the direction opposite to wave propagation for a wave that stimulates the super-radiating coherent state. Thus, coherent spontaneous emission can be used for wavefront reversal. In this case the frequency of the reversed signal should practically coincide with that of the incident wave.

The author is deeply grateful to N. G. Basov, B. Ya. Zel'dovich, Yu. Yu. Stoylov, V. S. Zuyev, I. I. Sobel'man and A. A. Orayevskiy.

REFERENCES

1. B. Ya. Zel'dovich, V. I. Popovichev, V. V. Ragul'skiy, F. S. Fayzullov, PIS'MA V ZHURNAL EKSPERIMENTAL'NOY I TEORETICHESKOY FIZIKI Vol 15, 1972, p 160.

2. B. Ya. Zel'dovich, V. V. Shkunov, Preprint FIAN [Lebedev Physics Institute], Moscow, No 196, 1976.

3. Ya. I. Khanin, "Dinamika kvantovykh generatorov" [Dynamics of Quantum Generators], Moscow, Sovetskoye radio, 1975, p 70.

4. A. N. Orayevskiy, "Molekulyarnyye generatory" [Molecular Generators], Moscow, Nauka, 1964, p 85.

5. A. Z. Grasyuk, I. G. Zubarev, A. V. Kotov, S. I. Mikhaylov, V. G. Smirnov, KVANTOVAYA ELEKTRONIKA, Vol 3, 1976, p 1062.

6. R. W. Hellworth, J. OPT. SOC. AMER., Vol 67, 1977, p 1.

7. A. Yariv, OPTICS COMMS, Vol 21, 1977, p 49.

8. S. N. Shostko, "Report to the Joint Seminar of the Lebedev Physics Institute on Quantum Electronics, 27 January 1978."

9. R. N. Dicke, PHYS. REV., Vol 93, 1954, p 99.

6610
CSO: 1870

PHYSICS

UDC 621.378.826:038.823

PARTICULARS OF DF + CO_2 ENERGY TRANSFER IN CHEMICAL LASERS BASED ON CHLORINE FLUORIDES

Moscow KVANTOVAYA ELEKTRONIKA in Russian Vol 6, No 1, Jan 79 pp 231-235

[Article by N. F. Chebotarev and S. Ya. Pshezhetskiy]

[Text] Experimental studies are done on the output parameters of lasers on mixtures of chlorine fluorides with deuterium, and also fluorine with deuterium where CO_2 is used as a component of the active medium. A qualitative analysis is done on the particulars of the transfer DF + CO_2 in laser systems based on ClF_5, ClF_3, ClF and F_2. It is shown that the most efficient transfer DF + CO_2 is realized in a mixture of F_2-D_2-CO_2.

The principal factor that determines the efficiency of chemical lasers based on HF (DF) is the rapid relaxation of these molecules on reaction products and on the initial molecules. Therefore the use of energy transfer from rapidly relaxing vibrationally excited molecules of HF or DF to molecules of CO_2 or others leads to an increase in the chemical efficiency. This idea was first expressed in Ref. 1. In Ref. 2-12 lasing was studied on mixtures of F_2-D_2-CO_2-He with energy transfer DF + CO_2. It was shown that the efficiency of a laser with transition on a CO_2 molecule is limited by heating of the gas during the time of the chemical reaction.

Laser systems based on other fluorides with energy transfer DF + CO_2 have been much less studied than systems with F_2, and data relative to the efficiency of energy transfer to CO_2 in these systems are contradictory.

Among investigated systems with energy transfer DF + CO_2 are mixtures of F_2O-D_2 and F_2O-D_2-CO_2 [Ref. 3]. At pressures of 20-50 mm Hg the laser with CO_2 is more efficient, and at pressures greater than 50 and less than 20 mm Hg, the laser without CO_2 is more efficient.

In Ref. 16, 17, chemical lasers were studied on mixtures of ClF_3-D_2 (-CO_2) and WF_6-D_2(-CO_2) and the energy was observed to approximately triple as

compared with a mixture without CO_2. In Ref. 12, attempts to achieve effective transfer on CO_2 in systems NF_3-D_2-CO_2 and N_2F_4-D_2-CO_2 were unsuccessful.

The possible disagreement of these results is explained by the different conditions of experiments (presence of impurities in the initial components, different conditions of mixing of reagents, initiation powers, temperatures and so forth). On the other hand, as shown in Ref. 14, the efficiency of systems with energy transfer passes through a maximum with increasing reaction rate, which is due to the change in initiation power; therefore it is difficult to interpret the results of experiments with addition of CO_2 to different chemical systems. We studied the energy transfer $DF \rightarrow CO_2$ in laser systems based on chlorine fluorides. The purpose of the work was to clarify the way that transfer efficiency depends on the kind of initial chlorine fluoride, the mechanism and kinetics of formation of DF, which differ for different molecules of ClF_n. The results are compared with data on the transfer $DF \rightarrow CO_2$ for the system F_2-D_2-CO_2-He.

Procedure

The experimental setup is described in Ref. 18. A quartz laser tube 17 mm in diameter and 75 cm long was placed in a cavity formed by a totally reflecting mirror R = 3 m and a Ge plate or a flat mirror with gold coating having a 1.5 mm aperture for coupling out the emission when measuring the duration of lasing. The ends of the tube were covered with NaCl windows oriented perpendicular to the optical axis.

The cavity was tuned by an LG-56 laser. Energy was measured by a KIM-1 calorimeter with recording of the lasing pulse by a GeAu sensor and an S8-11 oscilloscope. The gases ClF_3 and ClF_5 were purifed by distillation in vacuum. ClF was produced from ClF_3 and Cl_2 by heating an equimolar mixture to 300°C. The reaction was initiated by flash photolysis of the mixtures. The presence of F_2 in the chlorine fluorides was checked from the intensity of the band $1 \rightarrow 0$ of DF emission in control experiments: in the presence of F_2 this band is of low intensity or is absent due to the formation of $DF_{v=0}$ when F_2 is "burned out."

Inlet of the mixture into the tube and mixing were done with constant circulation to avoid thermal reactions. In experiments with mixtures of F_2-D_2 and F_2-D_2-CO_2 at pressures below the upper limit, the laser tube was cooled by a stream of nitrogen to a temperature of -80°C. At high pressures the F_2-D_2 mixture was stabilized with oxygen.

Results and discussion

As was shown in Ref. 19, one of the criteria for evaluating the chemical efficiency of a laser system is lasing duration τ_{la}. Comparing the lasing duration for different systems under identical conditions of initiation and at identical pressures of components, we can get an idea of the part played by secondary elementary stages in the creation of stimulated emission.

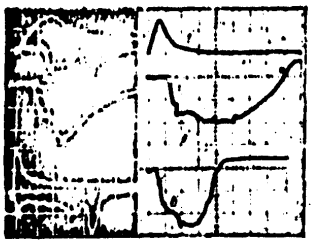

Fig. 1. Oscillograms of pulses of initiating light (1) and corresponding integrated stimulated emission in lasers on the following mixtures (pressure given in mm Hg): 0.5 ClF_5 + 0.5 D_2 + 0.5CO_2, (2); 0.5ClF_5 + 0.5D_2, (3); 1.2F_2 + 1.2D_2 + 2CO_2, (4); 6.7ClF + 2.54D_2 + 17.4He + 13.14CO_2, (5); 6.7ClF + 2.54D_2 + 17.4He, (6) (scanning 2 (2, 3) and 20 μs/div (4-6))

The systems ClF_5-D_2(-CO_2) and ClF_3-D_2(-CO_2) are characterized by short lasing duration comparable with the flash duration; CO_2 slightly increases the τ_{1a}. The difference in behavior of these systems may be due to both kinetic and relaxation phenomena. Energy transfer from DF to CO_2 may lead to an increase in chemical efficiency if the reaction rate is comparable, and the deactivation of CO_2 in collisions with a third body is low compared with the rate of energy transfer, which is more probable at low pressures.

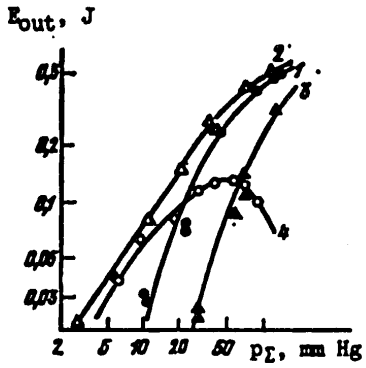

Fig. 2. Curves for laser output energy as related to the total pressure of fluorine and deuterium for mixtures: F_2:D_2:O_2:He:CO_2 = 1:0.38:0.15:7.3:0 (1); 1:0.38:0.15:4.3:3 (2); 1:0.38:0.13:6:0 (3); 1:0.38:1.13:6:3.83 (4) (U = 20 (1, 2) and 13 kV (3, 4))

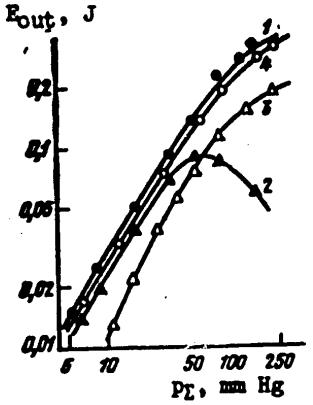

Fig. 3. Laser output energy as a function of the total pressure of ClF and deuterium for the mixtures: ClF:D_2:He:CO_2 = 1:0.38:2.6:2 (1, 2); 1:0.38:2.6:0 (3, 4) (U = 20 (1, 4) and 13 kV (2, 3))

Shown in Fig. 2-5 are curves for emission energy of lasers on mixtures of F_2-D_2(-CO_2), ClF-D_2(-CO_2), ClF_5-D_2(-CO_2) and ClF_3-D_2(-CO_2) as dependent on

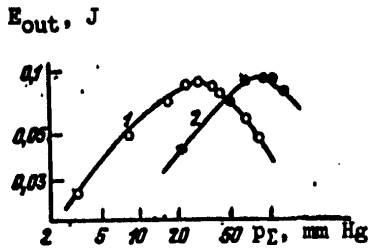

Fig. 4. Laser output energy as a function of integrated pressure of ClF_5 and D_2 for mixtures: $ClF_5:D_2:He:CO_2 = 1:0.5:0.44:0$ (1) and 1:0.5:0.44:1 (2)

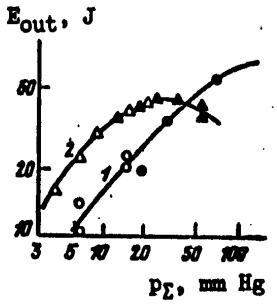

Fig. 5. Laser output energy as a function of integral pressure of ClF_3 and D_2 for mixtures: $ClF_3:D_2:CO_2 = 1:1.5:1$ (1) and 1:1.5:0 (2) (the points show data for experiments on different days)

the overall pressure of deuterium and fluoride. The errors of measurements shown in these figures were no more than 20%, and the reproducibility of results was good. For the first two systems, strong dependence on the initiation energy was observed. The major patterns for both systems are analogous.

The two other systems also give a similar pattern; however, this pattern differs considerably from the first. The differences are apparently due to the competition of processes of deactivation of CO_2 and the rate of formation of DF^*, which is determined mainly by the rate of the elementary process $F + D_2 \rightarrow DF^* + D$ and the process $D + F_2$ or $D + ClF_n$, as well as by the ratio of this rate to the rate of chain breaking. The latter determines the lasing threshold in a system without CO_2.

A peculiarity of the systems ClF_3-$H_2(D_2)$ and ClF_5-$H_2(D_2)$ is that in these systems the formation of HF^* (DF^*) due to the reaction $H + ClF_n \rightarrow HF^* + ClF_{n-1}$ takes place much more slowly†, and as was shown in Ref. 20, does not make any significant contribution to stimulated emission. At the same time, the measurements of Ref. 22 imply that relaxation of HF^* on molecules of ClF_5 and ClF_3 takes place two orders more efficiently than on molecules of F_2 and ClF. With an increase in pressure, when a maximum of energy is observed without CO_2, the addition of CO_2 leads to a reduction of output energy, as can be seen from Fig. 4 and 5. (If we restrict ourselves in Fig. 4 to a pressure of 70 mm Hg, the behavior of the curves in Fig. 4 and 5 will be identical.) In other words, the addition of CO_2 to systems based on ClF_3 and ClF_5 is

†In Ref. 21 the EPR method was used to find the rate constant of the reaction $H + ClF_3 \rightarrow HF^* + ClF_2$, equal at 300 K to $10^{11.652}$ $cm^3/mole \cdot s = 0.0267$ $(\mu s \cdot mm\ Hg)^{-1}$.

effective only at pressures that exceed the optimum for these mixtures without CO_2, which is implied by experimental data.

For the systems F_2-D_2 and ClF-D_2, vice versa, high gain in output energy at low pressures of the reagents is observed when CO_2 is added, particularly for the system F_2-D_2. With an increase in pressure, the E_{out} in systems with CO_2 approaches that in systems without CO_2 (see Fig. 2 and 3). In the case of low-power initiation as the pressure rises the output energy on mixtures without CO_2 is greater than with CO_2. For the system ClF-D_2 with initiation by discharge of a condenser $C = 5.5$ μF, $U = 20$ kV, the output energy was about the same for mixtures with and without CO_2.

For the system F_2-D_2 at low pressure the output pressure is very sensitive to the purity of F_2 and to the presence of $DF_{v=0}$ formed as a result of the dark reaction. It was shown in Ref. 13 that the presence of a small amount of HF in a mixture of F_2-H_2 leads to a reduction of output energy by a factor of 50. When a mixture of F_2-D_2-CO_2 is used, the presence of $DF_{v=0}$ has little effect on the output energy because of the rate of the transfer $DF \rightarrow CO_2$. Therefore an increase is observed in output energy when CO_2 is added to the mixture at low pressures [Ref. 2]. Besides, the addition of O_2 to stabilize the flow has an effect on the threshold pressure of the mixture F_2-D_2 and leads to a reduction in the output energy at low pressures.

As can be seen from Fig. 2, the addition of CO_2 to the system F_2-D_2 is most effective at comparatively low pressures of the reagents (up to 50 mm Hg). At higher pressures with intense initiation, the addition of CO_2 is less effective. For the system ClF-D_2-CO_2 the effectiveness of adding CO_2 is low at all pressures, as implied by Fig. 3.

In the best case the increase in output energy is 100% at low values of specific power output. This can be attributed to the following causes: 1) a lower rate of the reaction $D_2 + ClF$ and less excitation of DCl molecules; 2) a lower constant of transfer $DCl \rightarrow CO_2$ as compared with $DF \rightarrow CO_2$, whereas DCl and DF are formed in a chain process in equivalent amounts; 3) lower exothermicity of the reaction $D + ClF$ as compared with $D + F_2$.

The measurements made in Ref. 16 and 17 showed an increase in the output energy for the system ClF_3-D_2-CO_2 by a factor of approximately three as compared with the mixture without CO_2 throughout the entire pressure range. The cause of lack of agreement with our data may be the presence of F_2 in the initial ClF_3. Then without CO_2, the presence of $DF_{v=0}$ leads to a reduction of the output energy, while with CO_2 the same amount of $DF_{v=0}$ has no effect on the output energy.

Thus the efficiency of systems with energy transfer on CO_2 depends on the relation between the different rates of the processes, and there are optimum conditions for each specific system. For some conditions and systems the use of the transfer $DF \rightarrow CO_2$ is ineffective from the standpoint of raising the power, and high specific parameters can be achieved in systems without CO_2 by selecting the appropriate conditions.

REFERENCES

1. N. G. Basov, A. N. Orayevskiy, V. A. Shcheglov, ZHURNAL TEKHNICHESKOY FIZIKI, Vol 37, 1967, p 339.

2. N. G. Basov, V. T. Galochkin et al. KRATKIYE SOOBSHCHENIYA PO FIZIKE, Lebedev Physics Institute, No 8, 1970, p 10.

3. P. W. Gross, J. CHEM. PHYS., Vol 50, 1969, p 1889.

4. T. A. Cool, R. R. Stephens, J. CHEM. PHYS., Vol 51, 1969, p 5175.

5. T. A. Cool, R. R. Stephens, J. A. Shirley, APPL. PHYS. LETTS, Vol 17, 1970, p 278.

6. J. Wilson, J. S. Stephenson, APPL. PHYS. LETTS, Vol 20, 1972, p 64.

7. N. G. Basov, S. I. Zavorotnyy, Ye. P. Markin, A. I. Nikitin, A. N. Orayevskiy, PIS'MA V ZHURNAL EKSPERIMENTAL'NOY I TEORETICHESKOY FIZIKI, Vol 15, 1972, p 135.

8. T. O. Poehler, M. S. Shandor, R. E. Walker, APPL. PHYS. LETTS, Vol 20, 1972, p 497.

9. S. N. Suchard, A. Ching, J. S. Whittier, APPL. PHYS. LETTS, Vol 21, 1972, p 274.

10. T. O. Poehler, R. E. Walker, J. W. Leight, APPL. PHYS. LETTS, Vol 26, 1975 p 560.

11. N. G. Basov, A. S. Bashkin, P. G. Grigor'yev, A. N. Orayevskiy, O. Ye. Porodinkov, KVANTOVAYA ELEKTRONIKA, Vol 3, 1976, p 2067.

12. P. T. Davis, MICROWAVES, Vol 13, 1974, p 14.

13. O. M. Batovskiy, V. I. Gur'yev, KVANTOVAYA ELEKTRONIKA, Vol 1, 1974, p 676.

14. V. I. Igoshin, "Trudy FIAN" [Proceedings of Lebedev Physics Institute], Vol 76, 1974, p 117.

15. L. V. Kulakov, A. I. Nikitin, A. N. Orayevskiy, KVANTOVAYA ELEKTRONIKA, Vol 3, 1976, p 1677.

16. G. G. Dolgov-Savel'yev, G. M. Chumak, "Kvantovaya elektronika" [Quantum Electronics], edited by N. G. Basov, No 4(10), 1972, p 108.

17. G. M. Chumak, Preprint, Institute of Nuclear Physics, Siberian Department, Academy of Sciences USSR, No 91, 1972.

18. M. F. Chebotarev, S. Ya. Pshezhetskiy, Ye. P. Poltolyarnyy, KVANTOVAYA ELEKTRONIKA, Vol 1, 1974, p 1551.

19. M. F. Chebotarev, L. I. Trakhtenberg, S. Ya. Pshezhetskiy, S. A. Kamenetskaya, KVANTOVAYA ELEKTRONIKA, Vol 1, 1974, p 1212.

20. M. F. Chebotarev, S. Ya. Pshezhetskiy, KVANTOVAYA ELEKTRONIKA, Vol 3, 1976, p 2263.

21. S. J. Pak, R. H. Krech, D. L. McFadden, D. J. Maclean, J. CHEM. PHYS., Vol 62, 1975, p 3419.

22. M. F. Chebotarev, L. I. Trakhtenberg, S. Ya. Pshezhetskiy, KVANTOVAYA ELEKTRONIKA, Vol 3, 1976, p 1331.

6610
CSO: 1870

PHYSICS

UDC 621.375.82

DIFFRACTION EFFECTS IN CW CHEMICAL HF LASER WITH UNSTABLE TELESCOPIC CAVITY

Moscow KVANTOVAYA ELEKTRONIKA in Russian Vol 6, No 1, Jan 79 pp 236-248

[Article by Ya. Z. Virnik, A. K. Piskunov, A. A. Stepanov and V. A. Shcheglov, Physics Institute imeni P. N. Lebedev, Academy of Sciences USSR, Moscow]

[Text] A solution is found for the self-consistent problem of the structure of the emission field of a supersonic cw chemical HF laser with unstable telescopic cavity (steady lasing mode). For typical conditions an analysis is made of the structure of amplitude and phase diagrams of the laser field in the near and far zones, energy characteristics are calculated and the angular divergence of laser emission is determined for different gains in the cavity. It is shown that the use of a telescopic cavity in cw HF lasers leads to a considerable increase in directionality of emission with a moderate reduction in system efficiency.

1. Introduction

Recently considerable attention has been given to the problems of using unstable cavities in lasers. The fundamental physical particulars of such optical systems were considered in Ref. 1-3, where it was shown that the use of unstable cavities can appreciably improve the directionality of laser output emission (in particular by natural mode selection).

Experiments with cw chemical HF lasers [Ref. 4, 5] have shown that the use of unstable cavities reduces the angular divergence of emission (right down to the diffraction divergence [Ref. 5]) although there is a concomitant drop of efficiency. In this paper a solution is found for the self-consistent problem of the structure of the emission field of a cw chemical HF laser (CWCL) in the "cold" state. The calculations that are done enable analysis of the structure of the amplitude and phase of the laser field in near and far zones for typical conditions, evaluation of the energy parameters of the system, and determination of the angular divergence of emission. The calculations directly imply recommendations on choosing optimum parameters of an unstable telescopic cavity.

This problem can be most completely examined on the basis of electrodynamic methods of calcualtion. Included in this category for instance are asymptotic and numerical methods that use Kirchhoff-Fresnel integrals [Ref. 8-11], and also the method based on solution of a wave equation in the quasioptical approximation [Ref. 12-14]. In our paper we will use the latter method since it gives the most consistent description of the interaction between the radiation and the active medium.

It should be emphasized that in contrast to works already published, the problem of the structure of the radiation field in the case of an HF laser of diffusion type is much more complicated. This is due first of all to the multiple-level nature of excitation, and hence to the large number of spectral lines that take part in lasing (which is particularly typical of an HF laser with a chain mechanism of excitation), and secondly to the fact that the kinetic processes responsible for the formation of the active medium in the CWCL take place against a background of diffusion "trails" beyond the nozzle tip. Let us note right away that as a rule, the major part in formation of the emission field structure is played by the gradient of longitudinal inhomogeneities of the active medium in the direction of gas motion, i. e. essentially by transverse inhomogeneities, rather than by the longituidnal inhomogeneities themselves in the direction of the beam. This situation means that in describing the process of mixing of reagents we can use a simplified approach based on a flame front model (see for instance Ref. 6, 7, 15-17). This approach, in describing the change in parameters of the chemically active stream in the cavity region in an averaged way, enables us to analyze the influence that transverse inhomogeneities have on the quality of laser radiation.

Since the angular directionality of laser radiation is determined both by cavity geometry and the degree of inhomogeneity of the active medium, let us briefly discuss the problem of the nature of inhomogeneities inherent in the CWCL. First of all let us note the influence of inhomogeneities caused by nonuniformity of amplification on individual vibrational-rotational transitions of HF molecules along the flow of working gas. Moreover, an essential part in formation of the structure of the emission field may also be played by inhomogeneities of the index of refraction, as happens in lasers of other types. In the general case, inhomogeneities of the index of refraction include resonant and nonresonant parts (see the Appendix). Let us note that inhomogeneities of resonant type are due to the contribution made by vibrational-rotational transitions of the working molecule with frequencies close to the lasing frequency, to the polarization of the active medium (on the given frequency). The nonresonant inhomogeneities include those due to a change in the chemical composition of the mixture, as well as to a change in particle density caused by thermal and gasdynamic effects in the stream. Let us also note that under typical conditions for a CWCL using a "cold" pumping reaction $F + H_2 \rightarrow HF + H$ (pressure at the nozzle tip $p \approx 5$-10 mm Hg, helium dilution of the oxidative stream -- 10-15) the mean gradient of the index of refraction corresponding to the mentioned inhomogeneities is 10^{-8}-10^{-7} cm^{-1} as a rule.

2. Initial equations

A simplified diagram of the investigated laser is shown in Fig. 1. We will restrict ourselves to the case of cylindrical mirrors (the two-dimensional problem), but it should be noted that such calculations, generally speaking, will also describe the structure of the emission field in the plane of symmetry for a cavity with spherical mirrors of rectangular shape [Ref. 7].

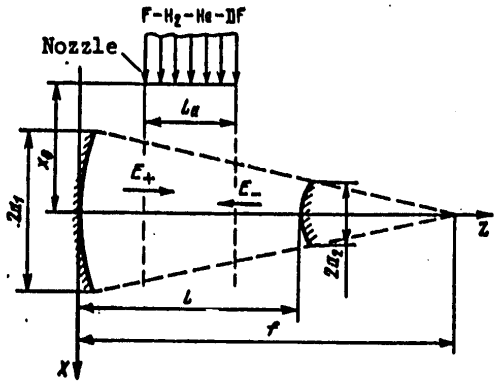

Fig. 1. Diagram of CWCL

In the general case, lasing in the CWCL can be stimulated on a large number of vibrational-rotational transitions of the P-branch v, $j_V - 1 \to v - 1$, j_V (v is the number of the vibrational level, j_V is the rotational quantum number). Clearly an adequate description of the emission spectrum of such a laser requires solution of a system of parabolic equations for the electromagnetic field (see the Appendix) combined with a system of kinetic and gasdynamic equations [Ref. 15, 17] at various possible values of v and j_V. In such a situation, calculation of the emission field demands excessive amounts of computer time, and therefore this approach is not feasible. In this connection, from here on we will study the lasing mode only on two vibrational-rotational transitions v, $j_V - 1 \to v - 1$, j_V (v = 1, 2), the rotational numbers being considered as given. It is shown below that such an approach is fairly sound.

Using the flame front model to describe the mixing of chemically active flows, we write the initial equations for the molar-mass concentrations of atomic fluorine y_F and molecules of hydrogen fluoride y_V in the usual form [Ref. 15]

$$\frac{\partial}{\partial x} y_F = -(\rho/u) Q_x + (y_F^0 - y_F) Q_{см}, \tag{1}$$

$$\frac{\partial}{\partial x} y_v = (\rho/u) \{\alpha_v Q_x + Q_{VV}(v) + Q_{VT}(v)\} - y_v Q_{см} + Q_p(v); \quad v = 0, 1, \ldots, 4. \tag{2}$$

Here $Q_x = k_x y_F y^0_{H_2}$; $Q_{CM} = (1/y_f)(dy_f/dx)$; the terms Q_{VV} and Q_{VT} describe VV exchange and VT relaxation of HF in the harmonic approximation; k_x is the rate constant of chemical pumping; α_v is the probability of formation of HF on the v-th vibrational level; ρ is the mass density of the mixture; u is the velocity of the flow; $y_f(x)$ is the half-width of the flame front; y^0_F and $y^0_{H_2}$ are the stoichiometric values of the molar-mass concentrations of atoms of F and molecules of H_2 on the flame front.

The radiation term Q_p in (2) takes the form

$$Q_p(v) = (1-\delta_{40})(1-\delta_{20}) \times$$
$$\times \left\{(1-\delta_{20}) g^{J_{v+1}}_{v+1,\,v} I_{v+1,\,v} - (1-\delta_{10}) g^{J_v}_{v,\,v-1} I_{v,\,v-1}\right\} / (\rho u),$$

where $I_{v,\,v-1}$ is the emission intensity in the band $v \to v-1$, and $g^J_{v,\,v-1}$ is the weak-signal gain (on the transition $v, j-1 \to v-1, j$) within the flame front surface;

$$g^J_{v,\,v-1} = \rho N_a \frac{c^2 A^J_{v,\,v-1}}{8\pi \nu^2_{vJ}} \frac{\theta_{rot}}{T} (2j-1) S_{vJ} f(0), \qquad (3)$$

where

$$S_{vJ} = \left[y_v - y_{v-1} \exp\left(-\frac{2\theta_{rot}}{T} J\right)\right] \exp\left[-\frac{\theta_{rot}}{T} J(J-1)\right]$$

and $f(0) = (\ln 2/\pi)^{1/2} (1/\Delta\nu_D) \exp(\beta^2) \operatorname{erfc}(\beta)$ is the form of the line for the case where lasing frequency coincides with the center of the line, $\beta = \Delta\nu_a \sqrt{\ln 2}/\Delta\nu_D$ and $\operatorname{erfc}(\beta) = 1 - (2/\sqrt{\pi}) \int_0^\beta e^{-t^2} d\xi$. The Doppler and Lorentz half-widths of the lines are equal to $\Delta\nu_D = 3{,}58 \cdot 10^{-7} \nu_{vJ} (T/20)^{1/2}$ and $\Delta\nu_a = pT^{-1/2} \sum_i \alpha_i \xi_i$, respectively, where $\xi_i = p_i/p$, and for the coefficients of impact broadening we can take $\alpha_{HF} = 2.3 \cdot 10^{-3}$ and $\alpha_{i \neq HF} = 1.14 \cdot 10^{-3}$ (in $K^{1/2}$/(cm·mm Hg). Thus for the HF molecule we get

$$\beta \approx 2{,}67 (p/T) [2{,}3 \xi_{HF} + 1{,}14 (1 - \xi_{HF})],$$

where the pressure p is expressed in mm Hg, and the temperature T of the mixture -- in kelvins.

For typical conditions of a CWCL of diffusion type β is always much less than unity, i. e. Doppler broadening of the HF lines predominates. In this case (3) implies that

$$g^J_{v,\,v-1} = \rho N_a \frac{c^2 A^J_{v,\,v-1}}{8\pi \Delta\nu_D \nu^2_{vJ}} (\ln 2/\pi)^{1/2} \left(\frac{\theta_{rot}}{T}\right) (2j-1) S_{vJ}.$$

Finally, the intensities $I_{v,\,v-1}$ of individual bands are related to the complex amplitudes of the vectors of electric intensity of electromagnetic fields $E_{v,\,v-1} = \mathcal{E}_{v,\,v-1} e^{i\omega_{v,\,v-1} t}$ by the expression $I_{v,\,v-1} = (\mathcal{E}_{v,\,v-1} \mathcal{E}^*_{v,\,v-1})/(204\pi)$, where $I_{v,\,v-1}$ is expressed in W/cm^2, and $\mathcal{E}_{v,\,v-1}$ is expressed in V/cm. Representing the fields $E_{v,\,v-1}$ in the form of the sum of the forward $E^+_{v,\,v-1}$ and reverse $E^-_{v,\,v-1}$ waves, separating out the rapidly varying phase factors

$$E^{\pm}_{v,\,v-1} = \mathcal{E}^{\pm}_{v,\,v-1}\exp[i(\omega_{vJ}t \mp k_{vJ}z)],$$

we find that the intensities $I_{v,\,v-1}$ are expressed in terms of the slowly varying complex amplitudes $\mathcal{E}^{\pm}_{v,\,v-1}$ of the forward and reverse waves as follows:

$$I_{v,\,v-1} = [1/(240\pi)]\,(|\,\mathcal{E}^{+}_{v,\,v-1}|^2 + |\,\mathcal{E}^{-}_{v,\,v-1}|^2 + \mathcal{E}^{+}_{v,\,v-1}(\mathcal{E}^{-}_{v,\,v-1})^{*}e^{i2k_{vJ}z} + \\ + \mathcal{E}^{+}_{v,\,v-1})^{*}\,\mathcal{E}^{-}_{v,\,v-1}e^{-i2k_{vJ}z}\,).$$

Let us note that the last two terms in this expression are due to the interference of opposed waves, and in virtue of the extremely fine structure of the interference pattern (characteristic period $\sim\lambda_{vJ}\sim 10^{-4}$ cm), they can be disregarded.

Furthermore, as estimates show, for the low pressures used in the CWCL we can totally ignore signal amplification on adjacent vibrational-rotational transitions with frequencies that differ from the frequency ω_{vJ} of the investigated signal, and under these conditions the parabolic wave equations for the slow complex amplitudes of the forward and reverse waves take the form ($v = 1, 2$)

$$\pm\frac{\partial}{\partial z}\mathcal{E}^{\pm}_{v,\,v-1} + (i/2k_{vJ})\frac{\partial^2}{\partial x^2}\mathcal{E}^{\pm}_{v,\,v-1} = \left[\frac{1}{2}G'_{v,\,v-1} - ik_{vJ}\overline{\Delta n}(\omega_{vJ})\right]\mathcal{E}^{\pm}_{v,\,v-1}. \quad (4)$$

Let us note that the "+" in (4) corresponds to the forward wave, while the "-" corresponds to the reverse wave; $G'_{v,\,v-1} = (y_f/h_a)\,g'_{v,\,v-1}$ is the effective (integral) gain of the active medium in the flame front model, and $\overline{\Delta n}$ is the index of refraction averaged with respect to the period h_a of the structure of the nozzle unit (see the Appendix).

To determine the structure of the fields in the cavity, the system of written equations supplemented by equations of gasdynamics in the quasi-one-dimensional approximation [Ref. 15, 17] is integrated by the usual iteration method with consideration of the corresponding boundary conditions. For the functions $y_P(x)$ and $y_V(x,z)$ the boundary conditions are obvious:

$$y_P(-x_a) = y_P^0;\quad y_v(-x_a,\,z) = 0,\ v = 0,\,1,\,\ldots,\,4.$$

With respect to the boundary conditions for the functions $\mathcal{E}^{\pm}_{v,\,v-1}$ on the mirrors of the cavity, we note the following. From the integral representation of the solution for $\mathcal{E}^{\pm}_{v,\,v-1}$ (for instance when the right-hand member of (4) is absent) we can easily see that in the case of a sufficiently large Fresnel number $N_\Phi = a_1^2/(\lambda_{vJ}L)$ the calculation of $\mathcal{E}^{\pm}_{v,\,v-1}$ requires a rather small integration step Δx in the transverse direction (this is due to the presence of a rapidly oscillating phase factor of the type $\exp(-ik_{vJ}x^2/2L)$). In the case of numerical integration of system (4), cofactors of this kind also show up in the boundary conditions on the mirrors [Ref. 13], thus complicating the investigation of cases that are of greatest practical interest. Nonetheless, the range of permissible Fresnel numbers (and cavity amplification factors) can be expanded if a

convergent coordinate system is used to integrate the reverse wave rather than a rectangular system (i. e. the cartesian system X, Z).

Let us note that the idea of introducing a convergent coordinate system is fairly simple [Ref. 12, 14]. In point of fact, the reverse wave is by nature divergent, and therefore in the case of cylindrical mirrors it is convenient to treat it in the first approximation as a cylindrical wave emanating from a common focus of the optical system. Since in the geometric approximation a divergent wave occupies a region on the XZ plane that is formed by rays emanating from a focus and passing through the edges of the mirrors (see Fig. 1), it is understandable that this region can be transformed by the relation

$$\xi = fx/(f-z),\ \eta = fz/(f-z), \tag{5}$$

where $f = R_1/2$ is focal length and R_1 is the radius of curvature of the large mirror, to a rectangular region on the plane $\xi\eta$. If now we set

$$\mathcal{E}^-_{v,\,v-1}(x, z) = (f-z)^{-1/2} W^-_{v,\,v-1}(\xi, \eta) \exp\left[-\frac{ik_{vj}x^2}{2(f-z)}\right], \tag{6}$$

thus isolating the rapidly varying phase factor in the transverse direction in $\mathcal{E}^-_{v,\,v-1}$, it can be readily demonstrated by direct calculations that the function $W^-_{v,\,v-1}$ satisfies the following parabolic equation ($v = 1, 2$):

$$-\frac{\partial}{\partial\eta} W^-_{v,\,v-1} + (i/2k_{vj})\frac{\partial^2}{\partial\xi^2} W^-_{v,\,v-1} = i(f-z)/f]^2 \left\{\frac{1}{2} G^j_{v,\,v-1} - ik_{vj}\overline{\Delta n}(\omega_{vj})\right\} W^-_{v,\,v-1},$$

where it should be considered that in virtue of (5), and the functions $G^j_{v,\,v-1}$ and Δn depend implicitly on $\xi\eta$. Since $\mathcal{E}^\pm_{v,\,v-1}$ and $W^-_{v,\,v-1}$ are slow functions $z(\eta)$, and the radii of the mirrors as a rule are rather large, it can be shown that $\mathcal{E}^+_{v,\,v-1}$ and $W^-_{v,\,v-1}$ are related in the planes of the mirrors by the following boundary conditions:

a) when $z = \eta = 0$

$$\mathcal{E}^+_{v,\,v-1}(x, 0) = (2/R_1)^{1/2}\,\rho_1(x)\,W^-_{v,\,v-1}(x, 0);$$

b) when $z = L$ and $\eta = ML$

$$W^-_{v,\,v-1}(\xi, ML) = (R_2/2)^{1/2}\,\rho_2(\xi/M)\,\mathcal{E}^+_{v,\,v-1}(\xi/M, L).$$

Here $M = R_1/R_2 = f/(f-L)$ is the gain of the cavity, R_2 is the radius of curvature of the small mirror, $\rho_1(x)$ and $\rho_2(x)$ are the amplitude coefficients of reflection.

Thus the special transformation of coordinates eliminates the rapidly varying phase factors in the boundary conditions for $\mathcal{E}^\pm$ and W^-; this appreciably facilitates the problem of numerical integration of parabolic wave equations and expands the range of permissible values of N_Φ and M. On the other hand, let us point out that such a transformation is helpful in reality only when the transverse gradients $\overline{\Delta n}$ are comparatively small. Clearly otherwise the mentioned difficulties remain in force.

3. Initial conditions. Particulars of the numerical method

Initial conditions. As in Ref. 6, 7, the calculations were done for a mixture of $(F_2-D_2-He)H_2$, and it was assumed that practically total dissociation of the surplus F_2 into atoms of F takes place with ignition of F_2-D_2 in the forechamber. Thus it was assumed that in the primary flow (i. e. in the flow of oxidant) emanating from the nozzle unit there is no molecular fluorine. It was also assumed that mixing of the reagents takes place under standard conditions, and the shape of the flame front is described by the relation $y_f/h_* = (x/x_д)^{\frac{1}{2}}$ characteristic of the mode of laminar mixing. Denoting the molar fractions of particles F, F_2, He and DF in the primary flow by ξ_i, we introduce the following parameters: $\alpha_F = \xi_F/(\xi_F + 2\xi_{F_2})$, $\beta_{He} = 2\xi_{He}/(\xi_F+2\xi_{F_2})$ and $\beta_{DF} = 2\xi_{DF}/(\xi_F+2\xi_{F_2})$. It is understood that α_F characterizes the degree of dissociation of F_2, β_{He} -- the degree of helium dilution of the primary flow, and β_{DF} -- the content of DF molecules.

The principal version for which the calculations were done is characterized by the following parameters of flows: primary flow $p_1 = 5$ mm Hg, $T_1 = 275$ K, $u_1 = 2.7$ km/s, $\alpha_F = 1$, $\beta_{He} = 15$ and $\beta_{DF} = 2$; secondary flow $p_2 = 5$ mm Hg, $T_2 = 110$ K and $u_2 = 2.3$ km/s.

The diffusion length (characteristic mixing length) in the calculations was taken as equal to $x_д = 30$ cm, the length of the active medium (height of the nozzle unit) $L_\alpha = 20$ cm. The telescopic cavity was assumed to be symmetric relative to the optical axis, the size of the larger (concave) mirror being $2a_1 = 3$ cm, and its radius of curvature $R_1 = 9$ m, which were taken as fixed in the model calculations. The latter means that when the quantity M is varied (coefficient of amplification) there is a change both in the size of the small mirror $2a_2 = 2a_1/M$, and in the radius of curvature, as well as in cavity length L. Let us also note that the distance from the nozzle tip to the optical axis of the cavity ($x_0 = 2.5$ cm) was likewise taken as fixed.

Particulars of the numerical method. In the computational approximation of parabolic wave equations for $\mathcal{E}^+_{v,\,v-1}$ and $W^-_{v,\,v-1}$ a two-layer implicit scheme of the second order of accuracy (Crank-Nicholson scheme) was used [Ref. 18], and the resultant system of algebraic equations for net-point functions was solved by the method of scalar sweep-out with complex coefficients (analog of matrix sweep-out). It should be pointed out that using a sweep method requires formulation of the corresponding boundary conditions on the side boundaries of the integration regions, i. e. at $x = \pm x_*$ and $\xi = \pm\xi_*$. As in Ref. 13, we used zero boundary conditions $\mathcal{E}^+_{v,v-1}(\pm x_*, z) = 0$ and $W^-_{v,v-1}(\pm\xi_*, \eta) = 0$ to simplify the algorithm, and to prevent the fictitious boundaries from influencing the structure of the fields in the cavity, they had to be shifted quite a distance (for instance we took $x_* \approx 2a_1$).

As a rule, the calculations used from 300 to 600 points in the transverse direction (along the x axis), and 40-60 points in the longitudinal direction. This number of points is completely sufficient for guaranteeing adequate

accuracy of integration both for the equations of the active medium and for the equations of the emission field. Let us note that the typical time for calculating a single variant (8-10 double passes of the cavity) on the BESM-6 computer was 1 hour, which is approximately double the time for calculating an analogous problem in the geometrical optics approximation [Ref. 6].

To speed up convergence of the iteration process we used (as is usually done [Ref. 12-14]) smoothing of the edges of the mirrors. To do this, we introduced the gaussian form of dependence of coefficients of reflection on coordinate ($i = 1, 2$):

$$\rho_i(x) = \begin{cases} \exp[-\gamma_i(x+a_i)^2], & x \leqslant -a_i, \\ 1 & |x| < a_i, \\ \exp[-\gamma_i(x-a_i)^2], & x \geqslant a_i. \end{cases}$$

In order for the edges of the mirrors to remain sufficiently sharp, the coefficients of smoothing γ_i were taken as equal to $\gamma_1 = \gamma_2 = 10^3$. If we consider the fact that the order of the least number still distinct from 0 in the BESM-6 computer is 10^{-19}, it can be estimated that the width of the smoothing sections in our case did not exceed $\Delta x \approx 0.2$ cm.

Finally, let us make one last remark. The calculation of energy characteristics of the CWCL (reduced power of stimulated emission, chemical efficiency and so on) is done according to relations found for $I^+_{v,\ v-1}(x)$ in a standard way [Ref. 6, 15, 17]. Knowing in addition the phase distribution in the plane of the output mirror, and using the Kirchhoff-Fresnel integral, one can readily find the distribution of the emission field in the far zone as well, i. e. the radiation pattern. Of course, we will not go into these problems further here.

4. Discussion of the results

In Ref. 6, where the energy characteristics of the CWCL were calculated in the geometric optics approximation, it was shown that under conditions of rotational equilibrium of working molecules stable steady-state emission for each of the vibrational lasing bands is realized only on the one rotational P-transition. In our research within the framework of the diffraction approach additional study involving this problem has been done. Investigation of the possibility of simultaneous stimulated emission on two adjacent transitions (with j_v and $j_v \pm 1$) of a single band has shown that regardless of the choice of initial conditions the mutual competition of two radiative transitions leads to suppression of one of them (see Fig. 2). For instance under the investigated conditions stable steady-state lasing was achieved only on lines $P_2(6)$ and $P_1(6)$, and therefore in further calculations it was assumed that $j_1 = j_2 = 6$.

Let us note that in the experiments we managed to observe several lines within the limits of a single band in the spectrum of the CWCL. As noted in Ref. 6, such a spectrum may be due for instance to effects of rotational

nonequilibrium of HF. In addition, under certain conditions effects may also arise that are associated with the phenomenon of self-oscillatory instability in flow-through lasers with unstable cavities [Ref. 19], and that cause a pulsation mode of laser operation on several vibrational-rotational transitions.

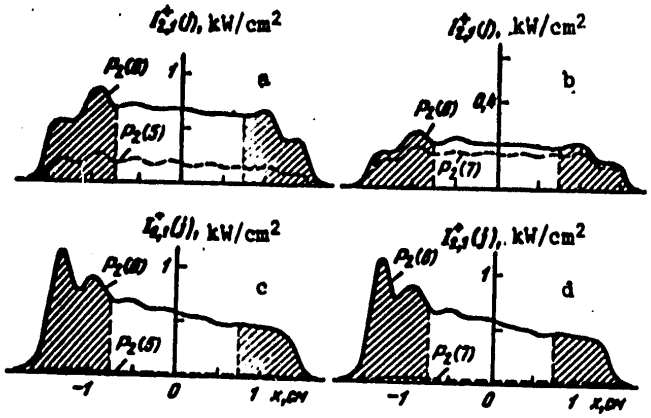

Fig. 2. Suppression of competing radiative transition with two-frequency lasing in a single band (M = 2) for iteration number i = 1 (a, c) and 15 (b, d), $j_2^1 = 5$ (a, b) and 6 (c, d), $j'' = 6$ (a, b) and 7 (c, d).

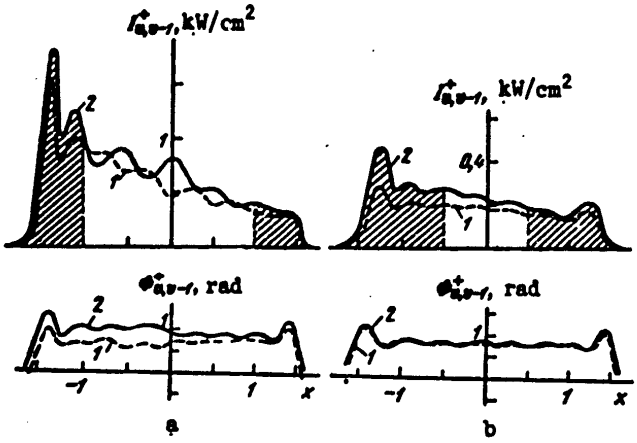

Fig. 3. Structure of fields in the plane of the output mirror with gain M = 1.5 (a) and 3 (b); values of v are shown on the curves.

The series of calculations that was done corresponded to a change of gain in the telescopic cavity over a fairly wide range of values (M = 1.3-8). The typical form of distribution of emission intensities of separate bands

and their corresponding phases $\phi_{\nu,\ \nu-1}$ in the plane of the output mirror for several values of M is shown in Fig. 3. The corresponding radiation patterns are shown in Fig. 4.

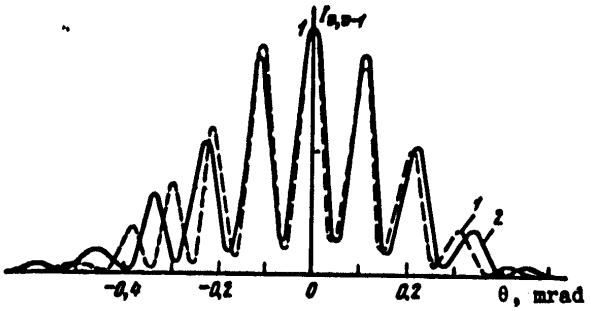

a

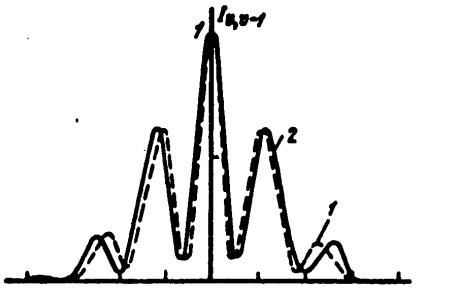

b

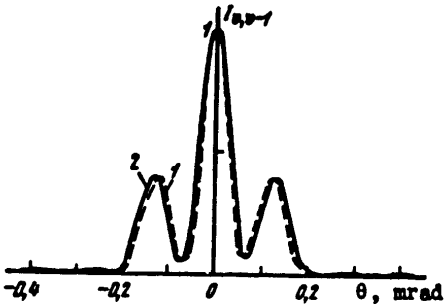

c

Fig. 4. Radiation patterns for M = 1.5 (a), 2 (b) and 3 (c). The values of ν are indicated on the curves

As noted in Ref. 13, a homogeneous active medium does not introduce any perturbations into the field structure of an empty telescopic cavity, and hence does not spoil its radiation pattern. On the other hand, in flow-through systems distortions are introduced into the field structure of the active medium of the laser [Ref. 12-14]. Let us note that the CWCL differs from the purely gasdynamic lasers studied in the cited works, generally speaking, in the way that the amplification properties depend on the flow coordinate. As a consequence, this also leads to less perturbation of the field structure of the unstable cavity by the active medium of the CWCL.

Of course, everything that we have said is true only in the case where transverse inhomogeneities of the index of refraction Δn are not too great, which is indeed the case in the given situation (with the possible exception of the conditions with slight helium dilution of the mixture). Actually, if nonuniformity of signal amplification leads mainly to skewing of the amplitude diagram, inhomogeneities of the index of refraction show up mainly on the

phase diagram. Clearly phase distortions have a much greater influence on the radiation pattern than amplitude distortions (see for instance Ref. 20).

It is clear from the given curves that in the investigated case when $M \geq 3$ the active medium of the CWCL introduces weak distortions into the field structure of an empty cavity, and as a consequence the radiation pattern of CWCL emission practically coincides with that of an empty cavity with the sole exception of a slight overall background. Let us note that the shift of curves $I_{1,0}(\theta)$ and $I_{2,1}(\theta)$ relative to one another on Fig. 4 can be attributed first of all to the difference in the wave numbers k_{vj} of the corresponding lines. With a further reduction in the gain of the cavity, asymmetry shows up both in the structure of the fields and phases relative to the optical axis of the cavity, and in the radiation pattern itself. The most appreciable asymmetry is observed at M fairly close to unity, i. e. in the region of strong radiation fields that lead to rapid depletion of the active medium in the direction of gas motion. Calculations show that the asymmetry also increases with a reduction in the degree of helium dilution of the mixture (with a reduction in β_{He}) and with an increase in the height of the nozzle unit (with increasing L_a) which can be attributed mainly to the same causes.

Nonetheless, despite these distortions and the appearance of a background, the characteristic angular width of the radiation pattern for each fixed M changes comparatively weakly, and as a rule increases by no more than a factor of 1.5-2 as compared with an empty cavity. This circumstance enables us to control the emission divergence of the CWCL by changing the gain M. It is also clear that the reduction in divergence with increasing M is due to an increase in the size of the luminescent region in the plane of the output mirror, but it should be noted that at the same time there is a drop in laser efficiency (Fig. 5). The latter is due of course to the fact that gains on individual vibrational-rotational transitions in the CWCL are comparatively low ($G^{j}_{v,v-1} \geq 0.05$-0.1 cm^{-1} and $G^{j}_{v,v-1}L_a < 2$).

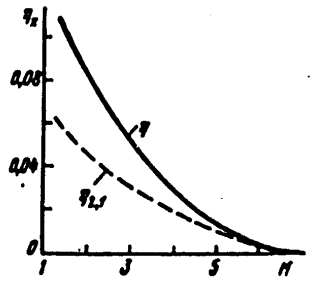

Fig. 5. Dependence of the chemical efficiency of an HF laser on gain of the cavity

It is of interest to estimate the limiting angular divergence in the case considered here. Considering that $\lambda_{vj} \approx 2.7 \cdot 10^{-4}$ cm, while the characteristic transverse dimension of the region is $\Delta x \approx 3$ cm, we get $\Delta\theta_{min} \approx \lambda/\Delta x \approx 10^{-4}$ rad for the half-width of the limiting angular divergence. Referring to the curves, we note that for $M = 1.5$-2 the divergence of the CWCL is close to the limit, and even moreso at large gains.

Consider now the case of a stable confocal cavity. It is known that in this case the half-width of the radiation pattern is evaluated by the relation $\Delta\theta \geq (\lambda/L)^{1/2}$, where L is the length of the cavity. When $L \approx 1$-3 m, this gives $\Delta\theta \geq 10^{-3}$ rad. Besides, with consideration of the multimode structure of the

radiation, the latter figure must be increased by a considerable factor. It is clear from these estimates that the use of telescopic cavities in the CWCL in principle enables an improvement in the directionality of emission by approximately an order of magnitude. Of course the actual radiation pattern will also depend on a number of additional factors not considered here: misalignment of mirrors, deviation of mirror surface from the ideal form (in particular due to nonuniform heating under the action of powerful laser radiation) and so forth. Accounting for these factors goes beyond the scope of this work.

Let us note a few more results of our research. In the first place, the calculations show that for a fixed M, a change in cavity length L, i. e. in the radius of curvature of the large mirror R_1 (R_1 being varied from 3 to 15 m) has extremely little effect on either the efficiency or the divergence of the radiation. Let us mention that with a reduction in $L(R_1)$, i. e. with an increase in the Fresnel number, efficiency drops somewhat, and there is an increase in the directionality of emission. Secondly, due to lack of space we will not give here the results of comparison of the diffraction and geometric-optics methods of calculating a CWCL with telescope cavity. Nevertheless, it should be noted that such a comparison shows complete applicability of the geometric optics approximation for calculating the energy characteristics of the CWCL. For this reason we will also omit here any discussion of the influence that individual parameters of the system (including cavity geometry) have on the energy properties of the CWCL (see for instance Ref. 6).

5. Conclusion

Thus our research shows that with a moderate reduction of efficiency the use of unstable cavities in a CWCL should lead to a considerable increase in the directionality of radiation. Even taking the losses in efficiency into consideration, it should nevertheless be acknowledged that this is quite sound in a number of applications. It should also be pointed out that losses in efficiency should decrease with an increase in the length of the active medium and in power.

Let us note further that nothing has been said in this paper about the inhomogeneities caused by weak shock waves and rarefaction waves that are formed when supersonic gas jets are discharged into the cavity space [Ref. 21]. There has been practically no mention either of the effects caused by flow turbulization. It can be noted with respect to the former effects that adequate consideration on the given stage is a fairly complicated problem, and to all appearances requires the use of Navier-Stokes equations. On the other hand, it is also clear that it is desirable in practice to realize modes of flow that are close to rated conditions, and in this case the influence of the given effects is minimized.

As to turbulent effects, in the case of a CWCL on a "cold" reaction short laser zones are usually realized, and as experiments have shown, turbulence

does not have time to develop in the cavity zone. Therefore it is not advisable to consider these effects here. It is completely possible that in the case of a chain mechanism of excitation (characterized by wide lasing zones) turbulence effects may take on special significance, but analysis of this question is beyond the scope of our paper.

APPENDIX

Form of parabolic wave equations in accounting for the vibrational-rotational structure of active molecules

Let the total electromagnetic field E be a superposition of fields $E_{vj} \equiv E^{v, j-1}_{v-1, j}$, corresponding to radiative transitions on individual spectral frequencies in the CWCL. In the general case we will assume that the lasing frequencies ω_{vj} do not coincide with the frequencies Ω_{vj} of molecular transitions in the center of the lines.

Disregarding the effects of interaction of waves E_{vj} with each other, we can get a wave equation of the form

$$\text{grad div } E_{vj} - \Delta E_{vj} = -\frac{1}{c^2}\frac{\partial^2}{\partial t^2} D_{vj}, \qquad (A.1)$$

from Maxwell's equations for each component of the electromagnetic field, where D_{vj} is the vector of electric induction.

We introduce into consideration the polarization P_{vj} of the active medium, and resolve it into resonance $P_{vj}(\omega_{vj})$ and nonresonance P_0 components; then

$$D_{vj} = \varepsilon_0 E_{vj} + 4\pi P_{vj}(\omega_{vj}), \qquad (A.2)$$

where $\varepsilon_0 = 1 + 4\pi\alpha_0$ is the nonresonant component of permittivity of the medium, and α_0 is dielectric susceptibility.

With consideration of (A.2), equation (A.1) takes the form

$$\text{grad div } E_{vj} - \Delta E_{vj} + \frac{1}{c^2}\frac{\partial^2}{\partial t^2}(\varepsilon_0 E_{vj}) = -\frac{4\pi}{c^2}\frac{\partial^2}{\partial t^2} P_{vj}(\omega_{vj}). \qquad (A.3)$$

Resolving the field in the cavity into a sum of forward and reverse waves

$$E_{vj} = E^{+}_{vj} + E^{-}_{vj}, \quad P_{vj} = P^{+}_{vj} + P^{-}_{vj},$$

we substitute these expressions in (A.3), first having separated out the rapidly varying phase factors in $E^{\pm}$ and $P^{\pm}$

$$E^{\pm}_{vj} = \vec{\mathcal{E}}^{\pm}_{vj} \exp\left[i\left(\omega_{vj} t \mp k_{vj} z\right)\right], \quad P^{\pm}_{vj} = \vec{\mathcal{P}}^{\pm}_{vj} \exp\left[i\left(\omega_{vj} t \mp k_{vj} z\right)\right].$$

We can easily get abbreviated parabolic equations by a conventional method (see for instance Ref. 22, 23) for slowly varying complex amplitudes $\mathcal{E}^{\pm}$

$$\pm\frac{\partial}{\partial z}\mathcal{E}^{\pm}_{vj} + (1/2k_{vj})\frac{\partial^2}{\partial x^2}\mathcal{E}^{\pm}_{vj} + (1/2)\,k_{vj}(\varepsilon_0 - 1)\,\mathcal{E}^{\pm}_{vj} = -i2\pi k_{vj}\mathcal{P}^{\pm}_{vj}(\omega_{vj}). \qquad (A.4)$$

Let us note that in the general case (for instance if the frequencies of radiative transitions corresponding to different v and j are fairly close or the contours of spectral lines are strongly broadened at high pressures)

many vibrational-rotational transitions of different bands of HF may make their contribution to polarization on the investigated frequency ω_{vj}. To demonstrate this, it is necessary to introduce the density matrix ρ for description of the multilevel active medium, and to determine the resonant polarization in the usual way:

$$P_{vj}(\omega_{vj}) = N_0 \mathrm{Sp}(\hat{\mu}\rho),$$

where N_0 is the density of HF molecules, and $\hat{\mu}$ is the operator of the electric dipole moment.

Limiting ourselves to the quasi-steady state approximation and using the approach outlined for example in Ref. 24, we can get the following expression (assuming combined broadening of spectral lines) for $\mathcal{P}_{vj}$

$$\mathcal{P}_{vj}(\omega_{vj}) = (\mathcal{E}_{vj}/4\pi)\sum_{p,q} k_{pq}^{-1} g_{p,p-1}^{q}(\omega_{vj})\left[\Phi\left(\alpha_{pq}^{vj},\beta\right)/F\left(\alpha_{pq}^{vj},\beta\right)\right]. \qquad (A.5)$$

Let us note that the summation in (A.5) is done with respect to all possible vibrational and rotational (p and q respectively) states of HF, the gain on the vibrational-rotational transition p, q-1 → p-1, q being written as

$$g_{p,p-1}^{q}(\omega_{vj}) = 8\pi^3 \nu_{vj}\left|\mu_{p,p-1}^{q}\right|^2 (\ln 2/\pi)^{1/2}/\left(3\hbar c\,\Delta\nu_{\mathcal{A}}\right)\times$$
$$\times\left[N_{p,q-1}/(2q-1) - N_{p-1,q}/(2q+1)\right]F\left(\alpha_{pq}^{vj},\beta\right),$$

where $\alpha_{pq}^{vj} = \left(\omega_{vj} - \Omega_{pq}\right)(\ln 2)^{1/2}/\Delta\omega_{\mathcal{A}}$ and $\beta = \Delta\omega_{\mathcal{A}}(\ln 2)^{1/2}/\Delta\omega_{\mathcal{A}}$, with $\Delta\omega_{\mathcal{A}} = 2\pi\Delta\nu_{\mathcal{A}}$ and $\Delta\omega_{\mathcal{A}} = 2\pi\Delta\nu_{\mathcal{A}}$ being the Doppler and Lorentz half-width of the line respectively.

Then the complex function $\Phi(x,y)$ appearing in (A.5) takes the form

$$\Phi(x,y) = \frac{1}{\pi}\int_{-\infty}^{\infty}\frac{e^{-t^2}dt}{(x-t)-iy} = L(x,y) + iF(x,y),$$

where
$$L(x,y) = \frac{1}{\pi}\int_{-\infty}^{\infty}\frac{(x-t)e^{-t^2}dt}{(x-t)^2+y^2}$$

and
$$F(x,y) = \frac{y}{\pi}\int_{-\infty}^{\infty}\frac{e^{-t^2}dt}{(x-t)^2+y^2}$$ is the Vogt function.

Thus with consideration of (A.5) we can now represent the parabolic wave equations for $\mathcal{E}_{vj}^{\pm}$ in the final form convenient for practical applications:

$$\pm\frac{\partial}{\partial z}\mathcal{E}_{vj}^{\pm} + (i/2k_{vj})\frac{\partial^2}{\partial x^2}\mathcal{E}_{vj}^{\pm} + ik_{vj}\Delta n(\omega_{vj})\mathcal{E}_{vj}^{\pm} = \frac{1}{2}\sum_{p,q} g_{p,p-1}^{q}(\omega_{vj})\mathcal{E}_{vj}^{\pm}.$$

In the latter equation we introduce the notation

$$\Delta n(\omega_{vj}) = (n-1) + \frac{1}{2}\sum_{p,q} k_{pq}^{-1} g_{p,p-1}^{q}(\omega_{vj})\left[L\left(\alpha_{pq}^{vj},\beta\right)/F\left(\alpha_{pq}^{vj},\beta\right)\right],$$

where n is the nonresonant index of refraction of the medium.

Let us note that for a mixture of gases in accordance with Ref. 25 we can assume

$$n-1=\frac{3}{2}\sum_i A_i N_i/N_a,$$

where A_i is the coefficient of molecular refraction, N_i is the density of the i-th component of the mixture, N_a is Avogadro's number.

In the case of the active medium of the HF laser, the molecular refractions of the individual components can be taken as (in cc/mole):

$A_{H_2}=2.09$, $A_{HF}=2.0$, $A_F=1$, $A_{F_2}=2.91$, $A_H=1.1$ and $A_{He}=0.52$.

REFERENCES

1. A. E. Siegman, PROC. IEEE, Vol 53, 1965, p 277; APPL. OPTICS, Vol 13, 1974, p 353.

2. Yu. A. Anan'yev, USPEKHI FIZICHESKIKH NAUK, Vol 103, 1971, p 705; "Kvantovaya elektronika" edited by N. G. Basov, No 6, 1971, p 3.

3. Yu. A. Anan'yev, L. V. Koval'chuk, V. P. Trusov, V. Ye. Sherstobitov, KVANTOVAYA ELEKTRONIKA, Vol 1, 1974, p 1201.

4. D. N. Mansell, J. A. Love, W. L. Snell, IEEE J., QE-7, 1971, p 177.

5. R. A. Chodzko, H. Mirels, F. S. Rohers, P. J. Pedersen, IEEE J., QE-9, 1973, p 523.

6. Ya. Z. Virnik, V. G. Krutova, A. I. Mashchenko, A. N. Orayevskiy, A. A. Stepanov, V. A. Shcheglov, KVANTOVAYA ELEKTRONIKA, Vol 4, 1977, p 2234.

7. Ya. Z. Virnik, V. G. Krutova, A. A. Stepanov, V. A. Shcheglov, KVANTOVAYA ELEKTRONIKA, Vol 4, 1977, p 2527.

8. D. B. Rensch, A. N. Chester, APPL. OPTICS, Vol 12, 1973, p 997.

9. A. N. Chester, APPL. OPTICS, Vol 12, 1973, p 2353.

10. A. E. Siegman, E. A. Sziklas, APPL. OPTICS, Vol 13, 1974, p 2775.

11. J. Thoenes, J. C. Kurzius, M. L. Pearson, AIAA PAPER, 75-20, 1975.

12. D. B. Bensch, APPL. OPTICS, Vol 13, 1974, p 2546.

13. Yu. N. Karamzin, Yu. B. Konev, KVANTOVAYA ELEKTRONIKA Vol 2, 1975, p 256.

14. E. A. Sziklas, A. E. Siegman, APPL. OPTICS, Vol 14, 1975, p 1874.

15. A. A. Stepanov, V. A. Shcheglov, ZHURNAL TEKHNICHESKOY FIZIKI, Vol 46, 1976, p 563; Preprint FIAN (Lebedev Physics Institute), Moscow, 1975, No 134.

16. A. N. Orayevskiy, V. P. Pimenov, A. A. Stepanov, V. A. Shcheglov, KVANTOVAYA ELEKTRONIKA, Vol 3, 1976, p 1896.

17. V. G. Krutova, A. N. Orayevskiy, A. A. Stepanov, V. A. Shcheglov, KVANTOVAYA ELEKTRONIKA, Vol 3, 1976, p 1919; ZHURNAL TEKHNICHESKOY FIZIKI, Vol 47, 1977, p 2383.

18. D. Potter, "Vychislitel'nyye metody v fizike" [Computer Techniques in Physics], Moscow, Mir, 1975; A. A. Samarskiy, "Teoriya raznostnykh skhem" [Theory of Difference Schemes], Moscow, Nauka, 1977.

19. Yu. A. Dreyzen, A. M. Dykhne, PIS'MA V ZHURNAL EKSPERIMENTAL'NOY I TEORETICHESKOY FIZIKI, Vol 19, 1974, p 718; H. Mirels, APPL. PHYS. LETTS, 1976, Vol 28, p 612.

20. V. I. Kuprenyuk, V. V. Sergeyev, V. Ye. Sherstobitov, KVANTOVAYA ELEKTRONIKA, Vol 3, 1976, p 1962.

21. Pai Shih-i, "Teoriya struy" [Theory of Jets], Moscow, Fizmatgiz, 1960.

22. L. A. Vaynshteyn, "Otkrytyye rezonatory i otkrytyye volnovody" [Open Resonators and Open Waveguides], Moscow, Sovetskoye radio, 1966.

23. V. N. Lugovoy, A. M. Prokhorov, USPEKHI FIZICHESKIKH NAUK, Vol 111, 1973, p 203.

24. R. Pantel, G. Putkhov, "Osnovy kvantovoy elektroniki" [Fundamentals of Quantum Electronics], Moscow, Mir, 1972.

25. M. Born, V. Vol'f, "Osnovy optiki" [Fundamentals of Optics], Moscow, Nauka, 1973.

6610
CSO: 1870

END

END OF FICHE DATE FILMED

APRIL 12, '71

APPROVED FOR RELEASE: 2007/02/08: CIA-RDP82-00850R000100040017-8

APPROVED FOR RELEASE: 2007/02/08: CIA-RDP82-00850R000100040017-8